12-2009

Dynamics of Ultrasonic Consolidation

James Gibert
Clemson University, jgibert@clemson.edu

Dynamics of Ultrasonic Consolidation

A Dissertation
Presented to
the Graduate School of
Clemson University

In Partial Fulfillment
of the Requirements for the Degree
Doctorate Of Science
Mechanical Engineering

---

by
James M. Gibert
December 2009

Accepted by:
Dr. Georges Fadel, Committee Chair
Dr. Mohammed Daqaq
Dr. Marian Kennedy
Dr. Henry Rack

Abstract

Ultrasonic consolidation (UC) is a solid state rapid manufacturing process derived from ultrasonic welding of thin metal foils coupled with contour milling to achieve functional accurate components. The bonding of metal is accomplished by the local application of high frequency vibration energy under pressure producing a metallurgical bond without melting the base material. Its unique nature allows the design and fabrication of structural panels for satellites, production of injection molding tools, functionally graded structures, metal-matrix composites, embedded sensors, armor, and fiber embedded adaptive structures. It is commonly theorized that interfacial motion and friction at the bonding interface play a prominent role in the bonding process by removing surface contaminants, allowing direct metal to metal contact, and producing sufficient stress to induce plastic flow. The substrates geometry is also crucial in the bonding process. Researchers have experimentally observed that as the height of build specimen approaches its width, the bonding process degrades, and no further foils may be welded. This work explores the process as the dimensions of the build specimen modeled as a standard parallelepiped, approaches the critical geometry through a combination of numerical, analytical and experimental analysis. We examine the resonances of a build feature due to a change in geometry and material properties using a three dimensional Rayleigh-Ritz model. A simple nonlinear dynamic model of the Ultrasonic Consolidation Process examines how the geometry change may influence the overall process dynamics. This simple model is use to provide estimates of how changes is substrate geometry affect the differential motion at the bonding interface and the amount of changing friction force due to build height. The trends of changes in natural frequency, and

differential motion, are compared to experimental limits on build height. These analyses lead to several predictions on build height that are verified experimentally. Finally, the work examines the effectiveness of using support material to extend the build height limit of the process. The results show that a proximity to a resonance excitation is clearly responsible for bonding degradation at features built with the nominal tape width of 0.9375 inches. However, for small widths other factors such as surface topography, and contact area may play an important role in bonding degradation.

Dedication

To Reneé and Naomi. You are always in my heart.

Acknowledgments

Above all, I would like to thank God for providing my life with a purpose. I would like to thank Renee, my wife, her love and support has sustained me over the years. Special thanks to my advisor, Dr. Georges Fadel, without his guidance and understanding I would have never completed this work. Thanks to Dr. Eric Austin for his help and advice. I am truly grateful to Dr. Fadel and Dr. Austin for their influence on my life. Thanks to my committee members: Dr. Mohammed Daqaq, Dr. Marian Kennedy, and Dr. Henry Rack. Your suggestions and comments have greatly improved my research.

I would like to recognize to my research colleague and friend, Daniel McCullough. The long nights in the office and machine shop passed quickly due to our interesting conversations. Special thanks to Dr. Todd Schweisinger for his friendship, it was great to know that I wasn't the only person to experience setbacks and delays. Special thanks to my friend, Dr. Balajee Ananthasyanam. I enjoyed our many interesting research conversations. I would like to acknowledge my friends and office mates Vincent Lee, Christian Davidson, Carlos Solano, Gregory Batt, Michael Baracky, Varun Praveen, Christopher Czech, Wenshan Wang, Santosh Tiwari, Justin Foster, Timothy Troy and Scott Hesser. I would like to recognize my friends at Solidica Inc., Mike Sheridan, Chris Fitzgerald, Grant Martin, Lea Ann Schwope, Jon Ayers, Tom Salvatore, and Samer Chanine.

I would like to acknowledge the support of the National Science Foundation through a graduate fellowship, and the South East Alliance for Graduate Education and the Professoriate through a fellowship. Finally, I would like to thank Solidica, Inc. for the use of their equipment and their financial support.

Table of Contents

List of Tables

List of Figures

Chapter 1

Introduction

1.1 Overview of Ultrasonic Consolidation

Prototyping is intrinsically linked to product development and manufacturing. In the early years of manufacturing, labor intensive manual prototypes were constructed by an artisan. The advent of digital computers brought a new phase of prototyping known as virtual prototyping. The prototype could now be tested, evaluated, and modified virtually as if it were a real component. In the late 1980's, prototyping evolved again with the introduction of the first rapid-prototyping techniques and machines. These processes construct a product or component using mostly additive methods called solid freeform fabrication [2]. Examples of these processes include: selective laser sintering, fused deposition modeling, stereolithography, laminated object manufacturing, and electron beam melting. Traditionally, these processes have been used in product visualization, experimentation, limited testing, proof of concept, and rapid-tooling. The current research trend is to expand the capabilities of rapid-prototyping into rapid manufacturing, i.e., the production of parts that can withstand the rigors of strenuous testing and may be used directly as finished components. Unfortunately, existing techniques have several flaws that prevent their expansion to manufacturing usable products, i.e., they are limited in their material structure and properties. They also suffer from the inability to integrate with prefabricated

components, and have high material costs. Typically, powder consolidation methods produce low density, porous structures with limited ductility, fracture toughness and corrosion resistance. Notable exceptions to these limits are laser engineered net shaping (LENS), direct metal deposition (DOM), electron beam melting (EBM) [3]. Processes such as selective laser sintering, fused deposition modeling, stereolithography, etc. are limited by using materials with low strength and low melting temperatures such as photopolymers, polymers that cure or solidify when exposed to light.

Ultrasonic consolidation (UC) is a solid-state fabrication process that creates three-dimensional components through ultrasonic welding of layered metal foils, and contour milling. The UC process is proprietary to Solidica, Inc. [4] and is implemented in their Formation machine (Figure 1.1) that is similar to a standard 3-axis CNC milling machine. UC can be used as a traditional rapid prototyping process, however it is better classified as

Figure 1.1: Current Commercial Version of Formation Machine

a rapid manufacturing process. It is a combination of a metal joining processes with contour milling. Its true potential is that it does not have many of the weaknesses associated with adapting rapid prototyping technologies to rapid manufacturing such as welding dissimilar metals that would be hazardous in powder form [5], where laser fusion techniques are

used. In addition, UC requires no inert gas shielding which is sometimes necessary in rapid prototyping processes. Typically, the process uses low cost aluminum foils, however, nickel, copper, magnesium, and titanium [6, 7] may also be used. Theoretically, the process can join the same material combinations as traditional ultrasonic welding (Figure 1.2). Experimental

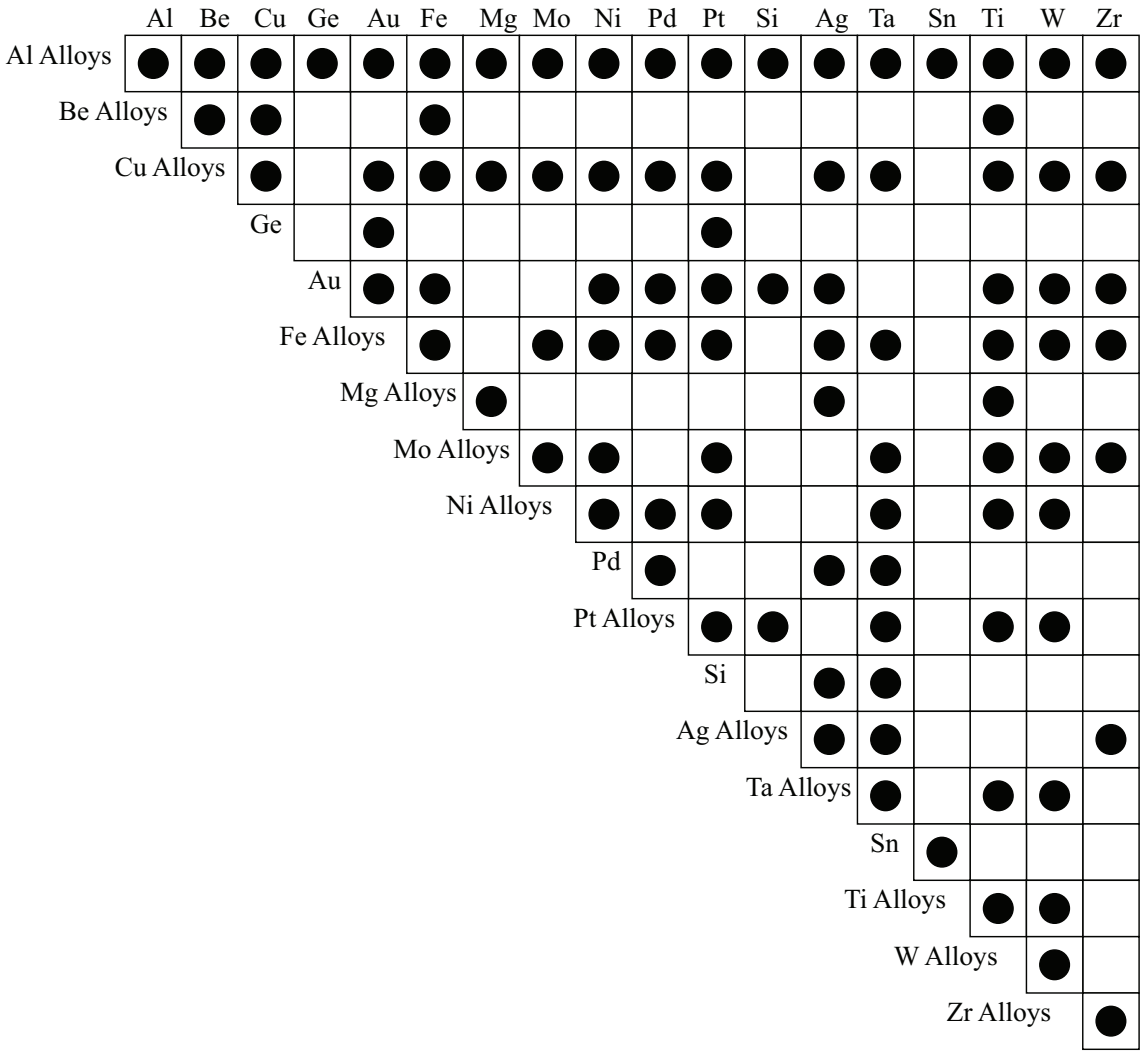

Figure 1.2: Metal Combinations that can be Ultrasonically Welded [7]

evidence indicates that the bond strength can approach that of the base metal allowing the production of durable, ready to use parts [5]. In addition to joining dissimilar metals, it allows the embedding of objects such as delicate fibers within a three dimensional metal structure. The bond is produced with no melted substructure reducing thermal gradients

that can lead to distortion and embrittlement [5].

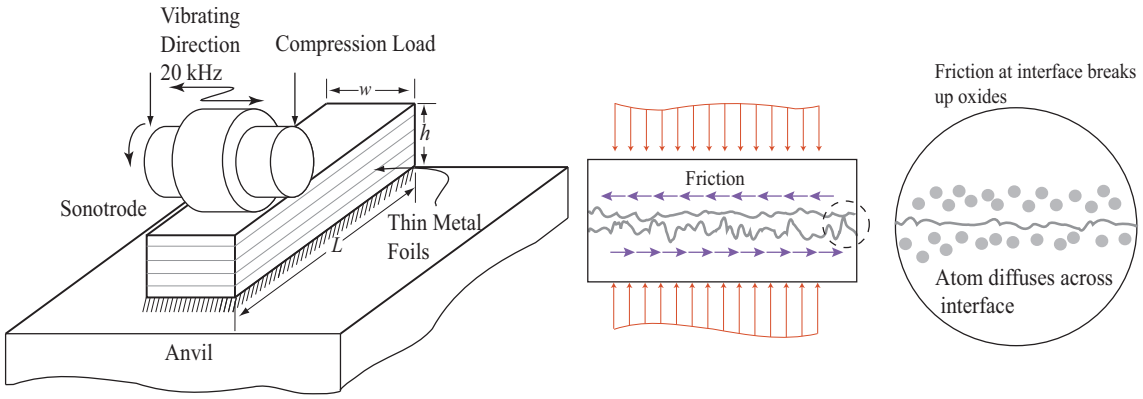

Figure 1.3: Overview of Ultrasonic Consolidation Process Reproduced from Kong [8]

While, there are several iterations of the Formation machine, the fundamental principles of the UC process remain unchanged. Figure 1.3 presents a basic overview of UC. A thin metal foil approximately 150 μm thick and 23.8 mm wide is placed on a sacrificial base plate that is bolted on an anvil. The foil is compressed under moderate pressure by a rolling ultrasonic horn, also known as a sonotrode, that vibrates nominally at 20 kHz with a peak to peak amplitude that ranges from 5-40 μm in the transverse direction. The sonotrode has a roughend surface; it is believed that the sonotrode grips the top surface of the foil vibrating it without slip. This causes relative motion between the foil and base plate. Performing the process at room temperature produces heat through the scrubbing of the mating surfaces at the bonding interface. The heat causes a temperature rise at the interface that is between 30 to 50% of the base metal's melting temperature [9]. Typically, the UC process is conducted at 300 °F by employing a heated base plate. Anecdotal evidence by Solidica, Inc. indicates that the added heat aids in the bonding process. Once one layer is bonded, additional layers are added and machined. The process is repeated until the desired dimensions of the feature are reached.

Ultrasonic consolidation is a relatively new technology. Its origin, however, is in ultrasonic welding and it utilizes some of the same principles of other ultrasonic joining methods such as ultrasonic ball bonding. However, UC differs from other processes in that

the substrate's geometry and therefore its stiffness is constantly changing.

Grouping UC and other ultrasonic joining processes in the larger framework of solid-state metal joining processes, UC lies somewhere between solid state diffusion bonding and linear friction welding as shown in Figure 1.4. In solid state diffusion bonding, there is no

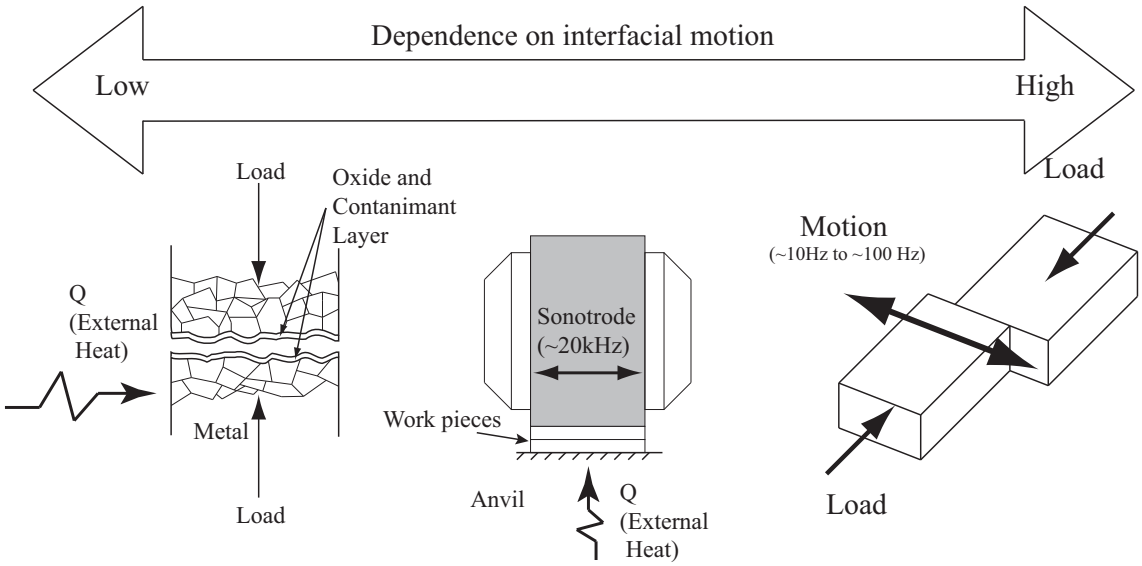

	Diffusion Bonding	Ultrasonic Consolidation	Linear Friction Bonding
Load	Varies (adequate to reach yield point of base metal)	Moderate (50-1400N)	Low during scrubbing, High during forging (max 200kN)
External heat	High (50% - 90% of Melting Temp)	Moderate (approximate 50% of Melting temp)	None
Interfacial Motion	None	Slip/ Gross Sliding	Gross Sliding
Time	Minutes to Hours	Rolling contact	Minutes

Figure 1.4: Continuum of Solid-State Fabrication Processes

scrubbing of the two surfaces. Diffusion bonding relies on elevated temperatures (50-90% of the melting point of the base material) and high pressure to flatten the bonding surfaces, fragment impurities, and produce atom to atom contact. When the surfaces are pressed together at high temperatures, atoms diffuse along grain boundaries closing voids in the contacting surfaces. The atoms condense and further reduce the size of any voids in the

interface [10]. The pressure can be applied for a few minutes or up to a few hours depending on the material being bonded.

Conversely, in friction welding, the bonding is solely dependent on pressure and frictional scrubbing at the interface. The process begins with two pieces that are statically clamped. Then next step depends on the process, inertia welding or linear welding. In inertia welding the parts are rotated and in linear welding the parts undergo linear reciprocal motion. The pieces are brought together under light pressure causing frictional heating. Finally, a forging pressure is applied, and the relative movement is stopped to form the final joint. The stressed on the material due to the scrubbing and forging causes the material to reach the plastic state which helps remove surface impurities. After the plastic state has been reached, the two surfaces are forced together [11].

While UC shares many aspects of both joining processes: it is performed at an elevated temperature similar to diffusion bonding and the interfacial motion of friction welding. It is unique in that ultrasonic waves travel through the bonding metals lowering the modulus and the stress needed to reach a plastic state [12, 13]. In fact, experiments have shown that the use of ultrasound in diffusion welding in an inert gas atmosphere or a vacuum reduces the time needed for bonding [14, 15]. The mechanism of bond formation during the ultrasonic welding of metals has been widely studied but the exact workings of the UC process are still not known, however, there are many theories about the physics that govern the process. The commonly accepted "theory" states that a combination of compression under moderate pressure and shear scrubbing caused by ultrasonic motion cleans off surface oxides through friction, fracturing and leveling of surface asperities [7, 5]. When two relatively flat surfaces are brought together, only peaks of the surface asperities actually touch. Thus, the physical contact area is less than the geometric area of contact. Ultrasonic consolidation causes the physical area to approach the geometric area. The process begins with the initial compressing of asperities, disrupting the oxide layer on the surface, allowing direct contact of pure metal resulting in metallic bonding. The bonds are in turn plastically deformed by shear vibrations resulting in heat which promotes diffusion

and crystallization of material between layers resulting in a true metallurgical bond [16]. In addition, the process is aided by the transfer of ultrasonic energy into the metal, which effectively acts similarly to localized heating, thus reducing the stress needed for plasticity. Specifically, in ultrasonic consolidation, there is evidence that the oxides are not removed, but are distributed in the bond zone [4].

Ultrasonic consolidation has been used in the fabrication of light weight structural panels for satellites [17], in the production of injection molding tools, functionally graded structures, metal-matrix composites, and fiber embedded adaptive structures [5].

The three processes: diffusion, ultrasonic consolidation, and friction welding rely on plasticity to initiate the mechanisms of bonding. Figure 1.5 shows a hypothetical relationship between applied stress, applied heat, and ultrasonic energy on the stress needed for plasticity. The amount of heat and stress generated are interdependent. The applied stress

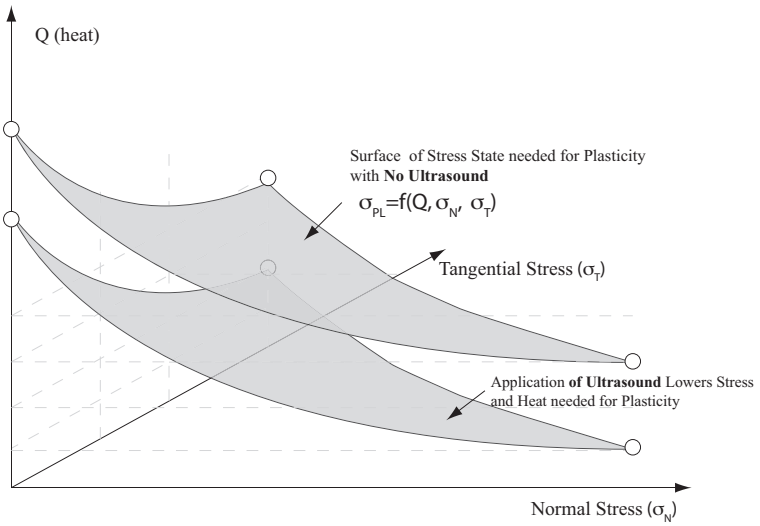

Figure 1.5: Effect of Heat and Stress on Plasticity

is a function of amplitude of vibration, relative motion, normal load, and stiffness of the workpiece. The heat generated is a function of friction at the interface, and of the plastic deformation of the work piece. Seemingly, there is a trade-off between heat and stress. Larger values of stress imply less heat is needed to reach plasticity, and consequently, the more heat the less stress one needs to reach plasticity. Ultrasonic energy shifts the curve

by reducing both the amount of heat and stress needed to reach the plastic stress state..

1.2 Motivation

Experimental observations by Solidica, Inc. indicate that additional layers cannot be bonded to a free standing aluminum feature if its dimensions exceed a critical value. Robinson *et al.* formally documented this finding [18] and theorized that if the substrate is not sufficiently stiff then no differential motion exists. This results in a lack of bonding. In the context of the accepted theory of ultrasonic bonding [7, 19, 16, 20, 21], this can be explained by realizing that, as the substrate becomes more compliant the amount of differential motion is reduced. The tangential force due to friction, is dependent upon the differential motion and is also reduced. The combination of tangential and normal force results in stress. Differential motion at the interface results in heat. The stress and heat produced must be of sufficient magnitude to break up the oxide layer and cause plastic deformation of asperities allowing metal to metal contact. The exact stiffness needed for adequate stress and differential motion between the bonding tape and substrate has not been quantified. In fact, the exact level of stress needed to breakup the oxide layer and cause bonding is not known, however, we assume the stress to be equal to that which causes plastic deformation in the workpiece. Furthermore, determining this required stiffness is problematic. The substrate's stiffness [22] changes with temperature, geometry, the location of the applied force, the type of deformation, the elastic modulus of the material and therefore the amount of ultrasonic energy the material absorbs [23]. Additionally, substrate stiffness cannot be considered in isolation in determining when differential motion will occur. Surface properties such as roughness and asperity height and distribution along with surface interactions such as the shearing of asperities, also affect the normal pressure and friction at the interface. The objective of this work is to quantify the exact nature of the relationship between stiffness, differential motion, and the force transmitted at the interface.

1.3 Principles of Operation of Ultrasonic Consolidation

While all of the techniques in this family of ultrasonic bonding utilize ultrasonic energy to aid in the bonding process; it is important to note that in the family there are differences between the various processes. Light, low power machines operate at high frequencies. Examples' of these machines include ultrasonic ball bonding, Figure 1.6, and wire bonding, Figure 1.7, used in joining wire to integrated circuit boards. They involve the bonding of objects with a diameter or characteristic length which varies from 25 - 500 μm. The materials used in bonding and the substrates are relatively ductlile, i.e., pure aluminum

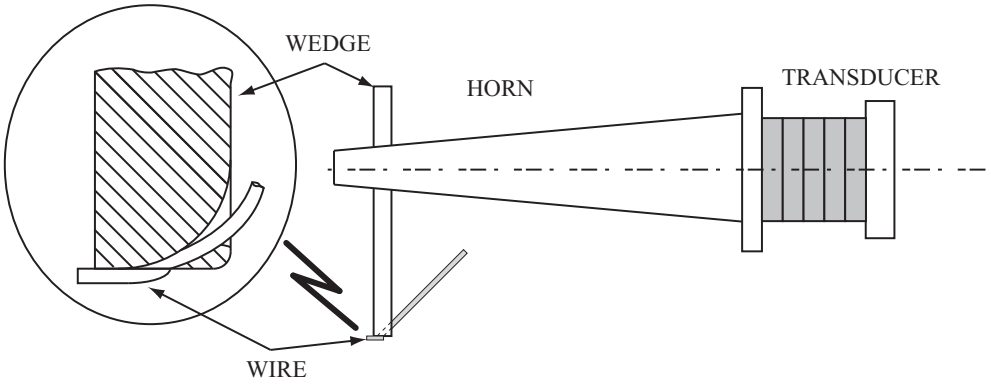

Figure 1.6: Wedge Bonding

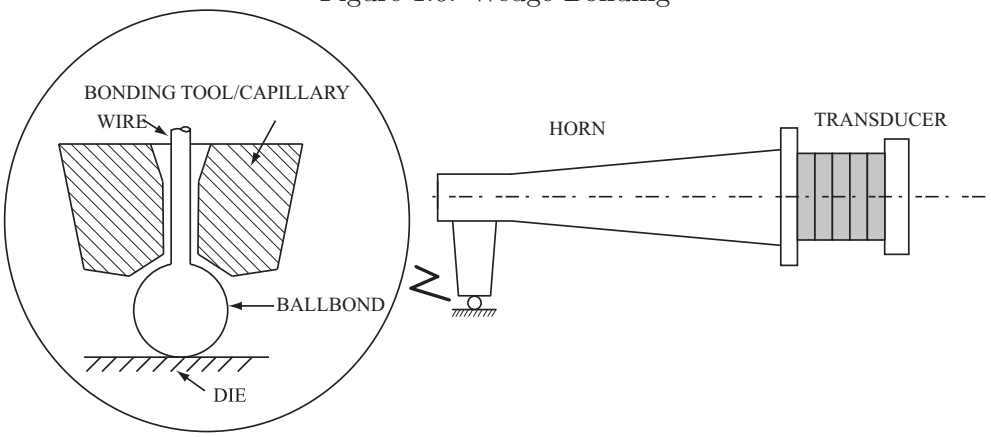

Figure 1.7: Ball Bonding

and gold [7]. The bonding units typically have an operating frequency range of 40 - 75 kHz with relatively low power levels, typically a few watts. Heavy, high power machines such

as ultrasonic welders used in metal joining usually operate a lower frequencies. Ultrasonic welders differ based on design and application. Operating frequencies are typically in the range from 10 to 20 kHz with an amplitude of vibration varying from 10-100 μm. Seam welders are able to bond metals of foil thickness around 150 μm, while wedge-reed welders can be used for metals as thick as 3mm and butt welders can weld aluminum sheets with a thickness up to 10 mm [24]. Ultrasonic welding is used to joined hard aluminum alloys. Despite differences in dimensions, materials, and the amount of power passing through the interface, the current theories of bond formation for ultrasonic wire bonding, ball bonding and welding share many similarities [7].

While the exact operational details of the ultrasonic welding assembly are proprietary to Solidica, Inc., the basic equipment used in the process consists of a three axis CNC mill and an ultrasonic seam welder. All ultrasonic bonding machines convert electrical energy into high frequency mechanical vibrations. They typically have the following components [7]:

- A power source or frequency convertor that changes electrical line power of 50 to 60 Hz to the resonant frequency on the welding system.
- A transducer-sonotrode system to convert the electrical power to elastic vibratory energy and deliver into the weld zone.
- A mechanism to apply compressive force to the weld zone.
- An anvil that supports the workpieces providing a reaction to the clamping force.
- A device to control the amount of energy supplied to weld. This device can take many forms. In spot welding, ring and line welding it is a simple timer that shuts the sonotrode off after a desired amount of time. In seam welding, it is the system used to rotate the sonotrode and translate the build piece i.e., the motors that determine the rolling speed of the sonotrode.

Of particular interest is the transducer-sonotrode system. The transducer can be

either magnetostrictive or piezoelectric. In the magnetostrictive effect a rod or bar of ferromagnetic or ferrimagnetic material is subject to a magnetic field and strains. Conversely, a mechanical stress applied to the rod or bar causes a change in intensity of magnetization [25]. Similarly, the piezoelectric materials generate an electric charge when their they are subject to a stress field and when exposed to an electric field they strain [25]. We focus on the piezoelectric actuator since it is used in the ultrasonic consolidation process. The actuator strains in the presence of an electric field; conversely in a stress field, it generates an electrical charge.

The transducer usually outputs a limited displacement, therefore horns are used to magnify the transducers' vibration. A horn is a mechanical velocity and displacement transformer, typically this is a rod of variable cross section. The force, and displacement vary along the cross section. There are four general types of horns: constant, linear or conical, exponential, and stepped. The designation refers to the degree to which the area changes from the base to the tip [26]. The term sonotrode usually designates the horn that transmits vibrations into the weld area. The sonotrode, may unlike other horns, have geometries that range from bars, to disks, to blocks depending upon the application. If the amplification of one horn is insufficient for a given application, multiple horns may be connected with each horn resonating at the transducers operating frequency.

Perhaps the most common and conceptually simple transducer-sonotrode assemblies are designed to resonate at the assembly's first longitudinal mode of vibration, i.e., the $\lambda/2$ mode. Lambda is the wave length of the fundamental mode of the horn. The $\lambda/2$ mode is the fundamental mode of a vibrating longitudinal rod with both ends free, i.e., half the wave length of a cosine wave. When multiple horns are used, these types of systems can be thought of as a series of rods each having the same resonant frequency. Figure 1.8 illustrates the principle for a seam welder. This rod approximation is an idealization, it neglects the poisson's effect. This eliminates the effect of shear stiffness and lateral motion on the modes of vibration. Furthermore, rod theory neglects other modes of vibration that may be present due to bending or torsion.

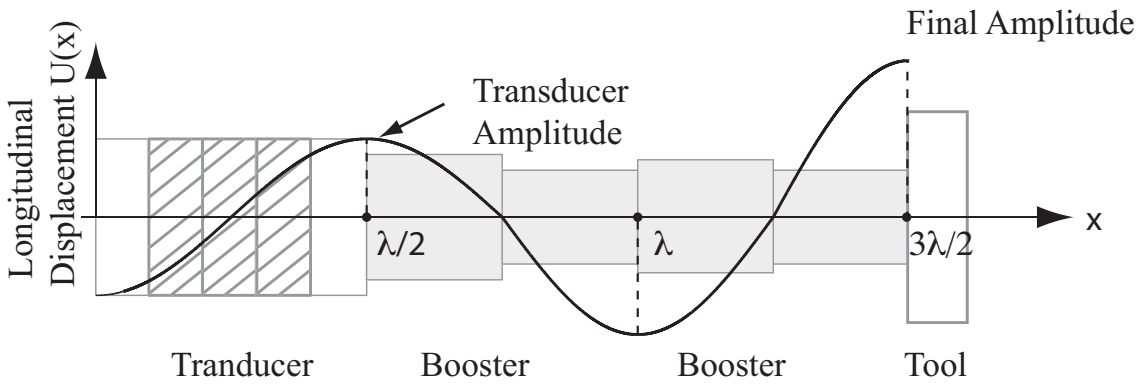

Figure 1.8: $\lambda/2$ Synthesis of Longitudinal Seam Welder Reproduced from Fu [27]

Transducer-sonotrode assemblies are not limited to this design, but can be designed to operate at higher resonant frequencies or to even utilize torsional and flexural modes of vibration. Again, the exact operation of the welding assembly used in the Formation machine is not known; however, the geometry of the assembly indicates that it works by exciting either the first or the second longitudinal mode.

There are several control schemes to maintain tip amplitude during welding. Communication from Solidica, Inc. states that the horn is calibrated in free air to determine the relationship between the amplitude of the voltage and the amplitude of the horn as measured by the laser vibrometer [28]. Once the calibration constant between the applied voltage and amplitude is determined, the operator inputs the desired amplitude, and a phase lock loop (PLL) algorithm then maintains the amplitude of vibration during the build process. The exact control algorithm for the PLL system is a trade secret of the Sonics and Materials Inc. and Branson Ultrasonics Corporation, the two manufacturers of UC power supplies. In general, PLL controllers of ultrasonic welding systems with voltage sources dynamically tune the sonotrode by adjusting the input voltage frequency to the transducers piezoelectric (PZT) actuator to eliminate the phase difference with the current output of the PZT during operation. In the mechanical domain, the velocity and force have zero phase difference at resonance. The PLL algorithm assumes the ultrasonic system is described by the Force-Voltage electromechanical analogy: the velocity is analogous to the current and the force

is analogous to the voltage [29]. Minimizing the phase difference between the current and voltage is equivalent to minimizing the phase difference between the forces that excites the sonotrode and its resulting velocity under load, thus always ensuring the system is driven at resonance.

1.4 Literature Review

In this section we review the prevalent literature describing the effect of ultrasound on metals, previous work on modeling the process as well as process optimization. The section begins by reviewing early work on the effect of the application of ultrasound on metals. It then proceeds to review research dealing with the types of motion at the bonding interface: interfacial slip and gross sliding. Next, we examine research on modeling ultrasonic rapid manufacturing. Finally, we detail work that focuses on optimizing the UC process.

1.4.1 Effect of Ultrasound on Metals

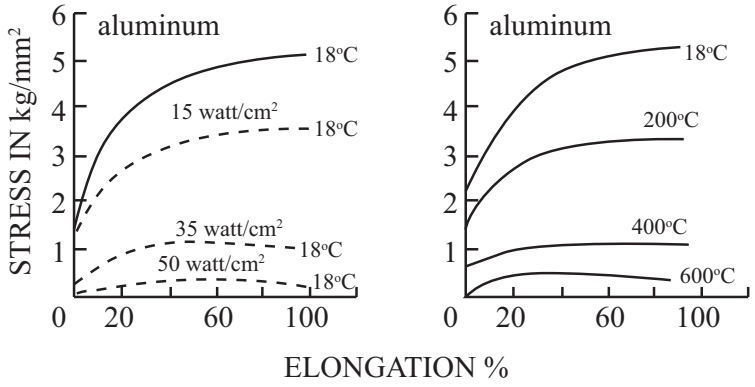

Figure 1.9: Acoustic Softening of Aluminum Reproduced from Langenecker [12]

Early research efforts on the effects of ultrasound on metals were conducted by Langenecker [12, 23], and Blaha [30]. They performed several experiments in which metal specimens were fastened directly to an ultrasonic horn that is allowed to vibrate at various levels of intensity (power supplied to specimen divided by the area). Langenecker [12]

summarizes two nonlinear effects caused by the application of ultrasound on metal: acoustic softening and acoustic hardening. Acoustic softening occurs during the application of ultrasound; it is a reduction in the modulus and apparent static stress necessary for plastic deformation. In fact, Langenecker states that the application of ultrasound and heat to metal appears to have similar effects on the stress needed for plastic deformation. Figure 1.9 shows the similarity between thermal and acoustic softening. Ultrasound is more efficient in reducing the apparent stress. He ascribes the difference to ultrasound energy being readily absorbed by dislocations in the microstructure, i.e., the irregularities or defects in the crystallline microstructure of metal. Disolocations in the metal lattice which are known to carry out plastic deformation. The acoustically excited areas of dislocations are "weak spotsinches in the metal and are movable at much lower stresses. Heat on the other hand, is distributed to all the atoms of the crystal including those not responsible for plastic deformation. Both heat and ultrasonic energy excite atoms in the lattice making it susceptible to slip. Langenecker also observed acoustic hardening in Zinc (Figure 1.10). This is an increase in apparent yield stress and occurs after the removal of acoustic radiation of high levels of intensity. Acoustic hardening is limited by the fact that too high of an intensity of ultrasound may cause plastic deformation and even fracture of metal crystals. Langenecker did not theorize why this occurs, but it may be a form of strain hardening.

1.4.2 Ultrasonic Bonding

In ultrasonic bonding techniques, there exist two types of motion: interfacial slip and gross sliding. Joshi [31] studied joint formation of ultrasonic wire bonds in different materials: pure aluminum, copper and gold in both similar and dissimilar combinations. He measured the temperature change, electrical resistance change, and interfacial motion during the process. Finally, he looked for evidence of hardening. Measurements indicated that during the process, no temperature exceeded 80 °C, and that decreases in clamping force , i.e., the force used to clamp the wire to the substrate by 50% caused a temperature rise of 40 °C. Joshi [31] found no evidence of gross slip in the process. He used a laser

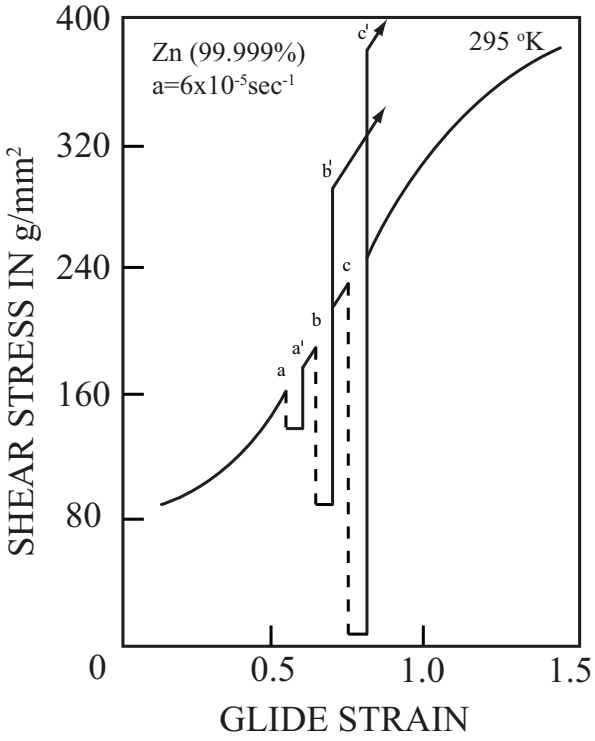

Figure 1.10: Softening and Hardening of Zn from [12]

interferometer to measure the motion of the tip, wire, and substrate. The amplitude of motion for each component reached a common constant value and retained that value during the process. Subsequent re-excitation did not change this pattern. In addition, he excited the system not only in the x direction; i.e, in the same direction as friction, but also in the y and z directions. Bonds formed in all three directions, however, in the x direction, the bonds were the strongest. There was no evidence of localized hardening in the weld region. Joshi concluded that the primary bonding mechanism was due to plasticity caused directly by acoustic softening, and that heat does not play a significant role in the process. There was evidence that bonding occurred after the cessation in ultrasonic energy. Mechanical interlocking and not diffusion seemed to be the primary cause of bonding. Finally, he found that long weld times caused cracking.

Research by Lum, Mayer and Zhou [32] clarified the results of Joshi [31]. They developed a model of ultrasonic wire bonding based on the classical microslip theory of

Mindlin [33]. They showed that both microslip and gross sliding occur in wire bonding. The transition in motion depends on the amount of ultrasonic power and normal load: for a given normal force, the motion switches from slipping to sliding as ultrasonic power increases. Consequently, by increasing the normal load, a greater amount of ultrasonic power is needed to change the type of motion. Gross sliding correlated well with high bond strength while localized slip indicated weaker bonds.

Early studies in ultrasonic welding were conducted by Chang and Frish [34] using a spherical radius horn and joined both 2024-T351 Aluminum alloy and OFHC Copper plates. In their system, motion at the interface consisted of localized slip and not gross sliding. The researchers measured the temperature, normal load and power output during the process. Analytically, they modeled the system using a Mindlin [33] analysis of an elastic sphere contacting a plane. This allowed them to develop expressions for the optimum tip displacement, power consumption, and coefficient from the damaged slip annulus produced by the slip between the bonding surfaces. They concluded that plasticity and interfacial slip aid in the bonding mechanism. They theorize that the mechanism's probable cause is either adhesion, mechanical interlocking, recrystallization, diffusion or a combination of these processes. Neppiras [35] considered the energy loss in ultrasonic welding. He found that, when the tangential force exceeds a critical value, macroscopic sliding occurs in ultrasonic welding

Harthoorn [36] compared ultrasonic welding to the joining of metals by fretting. He defines fretting as the reciprocating sliding between two surfaces, where the sliding distance is significantly less than the contact length. The frequency of the oscillatory motion in fretting is much smaller than that of ultrasonic welding. He noted that the tensile shear strength of welds produced by both processes is nearly the same, the shape of the bonded areas is similar, and plastic deformation is present at the interface in both processes. Fretting, however, does not result in a gross temperature rise.

Harthoorn concludes that the method of joining in both processes is the plastic deformation of asperities, breaking surface layers and allowing adhesion between the metals.

These bonds grow in the direction of oscillating movement. The process continues resulting in the interface being welded and plastically deformed in a layer of 30 μm. He excludes the possibility of diffusion and recrystallization of metal across the bond interface,

1.4.3 Theoretical Modeling

Some of the earliest published analysis concerning ultrasonic bonding in rapid prototyping was by Yadev and Doumandis [16] and Gao and Doumandis [19]. Yadev and Doumandis [16] developed an ultrasonic rapid manufacturing platform and analyzed the thermomechanical aspects of the process. In their analysis, they considered heat generation originating from inelastic hysteresis (due to high loading rates) and plastic deformation in the volume of the material. Heat at the interface surface originates from friction. Based on experimental measurement and theoretical modeling they set forth the following possible evolution of bond formation based on temperature measurements. As the horizontal scrubbing is superimposed on the normal force, there is a rapid increase in temperature due to frictional heating. When the bonding foil reaches the elastic limit, the relative displacement at the loading edges approaches zero due to impending welding. This results in decreased slip and heat generation. Heat generation completely subsides at the yield point indicating local welding. Next, plastic deformation occurs, which produces significantly less heat than friction.

Gao and Doumandis [19] theorized that the coefficient of friction at the interface changes during the welding process due to the shearing and plastic deformation of asperities. In their study, they bonded Aluminum 1100 to Aluminum 6061. A finite element analysis with Coloumb friction at the interface modeled the progression of strains and stresses in the substrate during a single ultrasonic bond using a coefficient of friction dependent upon the amount of plastic deformation. A simple analytical model in combination with experimental strain measurements was used to determine a functional relationship between the coefficient of friction and the amount of plastic deformation. Finally, they conducted simulations using both a quasi-static analysis and full dynamic analysis. They validated

the models by comparing predicted strains to the actual strains produced in welding. The simulation predicted the evolution of the bonding process. The normal load and motion of the sonotrode results in friction on both sides of the bonding tape. The friction results in elastic shear stresses and strains in the tape and substrate. Initially, the shear strains are discontinuous and there is relative slip at the bonding interface. The coefficient of friction increases, amplifying the elastic deformations, but the slip at the interface persists. The stress then reaches the yield point in the softer foil, resulting in excessive shear deformation. Strain hardening occurs in the foil until the plastic limit of the substrate is reached. The plastic deformation bridges the gap between the interfaces, and no further slip occurs. They considered a rectangular shaped horn, therefore local bonding began at the sonotrode edges where the stress concentrations occur. The plastic deformation propagates inward eliminating slip and increasing the bond size.

Zhang and Li [37] performed a two-dimensional dynamic finite element analysis that included elastic, plastic, and thermal strainches The simulation showed that as h/w approaches unity the magnitude of the frictional stress decreases. Subsequently, stress increases as the problematic geometry is passed. The researchers attributed this to positive wave interference that resulted in minimum interfacial displacement. While the work showed a height dependence for the wave superposition. What is unclear from their analysis is how the width plays a role in this behavior.

In the literature there are several three-dimensional coupled finite element dynamic models of the UC process [38, 39]. Zhang *et al.* [37] hypothesized that interactions between the mechanical and thermal domains result in bonding. Specifically, they show that ultrasonic vibrations generate heat at the interface through friction. Heat changes the mechanical properties of the material promoting localized plastic deformation and therefore initiates bonding. Increasing the plastic deformation generates more heat and friction perpetuating the process.

Huang and Ghaseemieh [38] in their three-dimensional finite element analysis utilize a plastic dependent coefficient of friction. They conclude that ultrasonic vibration leads to

a periodically changing stress field, the upper surface of the foil experience severe plastic deformation, and the major source of generated by heat is by the interaction heat is by the interaction between the sonotrode and the foil.

1.4.4 Weld Strength and Process Optimization

Much of the recent research effort in UC has been in determining weld strength and process optimization for various materials. Kong, Soar and Dickens [8] adapted peel tests associated with adhesive bonding to examine the weld strength of Aluminum 6061 specimens, Figure 1.11. They compared the peel strength and linear weld density (the ratio

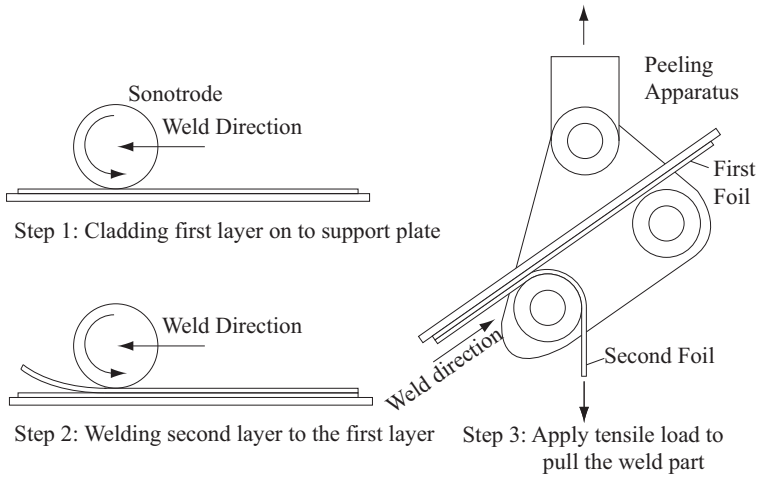

Figure 1.11: Testing Strategy of Kong, Soar, and Dickens [8]

of bonded area to unbonded area along the interface) of specimens composed of unprepared aluminum foil to those cleaned with a degreaser. They believed that a tenacious layer of oxides is on the surface of Aluminum 6061 and that may be removed or weakened by treatment with degreaser. The specimens were welded at various displacement amplitudes, speeds, and contact pressures. They noted that the unprepared specimens had a high resistance to peeling if consolidated at high contact pressures and low weld speeds. Increases in amplitude did not significantly increase bond strength. Unprepared specimens processed at low contact pressure and temperature suffered from "peel-off" or delamination. The prepared foils could not bond at low speeds and high amplitude settings without prema-

ture failure due to rearing and cracking in the weld. Similarly, they could not bond with prepared foils at low contact pressures and high weld speeds. Of the specimens that were able to bond, they found a 6-7% increase in weld strength of the prepared specimens over the unprepared specimens. In examining the microstructure of the unprepared specimens, researchers observed near 0% density due to a persistent oxide layer at the interface. In addition, the interface did not show any sign of mechanical bonding, i.e., interlocking of surface asperities. In fact, the interfaces were separated by a barrier layer made of oxides and other surface contaminants. Conversely, the prepared specimens had a maximum weld density of 45%. The weld density generally increased with slower weld speeds, high amplitude, and high contact pressure. Specimens produced with slow weld speeds and low contact pressures exhibited similar weld densities to those prepared at high pressures and fast weld speeds. They concluded that the high level of oxides in the unprepared specimens caused ceramic bonds, i.e., oxides in the layer to bond, to the oxides in the foil. In addition, they gave a general process window to use when bonding Aluminum 6061 alloy.

Kong, Soar and Dickens [21] also characterized Aluminum 3003-H18 for the UC process. The researchers used the same methodology as [8]; however, they added lap shear tests to the peel tests. The specimens in the lap shear test failed by tension in the foil. Again, the specimens for the test were produced using a range of contact pressure settings, ultrasonic amplitudes and weld speeds. Their results were scattered, but they drew the following conclusions: specimens produced at low amplitudes, low contact pressures and fast weld speeds produced weaker bonds than any other combination of process parameters. Increasing the amplitude of the process increased the linear weld density. Other results were conflicting. High contact pressures correlate well to an increase in weld density. They found evidence that linear weld density could be relatively high with low peel test strength due to the presence of a large amount of oxides and contaminants in the bonded interface.

Similar studies were performed by Janaki Ram *et al.* [40]. They focused on strategies to improve linear weld density without considering weld strength. Oscillation amplitude had the greatest effect on weld density. In general they found upper limits on oscillation

amplitude and normal force for increasing linear weld density; if the parameters are increased past these limits, the linear weld density decreases. Lower weld speeds increased linear weld density. Increasing the temperature resulted in an increase in weld density. They identified sonotrode induced surface roughness as the primary cause of defects in the UC process. Observations indicated that machining removes surface roughness facilitating intimate contact between mating surfaces, removes the sonotrode damage that results in defects and entrapped air, and partially or completely removes the work hardened layer.

Kong, Soar, and Dickens [5] determined a critical load associated with failure in the pull test: failure occurring below this critical load was in the weld region, above the critical load the failure was in a single foil. The implication being that for specimens with sufficient weld strength, the weld is stronger than the base metal. They explained the increase in weld strength by considering the surface and volume effects present in ultrasonic welding. The surface effect describes the interfacial friction between two bonding surfaces, while the volume effect deals with the internal stress, strain hardening and plastic deformation within the metal during the welding process due to absorption of ultrasonic energy. They could not test the weld strength above the critical peeling load: however, they confirmed changes in the weld by examining its hardness. Measurement of hardness showed that both acoustic softening and hardening occurred depending on the contact pressure and weld speed used to weld the specimens. They concluded that the increase in hardness mirrored an increase in weld strengths. The gains in strength occurred for specimens produced at high contact pressures, high amplitudes, and low weld speeds. These parameters would allow for more ultrasonic energy into the bonded area causing acoustic hardening.

Robinson *et al.* [18] explored the connection between effective build height and stiffness experimentally by welding ribs at three different orientations: longitudinally (in the direction of sonotrode travel), laterally (perpendicular to the direction of sonotrode travel), and at 45 degree angle with respect to sonotrode travel, Figure 1.12. Changing the orientation alters the effective substrate stiffness with respect to the ultrasonic excitation. For the various orientations the researchers built features at various widths (0.25 inches,

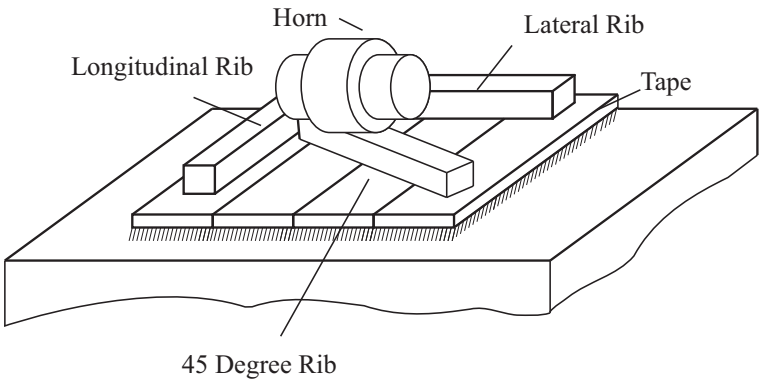

Figure 1.12: UC Free-Standing Rib Build Orientation Reproduced from [18]

0.125 inches, 0.063 inches), each with a length to width ratio of 10:1. However, for the longitudinally orientation they built additional features at widths of 0.50 inches and 0.93 inches Each feature was built to the maximum height possible. They attempted to minimize the effects of trimming by performing the operation after each deposition. They found that the maximum height to width ratio over the three common build widths was 0.943 for the longitudinal rib, 0.943 for the lateral rib, 1.0017 and for the angled rib. The average obscured some of the more interesting results. The minimum build heights for the longitudinal and angled ribs were for features with widths of 0.125 inches In the longitudinal ribs, the mode of failure was detachment during the machining process. In addition, they found that weld density did not change much with height; however, it was well bonded in the center of the feature and showed defects near the edges. In the lateral ribs, the effective stiffness was the greatest; however, the layers were easy to peel off, even at high density, since the weld area for the tapes were small. Failure in this direction was attributed to lack of bonding, and there seemed to be some evidence that weld density was a function of height. The angle oriented builds had regions that saw little force since the process is based on constant pressure. In these areas the tape was prone to peel during the machining operation. Overall, they found the largest height to width ratio was obtained for features with widths of 0.063 inches regardless of orientation, and that the highest weld density occurred in features produced at the angled orientation. The researchers attempted to understand their results

analytically through a two-dimensional finite element model of the process.

Recently, Kulakov and Rack [41] explored the effect of normal load, vibration amplitude and sonotrode velocity on linear weld density using design of experiments. They welded over Aluminum 3003 H-18 specimens. In their study the normal load and vibration amplitude were the primary factors influencing linear weld density while the velocity of the sonotrode had a negligible effect. Based on this literature review, it is clear that the UC process still needs to be studied and better understood. This dissertation is a step in this direction. From the literature survey and from our own investigations, a number of hypotheses and questions surface, these are presented next.

1.5 Hypotheses and Research Questions

The current theory of ultrasonic welding provides a general description of how bonds are formed in the UC process. Yet, it does not clearly indicate how each of the process's system and material parameters, seen in Figure 1.13 affect bond formation. System parameters and their possible effects on the UC process include:

Weld speed - Weld speed determines the energy per unit length put in the weld.

Amplitude of vibration - As long as the limiting value of friction is not reached, the amplitude of vibration affects the dynamic stresses at the interface. Depending on the magnitude and flow stress of the material, it may determine when plasticity occurs and the degree of strain hardening.

Normal load - The compressive load flattens asperities, and determines the magnitude of the limiting value of friction force and consequently the stresses at the interface.

Texture of sonotrode - The sonotrode texture directly affects the amount of damage to the surface of the bonding tape. Excessive damage may lead to large gaps in the bonding interface [40]. In addition it affects the "grippinginches of the sonotrode on

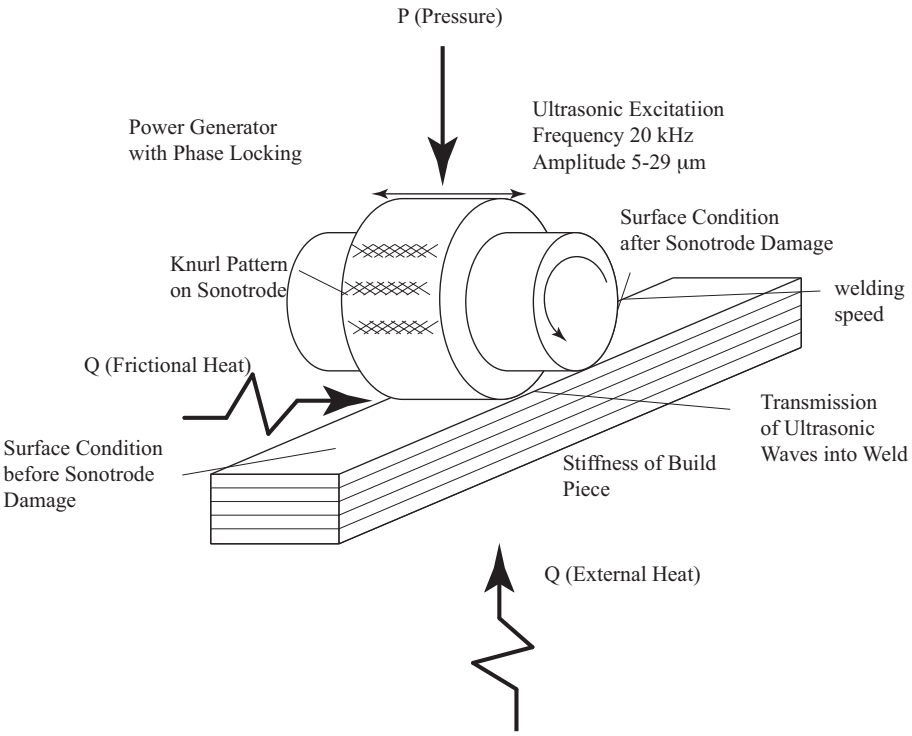

Figure 1.13: Parameters in the Bonding Process

the tapes's top surface. Ideally, the texture would grip the tape so that no differential motion exist at the tape-sonotrode interface.

Temperature of base plate - External heat could serve to reduce the apparent stress for plasticity, enhance atomic diffusion, reduce strain hardening due to plasticity.

Electrical power draw - It is a measurable quantity that may reflect the different conditions of stick and slip at the interface. One can easily see the sonotrode requiring more power to counteract friction when it is sliding than microsliding or even sticking.

Stiffness of the machine - Directly affects the amount of force transmitted to the bonding interface.

While material parameters include:

Surface topography - The surface topography affects the initial contact area through the touching of asperities and therefore influences the frictional and normal stress at the

interface.

Presence of surface containments and oxides - Surface contaminants prevent metal-metal contact. They must be displaced in order for bonding to beginches

Stiffness (geometry and modulus) - The stiffness of the substrate directly influences the resistive force produced by friction at the bonding interface.

Hardness - Hardness directly influences the coefficient of friction between two metals. Empirically, it has been shown to influence the amount of energy required to form a bond [7].

Researchers have examined some of these parameters in the past, specifically in the area of weld speed, amplitude of vibration and normal load. Much work remains to be done before the physics of the UC process are truly understood.

This work addresses the dynamic motion that maybe the major contributor in bonding during ultrasonic consolidation. In terms of the system parameters we focus on load, and amplitude of vibration. In terms of process parameters we deal with the stiffness of the substrate. The work is based on the hypothesis that both a certain amount of tangential force and relative motion is needed for bonding. This amount of force and relative motion are directly dependent on the substrate's stiffness and its properties at its bonding interface. We hypothesize that the system undergoes a qualitative change of dynamics or bifurcation that results in debonding. It is evident that this change in dynamic behavior is a function of the build pieces geometry but no quantifiable explanation has been put forth. The geometry dependence may obscure the true physics of the problem. Our hypothesis is that there must exist some functional relationship between the required stiffness and the forces developed at the interface. This relationship will also dictate the energy at the welding interface. We believe that the ultrasonic energy at the welding interface is converted to friction when slipping occurs, and to elastic strain energy when sticking occurs. If micro slip occurs the ultrasonic energy is split into friction and to strain energy. The interaction of these parameters leads to our research hypotheses.

1.5.1 Primary Hypothesis

Our primary hypothesis is that in order for bonding to occur in the process there is a minimum amount of differential motion and stress needed. The stress depends upon the frictional force, normal force at the interfaces as well as the size of the contact area, Figure 1.14. The relative motion directly depends upon the features' stiffness, the amplitude of vibration and the effective coefficient of friction at the interface, Figure 1.15. This leads to our two sub hypotheses.

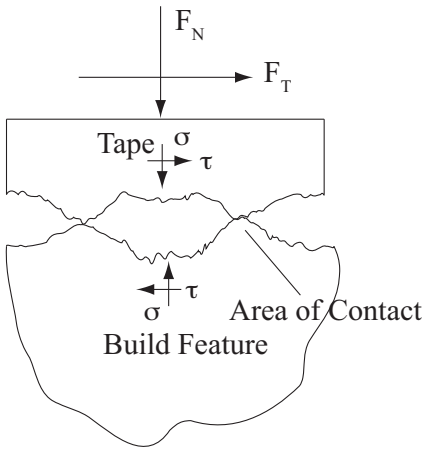

Figure 1.14: Stress at Interface

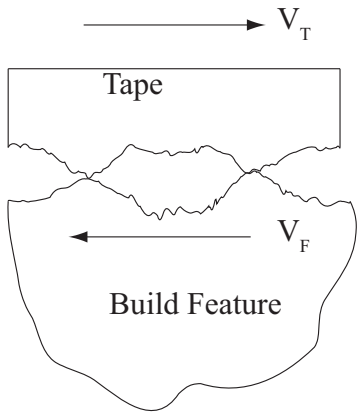

Figure 1.15: Interfacial Motion

1.5.2 Secondary Hypotheses

First, changes in the geometry while building causes a quantitative change in the dynamics to occur. Figure 1.16 presents the one possible scenario based on a stick slip model of the UC process. Assuming that there is no gross slip between the sonotrode and the tape a short build feature is of sufficient stiffness to cause differential motion between the tape and the feature. As the features height increases, it becomes more compliant, and no differential motion occurs. It is evident that this change in dynamic behavior is a function of the build pieces geometry; however, there is no quantifiable explanation. In fact the geometry dependence may obscure the underlying physics of the problem.

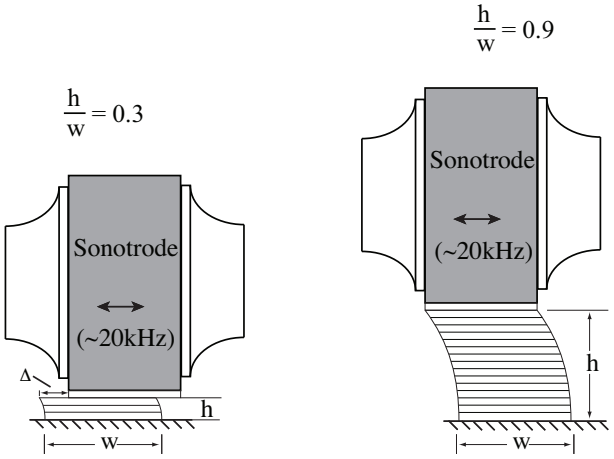

Figure 1.16: Change in Dynamic Behavior Based on Stick-Slip Interaction Between Tape and Build Feature

Second, there exists a functional relationship between the required stiffness and the forces developed at the interface. By quantifying the functional relationship between stiffness and force we may able to suggest strategies to extend the build height.

1.5.3 Research Questions

Quantifying the research hypotheses leads to several questions :

1. Are parasitic vibrations caused by a change in geometry of the workpiece responsible for bonding degradation?

2. Under what exact geometries does bonding degradation occur?

   - Degradation for all heights and widths that have ratios of h/w ranging from 0.8 to 1.2, regardless of width?
   - Are there quantifiable differences between a wrought build feature and consolidated feature?

3. Can we experimentally detect a change in the dynamic response of the build piece and or sonotrode from optimal build geometries to those at or near bonding degradation?

Perhaps by considering changes in amplitude or the frequencies present in the time response.

4. How does friction act at both tape interfaces, i.e., between the tape and the sonotrode and between the tape and build feature? Is it gross sliding versus micro slip? Can we determine how friction acts based on experimental evidence or thru analytical methods such as Finite Element modeling?

5. How do we determine a reasonable estimate of the effective stiffness and mass of the feature and sonotrode?

6. What is a suitable model of the sonotrode? Under what process conditions, if any, can we assume the sonotrode displacement, velocity and acceleration to be enforced?

Answering these questions will lead to a dynamic model of the UC process that may yield insight in how the various process parameters effect bonding. In addition, it will provide the framework for more detailed studies in the bond formation by providing some bounds on the energy at the interface. The primary focus in this work is to study the dynamic behavior of the substrate and this behaviors affect on bonding.

1.6 Dissertation Outline

The remainder of the dissertation is organized as follows.

Chapter 2 models free standings features as a cantilevered parallelepiped. We use this model to determine the natural frequencies of the feature. We use the model to determine the geometries whose natural frequencies are in proximity to the sonotrode's excitation frequency. In addition, the model is used to examine the response to a rolling sonotrode represented as a moving, vibrating load. The models

Chapter 3 presents a lumped parameter model whose results of are compared to a more detailed finite element model for verification. Finally, we use the lumped parameter model to explore changes in process parameters.

Chapter 4 introduces the general procedure, equipment and setup for two tests to validate the models of the UC process.

Chapter 5 discusses the results of the tests presented in Chapter 5.

Chapter 6 explores the use of two candidate support materials in extending the build height limit.

Chapter 7 provides concluding remarks and the suggested direction of future work.

Chapter 2

Vibrations of the Workpiece

2.1 Introduction

Essentially, the ultrasonic consolidation can be viewed as a forced vibration problem with respect to the build piece. A logical hypothesis is that one mode of degradation in bonding may be due in part to an increase in response at resonance leading to fatigue failure in the bond. Unfortunately, the author is unaware of any published research that directly addresses the influence of vibrations on the ultrasonic consolidation process. Vibrating work pieces, however, has been a concern in ultrasonic welding since its inception. These problems manifest themselves as parasitic vibrations, i.e., vibrations outside the weld zone at the excitation frequency [6]. Vibrations can be both harmful and helpful in ultrasonic joining process; a resonance excitation of the top part in contact with the sonotrode facilitates bonding at the interface. Perhaps, the most dangerous form of parasitic vibrations occur when the bottom workpiece is excited at a resonant frequency. Researchers believe that resonance excitations lowers the weld strength of joints already formed, cause rises in dynamic loading of the work pieces which may manifest in cracks at sites of stress concentrations. Solutions to eliminate the undesirable effects of parasitic vibrations range from shifting the excitation relative to the direction of vibration, altering the dimensions of the work pieces to avoid possible resonances and, damping the vibrations through the use of

heavy clamps [7].

2.2 Rod Approximation of Workpiece in Ultrasonic Welding

Most researchers investigating the effects of parasitic vibrations in ultrasonic spot welding assume that the longitudinal motion of the plates is approximated by rod theory whose governing equation is given by

$$c^2 \frac{\partial^2 u(x,t)}{\partial x^2} = \frac{\partial^2 u(x,t)}{\partial t^2} \tag{2.1}$$

where c, is the wave speed, i.e., $\sqrt{\frac{E}{\rho}}$, E is the young's modulus, ρ is the density, and $u(x,t)$ is the longitudinal motion along the beam. Therefore, before elaborating on the literature, it will be helpful to review some fundamentals on the presence of waves and resonances in longitudinal rods. The wavelength, λ, of a traveling wave for a given excitation frequency in a rod is

$$\lambda = \frac{c}{f} = \frac{1}{f}\sqrt{\frac{E}{\rho}} \tag{2.2}$$

where f is the frequency of the wave. Resonances occur in an elastic body when two waves reflect from the boundaries of an object with the same velocity; they interfere constructively and produce a standing wave. The shape of the standing wave is governed by the boundary conditions of the rod. The first frequency a standing wave occurs is known as the fundamental frequency, multiples of this frequency also produce resonances and are known as the higher modes or harmonics and correspond to different shapes of waves, i.e., higher multiples of the wavelength that satisfy the boundary conditions. Figure 2.1 shows the first three modes of longitudinal rods with both ends fixed and both ends free. The fundamental mode of fixed-fixed rod and free-free rods are the half wavelengths of sine and cosine waves, respectively. Both occur when the dimension of the part is half the wavelength, $\lambda/2$. Typically, the plates welded in ultrasonic consolidation are assumed to have both ends free. Given a set of boundary conditions and an excitation frequency one can easily

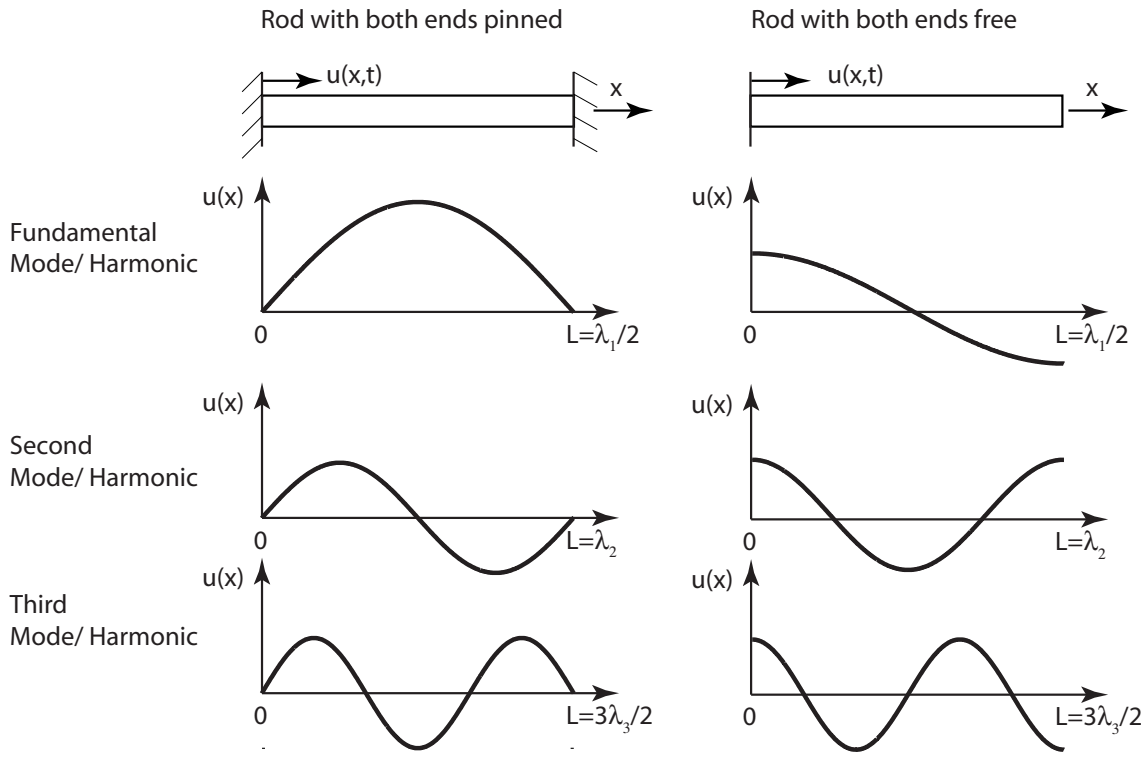

Figure 2.1: First Three Modes of a Rod with Both Ends Fixed, Both Ends Free

use Equation 2.2 to calculate the length of the rod so that excitation frequency excites a fundamental mode or one of its harmonics.

2.3 Investigation into Parasitic Vibrations in Ultrasonic Welding

Rozenberg [6] performed a set of experiments that examined the effects of longitudinal and flexural waves on the spot welding of aluminum alloy plates. He assumed that the longitudinal and flexural motion of the plate can be approximated by rod and plate theory, respectively. He chose the length of the plate so that the ultrasonic welding frequency excites one of the plate's higher harmonics. This was done by placing the excitation at an anti-node position, points of maximum vibration, and clamping the plate at both node and anti-node positions. Rozenberg observed the vibration during welding by several

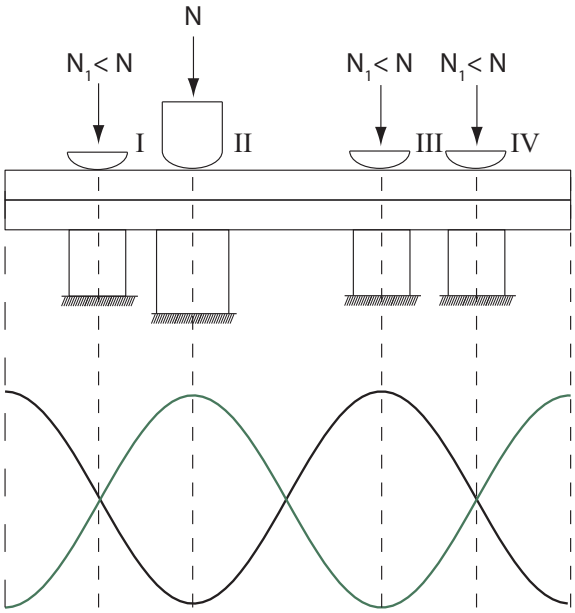

Figure 2.2: Experimental Arrangement for Investigation of the Nature of Vibrations in Plates During Welding Reproduced from Rozenburg [6]

methods. First, a thin layer of lead foil was inserted between the plates. He reasoned that the stresses in the foil will exceed its yield point during welding and therefore rupture indicated welding occurred at that particular spot. Second, he observed the vibration pattern directly by placing a fine powder on the plate's surface. The powder settled around the nodal positions of the plate allowing him to observe the standing wave pattern. Finally, he examined the lateral edges of the plate under a microscope during welding and he observed both the longitudinal and flexural vibrations of the plate. Rozenberg found that the lower plate vibrates far less than the top part which is in direct contact with the Ultrasonic horn. Rupturing of the lead foil indicated the excitation point as well as at the other clamped anti-nodal points. He also remarks without justification that flexural (shearing) modes are hazardous to the spot welding of plates. However, due to the nature of shearing vibration one may theorize they would subject the weld to cyclic loading and fatigue.

Wodara [42] observed that the dimension of the top plate that is parallel to the excitation direction plate influences weld strength. Figure 2.3 shows the breaking load of copper plates. We note that the weld strength decreases when the width is parallel to

excitation, the excitation is in the middle of the plate, and the width of the plate is half of the longitudinal wavelength, and the excitation frequency equals the fundamental frequency of the top plate. This is to be expected since the middle of the plate corresponds to a node position of the fundamental harmonic of a longitudinally vibrating bar and the fundamental mode will not be excited and no motion will be transmitted to the bonding interface. This is clearly shown in Figure 2.3 which shows the break strength of welding of two 0.5 mm thick copper sheets. Note the decrease in weld strength when the width of the top part reaches 86 mm. Copper has a wavelength of 172 mm at 21.5 kHz, as the width of the part increases to $\lambda/2 = 86$ mm, i.e., the dimensions are such that fundamental resonance is not excited which causes a clear decrease in weld strength.

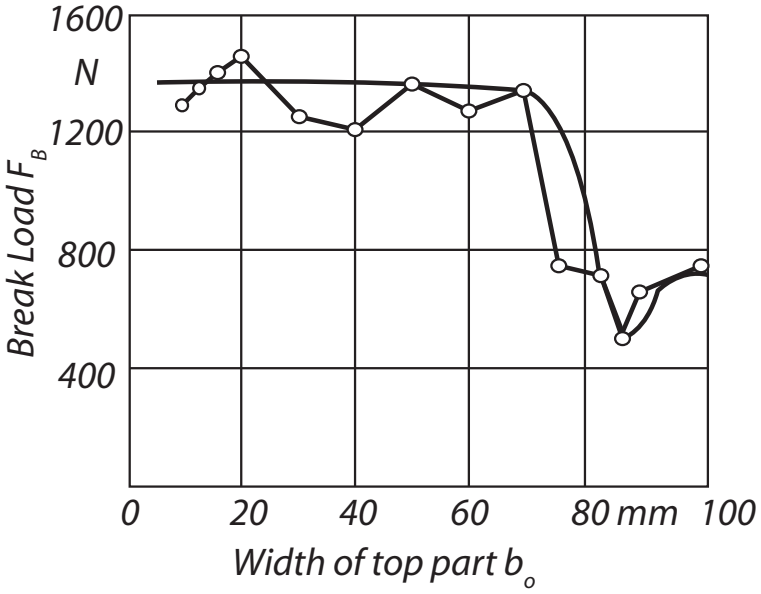

Figure 2.3: Breaking Load Versus Width of Top Part Reproduced from Wodara [42]

Wodara also noted similar trends if the plate is arranged so that its length is parallel to excitation direction. In this case, he performed welds on the edge and not the middle of the plate. The fundamental mode still occurs when the length is $\lambda/2$ and higher harmonics occur when the length is $(2n)\lambda/4$, $(n = 1, 3, 4 \ldots)$. Figure 2.4 shows the failure load as a function of the length of the plate. At these lengths the top part vibrates in resonance and the sonotrode's motion was easily transmitted to the weld interface. If the length of

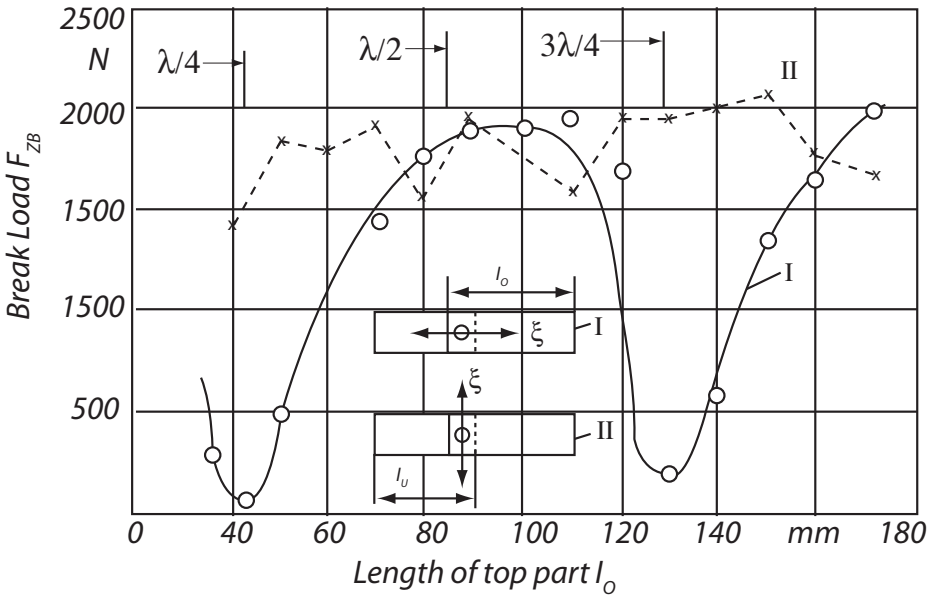

Figure 2.4: Breaking Load Versus Length of Top Part Reproduced from Wodara [42]

the top part is $(2n+1)\lambda/4$, $(n = 1, 3, 4\ldots)$ it offers resistance to the excitation and the oscillation of the sonotrode was insufficiently transmitted to the weld. He also notes that if the vibration direction was rotated 90 degrees so that it acts parallel to width then there is little or no effect on the breaking load.

Finally, Wodara studied the effect location of the welder along the length of the plate on weld strength, Figure 2.5. First, he welded directly at the bonding interface. Next, the welder was placed at a nodal position where no motion was transmitted to the flaying surfaces and the welds were weak. Conversely, welding at antinodes position caused bonds that were comparable in strength to directly welding at the bond interface.

2.4 Parallelepiped Model of Workpiece

The majority of the research in ultrasonic welding focuses on the influence of welding strength by resonances in the top part corresponding to a critical dimension. However, experimental evidence by Solidica, Inc. indicates that bonding degradation is seen at height

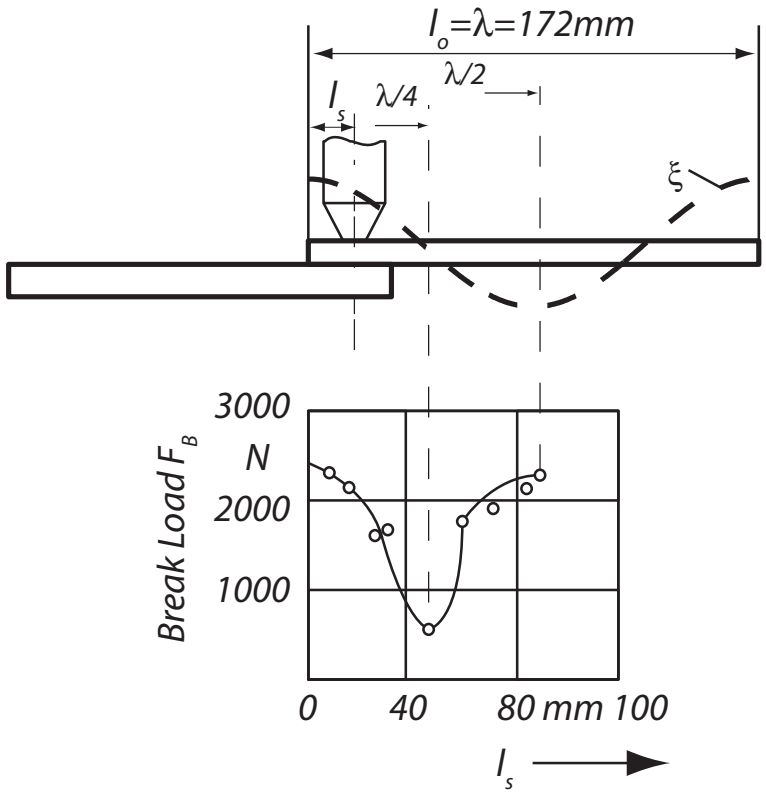

Figure 2.5: Influence on Excitation on Break Load form Wodara [42]

to depth ratio (h/w) of 0.8 while [18] indicates that h/w can be extended to near unity under certain build condition, i.e. normal load, vibration amplitude, specimen orientation and welding speed. This leads to the natural conclusion that the degradation in bonding may be due in increase in vibrations at resonance. We theorize that in the UC process a resonance excitation can lead to fatigue failure due to an increase strain in the build feature. The stack will vibrate with the sonotrode creating little differential motion and force at the bonding interface. Figure 2.6 shows Frequency Response Function (FRF) plot. A FRF can be viewed as a plot of the compliance of a system versus changes in applied forcing frequency. Any force or displacement applied at a frequency close to the natural frequency of the system, i.e., at resonance, will cause the amplitude of vibration of the system to become large. At resonance, the compliance is at a maximum, i.e., the stiffness is

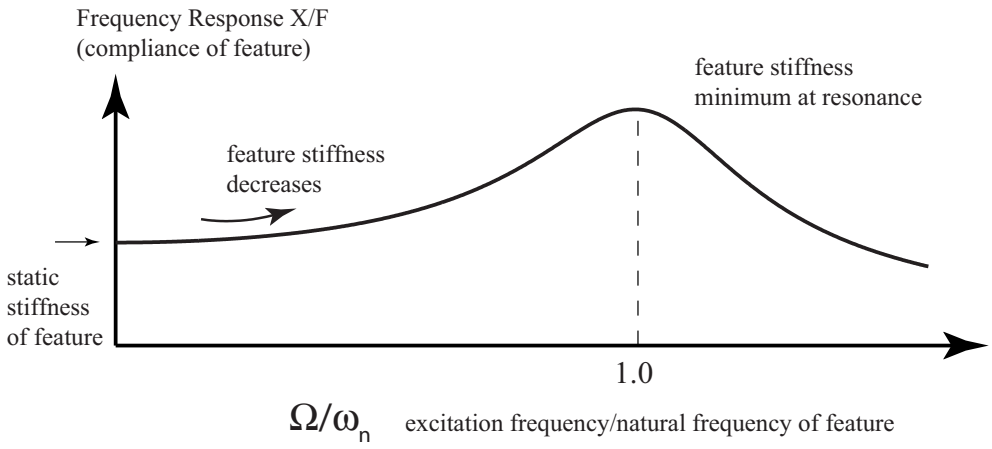

Figure 2.6: Frequency Response Function in Terms of UC Process

at minimum. Past the resonance the system may again become stiff. Specifically, the FRF in Figure 2.6 is for a single degree of freedom oscillator. The features built by UC process are continuous and thus have infinite number of natural frequencies. This lead to regions intermediate regions of stiff and compliant features based on the geometry.

However, before any assertion can be made, the natural frequencies of the bonded stack must be determined. A first estimate in modeling the three-dimensional vibration of the stack is to treat it as a single rectangular parallelepiped whose bottom face is fixed, as seen in Figure 2.7.

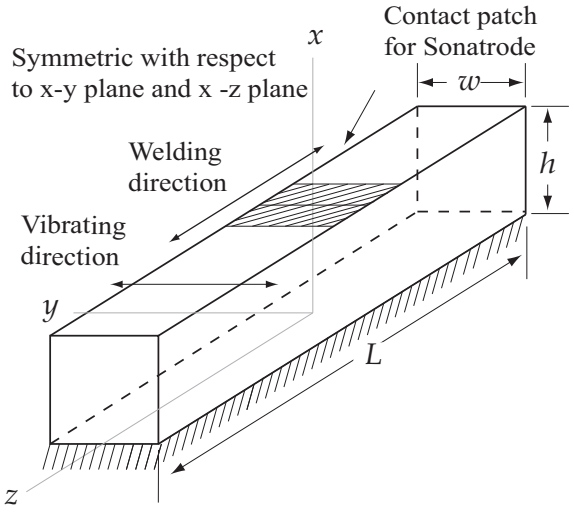

Figure 2.7: Coordinates System and Dimensions of Rectangular Paralleliped

Exact solutions of the free vibrations of three-dimensional finite bodies have received little attention due to their complexity. Usually, a geometric assumption is made on the displacement field that reduces the problem to one or two dimensions, i.e., beam, plate, or rod approximations. The simplification allows one to determine the deformation versus time exactly as a series of sines and cosines depending upon the boundary conditions of the problem. Unfortunately, the parallelepiped has only three sets of boundary conditions that yield exact solutions. The first exact solution corresponds to a parallelepiped that is completely stress free [43]. The second corresponds to a parallelepiped with all faces restrained normally but unrestrained tangentially. In the third solution, the faces of the parallelepiped are restrained tangentially and unrestrained normally. Alternatively, approximate methods have also been used to study the vibrations of three-dimensional finite bodies. Leissa and Zhang [44] later investigated the vibrations of rectangular parallelepiped using the popular energy based Rayleigh-Ritz method. We depart from the work of Leissa and Zhang [44] by using orthogonal polynomials as the basis functions.

Figure 2.7 shows a rectangular parallelepiped of dimensions $h \times w \times L$. The coordinate system lies on the bottom face of the rectangular parallelepiped with the x coordinate normal to the fixed face. We denote the displacements in the x, y, and z directions by u_1, u_2, and u_3, respectively. The block is completely constrained at $x = 0$ and at the fixed face the boundary conditions are

$$u_1(0, y, z, t) = u_2(0, y, z, t) = u_3(0, y, z, t) = 0. \tag{2.3}$$

In the free vibration problem, the remaining faces are stress free.

Following the Rayleigh-Ritz Method to solve the free vibration problem of the parallelepiped, the basis functions for the displacements are simple kinematically admissible polynomials. This allows a displacement field of the form

$$u_i(x, y, z, t) = U_i(\xi, \eta, \zeta) \sin \omega t, \quad i = 1, 2, 3 \tag{2.4}$$

$$U_1 = \sum_{i=1}^{I}\sum_{j=0}^{J}\sum_{k=0}^{K} A_{ijk}\hat{P}_i(\xi)P_j(\eta)P_k(\zeta), \tag{2.5}$$
$$U_2 = \sum_{l=1}^{L}\sum_{m=0}^{M}\sum_{n=0}^{N} B_{lmn}\hat{P}_l(\xi)P_m(\eta)P_n(\zeta),$$
$$U_3 = \sum_{p=1}^{P}\sum_{q=0}^{Q}\sum_{r=0}^{R} C_{pqr}\hat{P}_p(\xi)P_q(\eta)P_r(\zeta)$$

where A_{ijk}, B_{lmn}, C_{pqr} are unknown coefficients, ω is the circular frequency of the response, and the nondimensional coordinates are $\xi = \frac{x}{h}$, $\eta = \frac{y}{w/2}$, and $\zeta = \frac{z}{L/2}$. The polynomiasl $\hat{P}_\kappa$ for $\kappa = i, l, p$ are defined on the interval [0,1] by the Gram-Schmidt process. We begin with

$$\bar{P}_\kappa(\xi) = \xi^\kappa, \quad \kappa = 1 \ldots K. \tag{2.6}$$

The orthogonal polynomials are generated using the following relationship

$$\hat{P}_\kappa = \bar{P}_\kappa(\xi) - \sum_{t=1}^{\kappa-1} \frac{\langle \bar{P}_\kappa(\xi), \hat{P}_t(\xi)\rangle}{\langle \hat{P}_t(\xi), \hat{P}_t(\xi)\rangle}\hat{P}_\kappa(\xi) \tag{2.7}$$

where

$$\langle \bar{P}_\kappa(\xi), \hat{P}_t(\xi)\rangle = \int_0^1 \bar{P}_\kappa(\xi)\hat{P}_t(\xi)d\xi, \tag{2.8}$$
$$\langle \hat{P}_t(\xi), \hat{P}_t(\xi)\rangle = \int_0^1 \hat{P}_t(\xi)\hat{P}_t(\xi)d\xi, \tag{2.9}$$

and the resulting polynomials satisfy the orthogonal condition

$$\int_0^1 \hat{P}_i(\xi)\hat{P}_j(\xi)d\xi = \frac{1}{2j+1}\delta_{ij} \tag{2.10}$$

This choice of polynomials automatically satisfies Equation 2.3 since the summation on $\hat{P}_\kappa$ for $\kappa = i, l, p$ begins at 1, while the other coordinates begin with zero. The polynomials P_κ for $\kappa = j, k$, $\kappa = m, n$ and $\kappa = p, r$ are the Legendre Polynomials on the interval $[-1, 1]$ and

they satisfy the orthogonal condition

$$\int_0^1 P_i(\xi)P_j(\xi)d\xi = \frac{2}{2j+1}\delta_{ij} \tag{2.11}$$

The total energy of the parallelepiped is defined by

$$\Pi = T - V \tag{2.12}$$

where T and V are the kinetic energy and strain energy of the block, respectively. They are defined by

$$T = \frac{\rho\omega^2}{2}\int_{-1}^{1}\int_{-1}^{1}\int_{0}^{1}\left(\sum_{i=1}^{3}U_i^2\right)d\xi d\eta d\zeta, \quad \text{and} \quad V = \frac{1}{2}\int_{-1}^{1}\int_{-1}^{1}\int_{0}^{1}\left(\sum_{i=1}^{3}\sum_{j=1}^{3}\sigma_{ij}\epsilon_{ij}\right)d\xi d\eta d\zeta. \tag{2.13}$$

The constitutive relationships between the stresses and strains are

$$\sigma_{ij} = \lambda e + 2\delta_{ij}G\epsilon_{ij}, \quad i,j = 1,2,3, \tag{2.14}$$

where e is the volume dilation, λ and G(shear modulus) are the Lamé constants and ν is Poisson's ratio

$$e = \sum_{i=1}^{3}\epsilon_{ii}, \quad \lambda = \frac{\nu E}{(1+\nu)(1-2\nu)}, \quad G = \frac{E}{2(1+\nu)}. \tag{2.15}$$

The stresses are related to the displacements by

$$\epsilon_{ij} = \frac{1}{2}\left[\frac{\partial u_i}{\partial x_j} + \frac{\partial u_j}{\partial x_i}\right]. \tag{2.16}$$

Minimizing the total energy of the rectangular parallelepiped yields

$$\delta\Pi = \frac{\partial\Pi}{\partial A_{ijk}}\delta A_{ijk} + \frac{\partial\Pi}{\partial B_{lmn}}\delta B_{lmn} + \frac{\partial\Pi}{\partial C_{pqr}}\delta C_{pqr} = 0. \tag{2.17}$$

Equation 2.17 must be true for all arbitrary variations δA_{ijk}, δB_{lmn}, δC_{pqr} This implies

that the following is true

$$\frac{\partial \Pi}{\partial A_{ijk}} = 0, \quad \frac{\partial \Pi}{\partial B_{lmn}} = 0, \quad \text{and} \quad \frac{\partial \Pi}{\partial C_{pqr}} = 0 \tag{2.18}$$

and leads to the homogeneous equation of motion

$$\left(\begin{bmatrix} \boldsymbol{K}_{11} & \boldsymbol{K}_{12} & \boldsymbol{K}_{13} \\ & \boldsymbol{K}_{22} & \boldsymbol{K}_{23} \\ \text{symmetric} & & \boldsymbol{K}_{33} \end{bmatrix} - \omega^2 \begin{bmatrix} \boldsymbol{M}_{11} & 0 & 0 \\ & \boldsymbol{M}_{22} & 0 \\ \text{symmetric} & & \boldsymbol{M}_{33} \end{bmatrix} \right) \begin{Bmatrix} \{\boldsymbol{A}\} \\ \{\boldsymbol{B}\} \\ \{\boldsymbol{C}\} \end{Bmatrix} = \begin{Bmatrix} 0 \\ 0 \\ 0 \end{Bmatrix} \tag{2.19}$$

each $\boldsymbol{K}_{ij}$ and $\boldsymbol{M}_{ij}$ are symmetric stiffness and mass matrixes, respectively. Equation 2.19 yields a set of $I(J+1)(K+1) + L(M+1)(N+1) + P(Q+1)(R+1)$ equations. We seek nontrivial solution of this system by setting the determinant of the coefficient matrix to zero we find eigenvalues and eigenvectors. The eigenvectors and eigenvalues in turn yield natural frequencies and mode shapes.

The Ritz based approach allows the separation of the mode shapes based on the choice of basis functions. The rectangular parallelepiped has two symmetry planes; the x-z plane and the x-y plane. This allows the modes to be separated into four classes. Fromme and Leissa identify the classes based on the shape of the axial displacement (U_1), i.e., whether U_1 is symmetric (S) or antisymmetric (A) about the x-z plane and the x-y plane. We refer to combinations as SS (symmetric symmetric), SA (symmetric anti-symmetric), and AS(antisymmetric symmetric). The symmetry classes utilize even or odd powers of η and ζ. However, ξ is expanded in all terms. Table 2.1 summarizes the symmetry classes and the appropriate powers of the polynomials. Due to the nature of excitation the SS modes are the most likely to be excited by the sonotrode. In addition, these modes do not change with the changes in the length of the specimen.

Table 2.1: Powers of η and ζ for Symmetry Classes

Class	U_1	U_2	U_3
SS	j = even, k = even	m = odd n = even	q = even, r = odd
SA	j = even, k = odd	m = odd, n = odd	q = even, r = even
AS	j = odd, k = even	m = even, n = even	q = odd , r = odd
AA	j = odd, k = odd	m = even, n = odd	q = odd , r = even

2.5 Experimental Validation

Typically, the measurement of vibrations of an elastic body with natural frequencies in the kilohertz range involves the use of ultrasonic transducers, or a specialized impact hammer. Excitement of high frequencies by an impact requires a hard contacting surface, small mass, and a small duration of impact. We use an alternative to the traditional approaches: the samples are impacted by a carbide ball bearing. The method although simple provides a short impact time coupled with the hardness of the carbide ball, which allows the system to be excited at frequencies in the kilohertz range. The simplicity and high excitation frequency come with a tradeoff; we cannot measure the time history of the force input and thus are unable to use to determine mode shapes of the build specimen. The test setup for the vibration test is shown in Figure 2.8. Samples were machined from

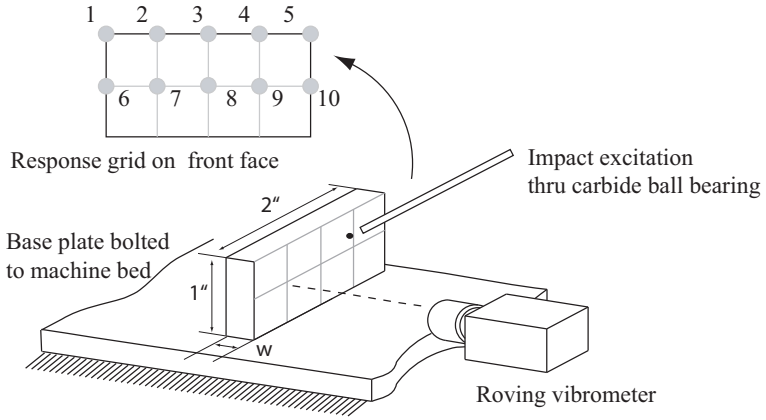

Figure 2.8: Test Setup for Verification of Parallelepiped Model

a slab of 50mm thick consolidated Al 3003 H-18 and wrought Al 6061. Wrought Al 6061

was used since Al 3003 H-18 is only available in plates or tapes. Each of the rectangular test features was 2.5 in. (63.5 mm) long by 1 in. (25.4 mm) high. Three samples of each of the following wdiths: 1/8 in. (3.175 mm), 1/4 in. (6.35 mm), 1/2 in. (12.7 mm), and 1in. (25.4 mm). Slots were left behind each feature Fig 2.8 for possible tests with filler materials at a later time. Figures 2.9 and 2.10 plots the auto spectrum of the response for points 1 and 2 with the predicted natural frequencies of the specimen of dimensions 2.5 in. x 1 in. x 1/4 in.

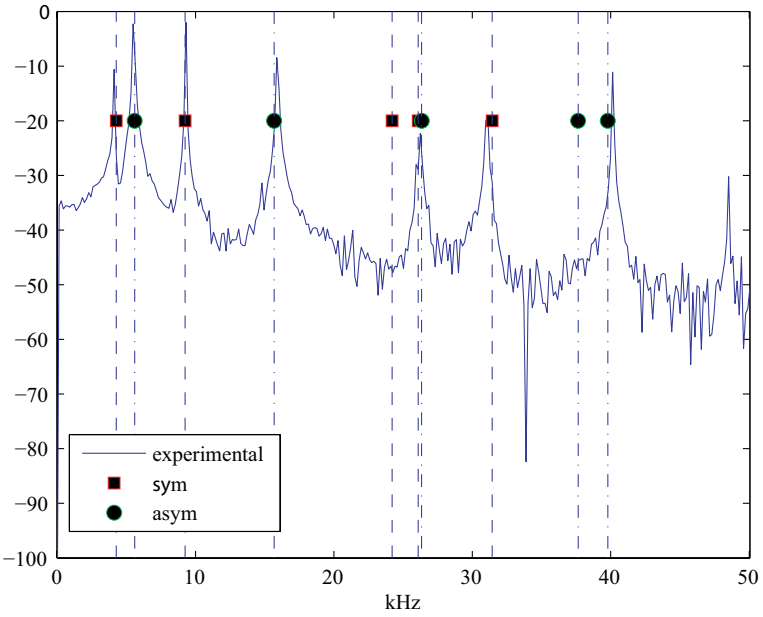

Figure 2.9: Autospectrum at Response Point 1 of 1 in. × 1/8 in. × 2.5 in. Al Sample

Table 2.2 summarizes the results of these tests. As expected the Rayleigh-Ritz Model captures the behavior of the wrought specimen accurately at all the tested dimensions; the maximum difference between the analytical model and experimental being on the order of 1 kHz. Both the Ritz model and the wrought specimen are stiffer than the laminate specimens.

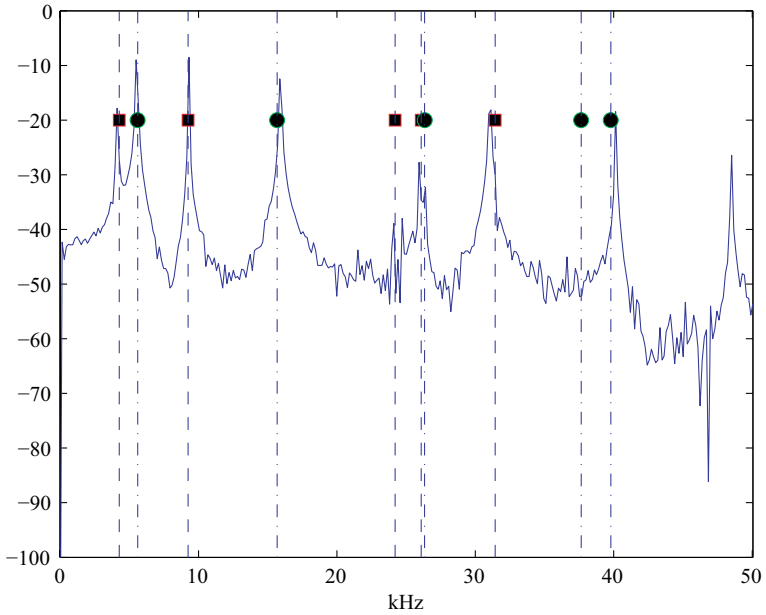

Figure 2.10: Autospectrum at Response Point 1 of 1 in. × 1/8 in. × 2.5 in. Al Sample

Table 2.2: Geometry and Natural Frequency for Wrought and Laminate Specimens

Width	Mode	Frequency (kHz)			
		Analysis	Wrought	Laminate	Difference[1]
1/8 in.(3.175 mm)	1	4.15	4.27	3.45	0.82
	2	5.49	5.61	4.72	0.89
	3	9.31	9.24	8.31	0.93
	4	15.9	15.7	14.8	0.9
	5	24.1	24.2	-	-
	6	26.28	26.33	-	-
1/4 in.(6.35 mm)	1	8.24	8.23	6	2.23
	2	10.58	10.1	8.5	1.6
	3	16.9	16.8	14.78	2.02
	4	27.0	27.0	25.5	1.5

2.6 Observation from Model of Build Feature

Figures 2.11(a) and 2.12(a) show contours of constant natural frequency of the first AS and SA modes for a nominally oriented build feature alone due to changes in height and width. In the plots, we restrict our attention to features with a length to width ratio of ten. The contour plots also contain lines of constant aspect ratio. Figure 2.11(b) and Figure 2.12(b) also show the corresponding deformation shapes of these modes. The frequencies of the sample with widths of 23.8 mm, the nominal tape width used in the UC process, for both AS and AA modes, are both roughly 25 kHz which is close to the 20 kHz excitation frequency of the sonotrode. This, in part, may explain the persistent wave shapes observed by [37] at this width. However, for other widths, the frequency of the features with an h/w of one is much higher than the frequency of the sonotrode. A trend emerges if we view the contour plots of Figures 2.11(a) and 2.12(a) in conjunction with Figure 2.6 We note that at low build height, for all widths, the natural frequencies are much higher than the sonotrode's frequency. In terms of a frequency response plot, the frequencies of the feature are greater than the operating frequencies of the sonotrode placing the response to the left of the resonance of a FRF. As the height of the features increases its natural frequency decreases and approaches the excitation frequency of the sonotrode. Features built at all widths see increases in compliance as the build height increases. The features built at the nominal tape width are closer to resonance and are likely to see a greater increase in compliance.

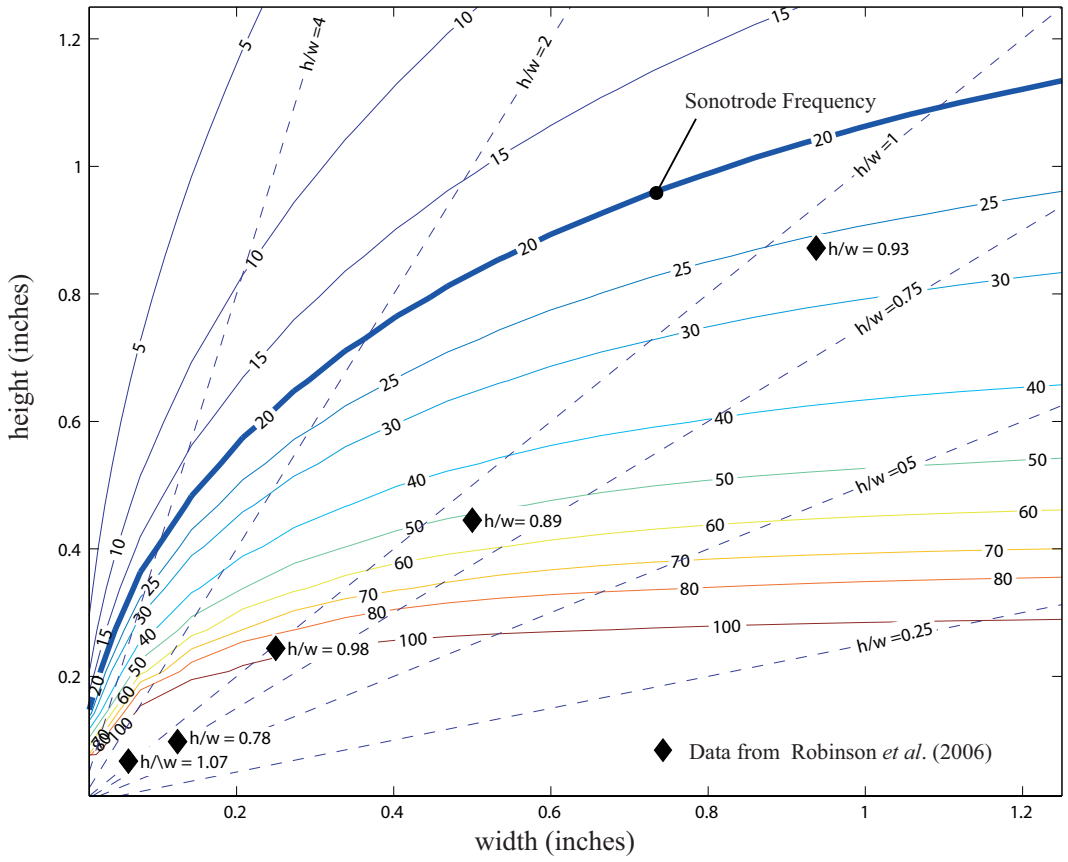

(a)

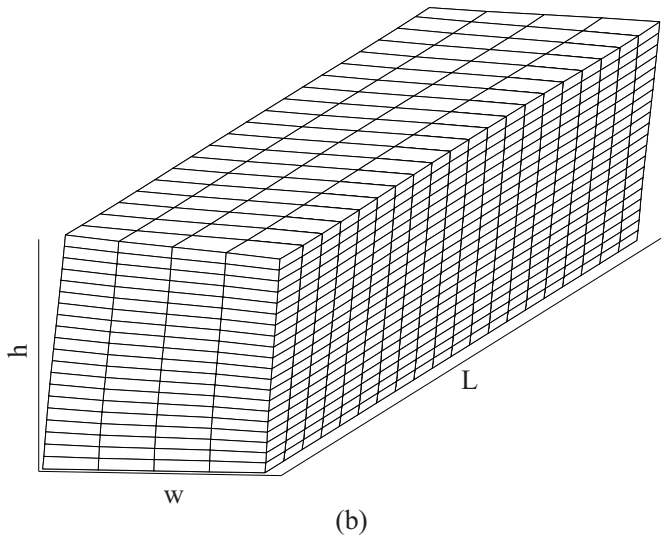

(b)

Figure 2.11: Contours of First AS Mode Frequency vs. Height and Depth of Build Piece, b) First AS Mode Shape h=w=0.9375 inches, L = 2.5 inches

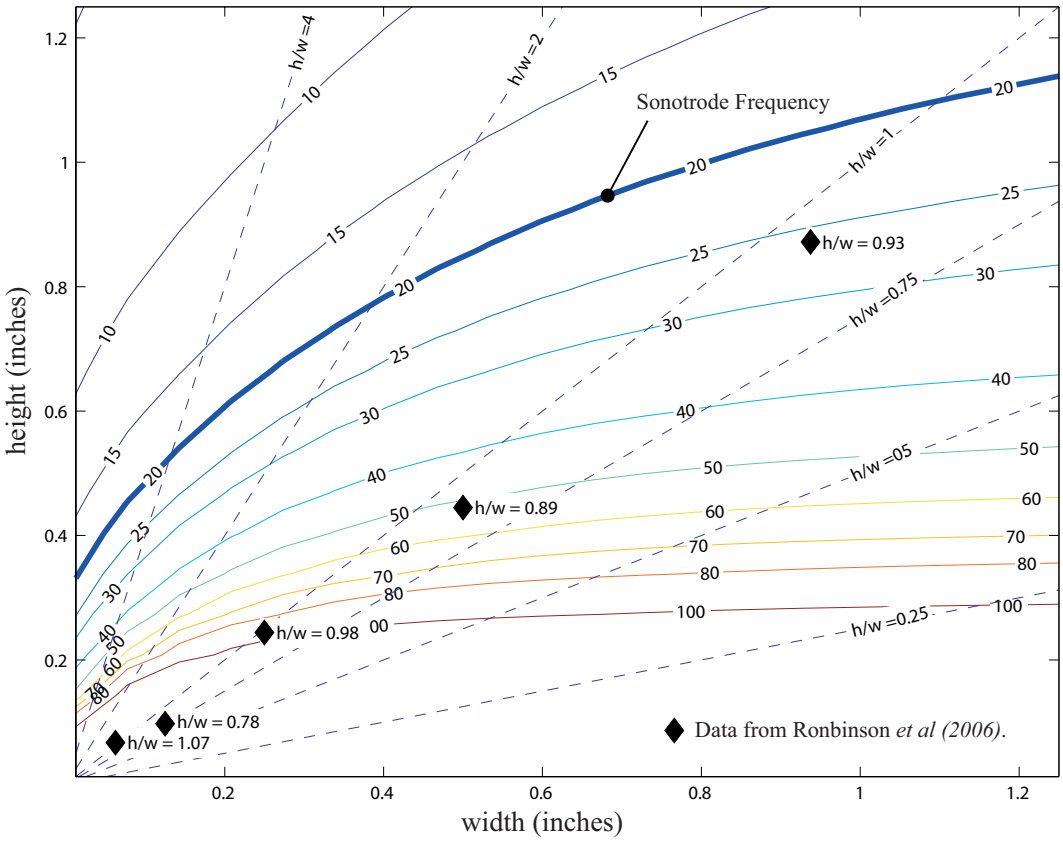

(a)

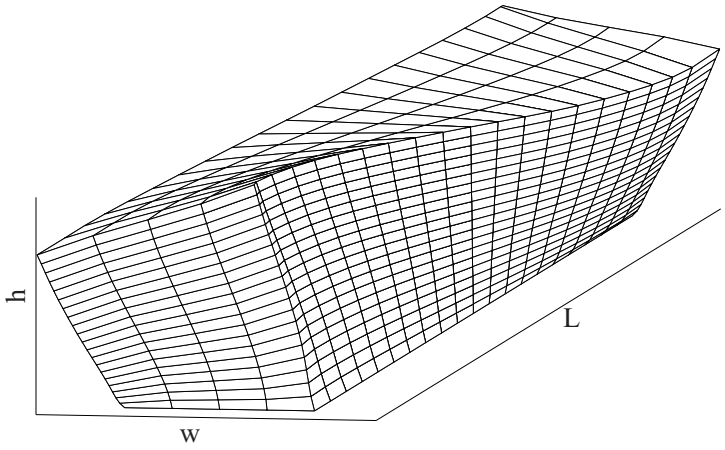

(b)

Figure 2.12: a) Contours of First AA Mode Frequency vs. Height and Depth of Build Piece, b) First AA Mode Shape h=w=0.9375 inches, L = 2.5 inches

Figures 2.13 (a) and 2.13 (b) show that at the nominal tape dimensions the natural frequency is weakly dependent on the length. However, these results do not indicate a lower limit on stiffness or upper limit on compliance necessary for bonding, i.e., at what point on the FRF does bonding degrade. In the next, chapter we formulate models to explore this limit on compliance and its affect on friction at the bonding interface.

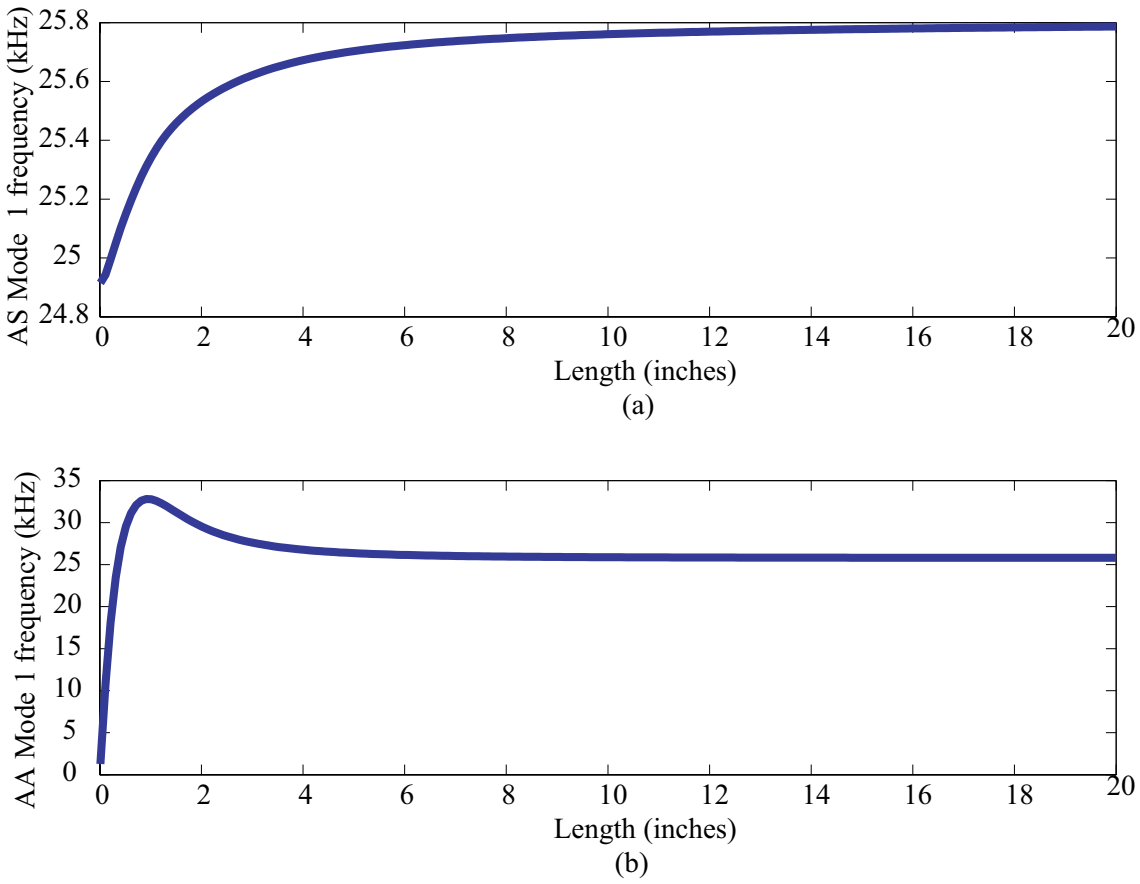

Figure 2.13: Length Independence of AS and AA Modes of Build Feature for $h = w = 0.9375$ inches

2.7 Temperature Effects

Zhang and Li [1] note that as the build piece is heated up to 300 °F the modulus drops to 45% of its nominal value, Table 2.3. The drop in modulus shifts the modal curves seen in Figure 2.14. A closer examination shows that for both the AS and SS modes at the

nominal tape width we see that primary natural frequencies of the build feature reduces to 20 Khz before the build height increase for widths of 0.75 inches and larger. We note that the nominal values reported in [1] are relatively low.

Table 2.3: Temperature-Dependent Mechanical Properties of AL 3003-H18 [1]

Temp. (°C)	Modulus of Elasticity (GPa)	Yield Strength (MPa
25	53.2	277.3
50	28.8	197.3
100	26.8	131.2
150	22.7	70.0
200	16.9	68.3
250	16.4	32.9
300	14.5	29.0
350	13.3	26.5

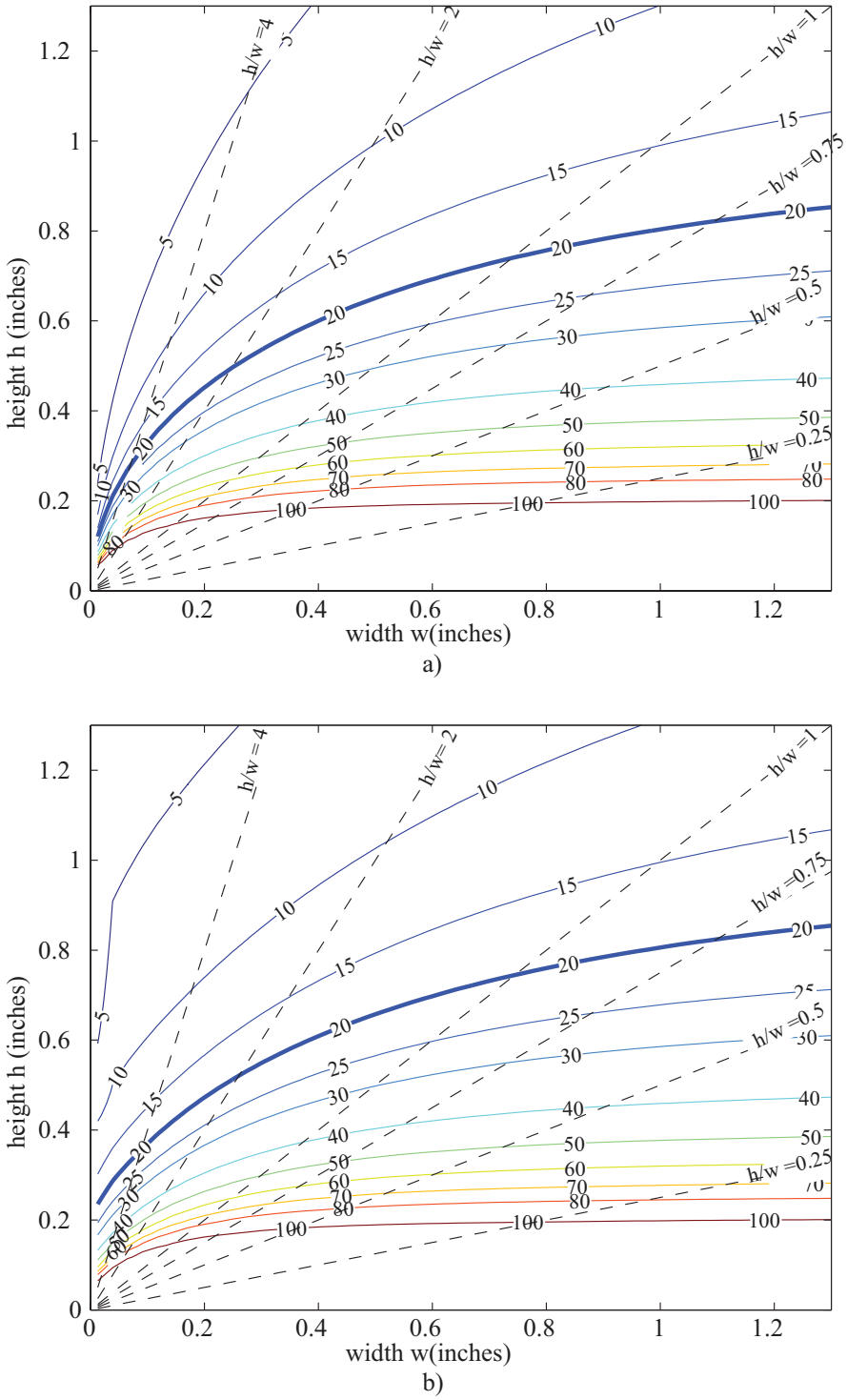

Figure 2.14: Contours First AS and SS Modes with a 45% Reduction in Modulus a) AS Mode, b) AA Mode

2.8 Secondary Modal Interactions

We focused on the first two modes of the parallelepiped for two reasons: first, the AS mode has no nodal region and will likely be excited regardless of the location by an excitation in the vicinity of the natural frequency. Similarly, the first AA mode has only one nodal region and thus for most of the process may also be excited. In practice other modes may be excited during the UC process depending upon the location of the sonotrode along the workpiece. Figure 2.15 shows the next three modes at $h = w = 0.9375$ inches, and $L = 2.5$ inches, i.e., at the problematic region of bonding degradation.

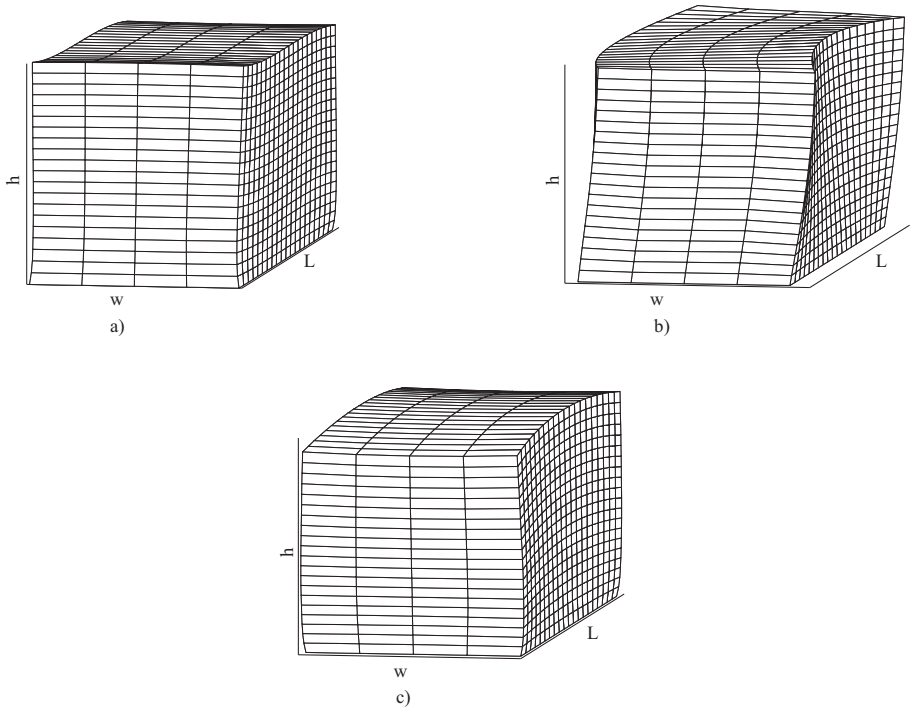

Figure 2.15: Third, Fourth and Fifth Modes for $h = w = 0.9375$ inches, $L = 2.5$ inches a) Third, b) Fourth c) Fifth

Solving the eigenvalue problem with the nominal properties of 3003 Aluminum at room temperature and search for the nearest natural frequencies in a 5 KHz radius of the sonotrode excitation we obtain a "Mode" Map of likely excited frequencies of the parallelepiped at the nominal temperature (Figure 2.16). The radius of 5 KHz was chosen arbitrarily. Length does not significantly change these results. For build features of widths

of 0.5 inches, the 20 kHz excitation excites the third natural frequency of the feature as the height approaches four times the width of the feature. Interestingly, at the nominal feature width and as the height increases we see regions where the excitation will not excite any mode. There are several implications of these observations. First, there may be more than one apparent limit on build height for high aspect ratio features and secondly, for the nominal width, once a certain critical height is passed there is no practical limit on build height. However, if we construct the mode map using the reduced modulus; the large region of no modal interaction disappear. However, for high aspect ratio features, i.e., h/w of two or greater the closest natural frequencies are near the fifth mode and higher. We must note that care must be taken in extrapolating any conclusions from these plots. They leave out three pieces of information: the modeshape, the presence of other modes in the search radius, and the exact difference between the closest mode and the sonotrode's excitation frequency. However, they provide a simple tool to examine possible modal interactions versus changes in geometry. Despite their shortfalls we will use them in Chapter 4 as a guide in producing test specimens.

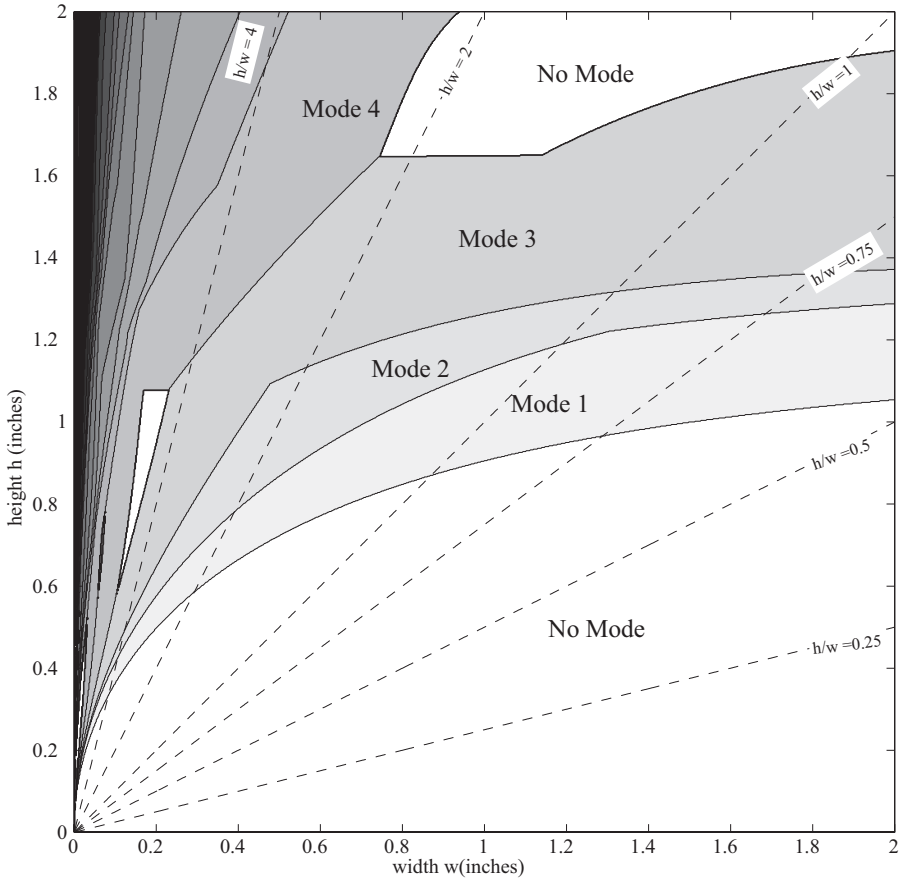

Figure 2.16: Map of Modes in a 5 kHz radius of the Excitation Frequency of the Sonotrode at Nominal Modulus

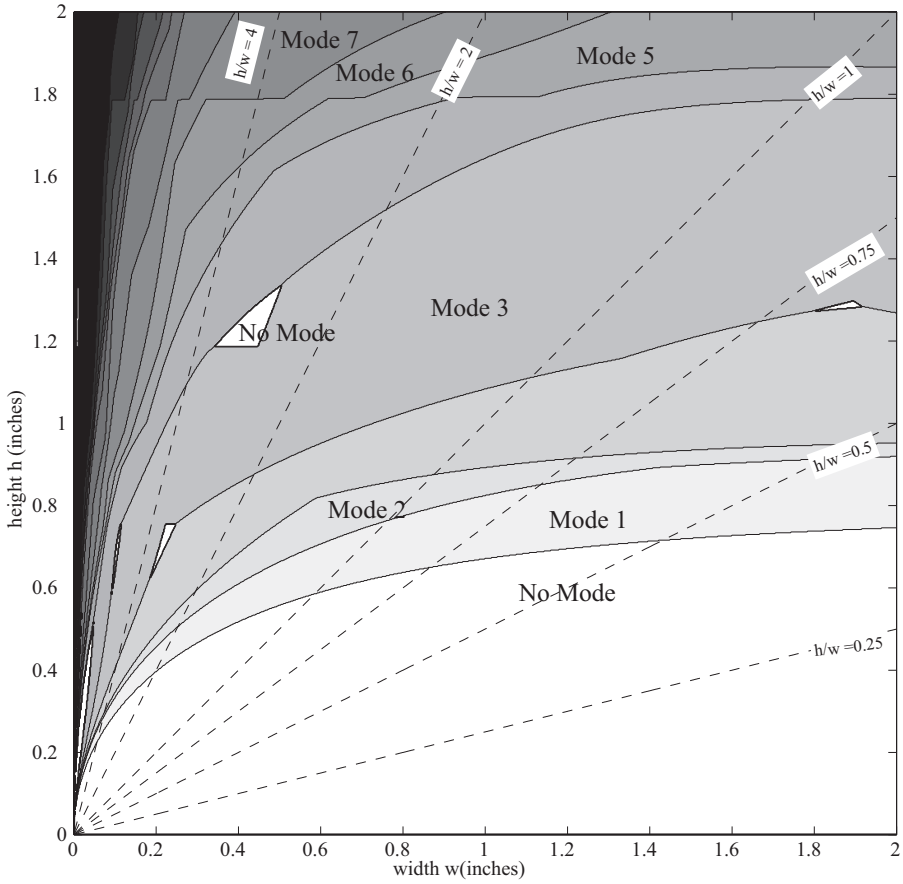

Figure 2.17: Map of Modes in a 5 kHz radius of the Excitation Frequency of the Sonotrode at Reduced Modulus

2.9 Modeling The Forced Vibration Problem

In this section, we present a model to explore the response of the parallelepiped to moving and vibrating sonotrode. We make several assumption in modeling the forced vibration problem. First, that the stress at the interface is below the limiting frictional stress and sinusoidal. Second, the sonotrode is represented as two moving loads of the form

$$P(x, y, z) = p(x, y, z)S(z) \tag{2.20}$$

$$Q(x, y, z) = q(x, y, z)S(z) \sin \Omega t \tag{2.21}$$

where $S(z)$ is defined as

$$S(z) = H_1(z - vt) - H_2(z - 2w_c - vt), \tag{2.22}$$

v is the rolling speed of the sonotrode, the functions H_i for $i = 1, 2$ are heaviside step functions defined generally as

$$H(z - a) = \begin{cases} 0, & \text{for } z < a \\ 1, & \text{for } z > a \end{cases} \tag{2.23}$$

and the point a is arbitrary. The variable w_c is the half width of the contact patch. We obtain the loads $p(x, y, z)$, $q(x, y, z)$ and the width of the contact patch, w_c, from a Hertzian Line Contact [45] analysis. The load $p(x, y, z)$ is defined using the average contact stress

$$p_m = \frac{P}{2w_c}, \tag{2.24}$$

where P is the applied normal load. The half width of the contact patch is

$$w_c^2 = \frac{PR}{\pi E^*} \tag{2.25}$$

The effective modulus E^* is defined by

$$\frac{1}{E^*} = \frac{1-\nu_{Ti}^2}{E_{Ti}} + \frac{1-\nu_{Al}^2}{E_{Al}} \tag{2.26}$$

In order to simulate the effects of a moving, vibrating load, we write the loads in the non-dimensional coordinate system and modify the total potential energy, Equation 2.12 to

$$\Pi_m = \Pi + \int_{-1}^{1}\int_{\zeta_2}^{\zeta_1} P(\xi,\eta,\zeta)U_1 d\eta d\zeta + \int_{-1}^{1}\int_{\zeta_2}^{\zeta_1} Q(\xi,\eta,\zeta)U_2 d\eta d\zeta \tag{2.27}$$

and the taking the variation for all δA_{ijk}, δB_{lmn}, δC_{pqr} coefficients yields the following set of equations

$$\begin{bmatrix} \boldsymbol{M}_{11} & 0 & 0 \\ & \boldsymbol{M}_{22} & 0 \\ \text{symmetric} & & \boldsymbol{M}_{33} \end{bmatrix} \begin{Bmatrix} \{\dot{\boldsymbol{A}}\} \\ \{\dot{\boldsymbol{B}}\} \\ \{\dot{\boldsymbol{C}}\} \end{Bmatrix} + \begin{bmatrix} \boldsymbol{K}_{11} & \boldsymbol{K}_{12} & \boldsymbol{K}_{13} \\ & \boldsymbol{K}_{22} & \boldsymbol{K}_{23} \\ \text{symmetric} & & \boldsymbol{K}_{33} \end{bmatrix} \begin{Bmatrix} \{\boldsymbol{A}\} \\ \{\boldsymbol{B}\} \\ \{\boldsymbol{C}\} \end{Bmatrix} = \tag{2.28}$$

$$\begin{Bmatrix} \{\boldsymbol{F_1}\} \\ \{\boldsymbol{F_2}\} \\ \{\boldsymbol{F_3}\} \end{Bmatrix}, \tag{2.29}$$

where the vector $\boldsymbol{F_i}$ is the force vector due to the moving load. In turn we write the equations of motion in state space form and simulate using Adam's Method [46]. We use a modulus reduced by 45% from it's nominal value of 10.6×10^6 ksi, a normal load of 315 lbs, rolling speed of 100 in./min, and a modulus of the titanium Sonotrode f 15.7×10^6 ksi, . Figure 2.18 shows the velocity of a point along the outer face that is directly beneath the contact patch for three geometries each having a width of 0.9375 inches and a length of 2.5 inches, while the height varied from 0.5 inches, to 0.9375 inches and to 2.0 inches. There is a clear indication from the plots that the response of the build feature increases as $h = w = 0.9375$ inches and decreases when $h = 2.0$ inches. This is indicative of the response one would expect due to a resonance excitation. Furthermore, we note a spatial

component to the compliance. In the specimens of height of 0.5 and 0.9375 inches the feature is substantially stiffer in the middle of its length. This is not true for the specimen of height 2.0 inches. It's minimum compliance occurs at roughly 0.1 seconds of travel time or at 1/5 of its length.

2.10 Summary

In this chapter, we focused on whether the system was excited near a resonance and due to a purely harmonic force. However, being excited at a resonance in itself does not provide a mechanism for bonding degradation. While a feature excited near a resonance will be susceptible to fatigue of previous bonded layers. Furthermore it is unlikely that one will ever excite the build feature exactly at a natural frequency. Thus we need a model that preserves the observation of no bonding at resonance but allows us to understand how close to resonance must the excitation be before bonding degradation occurs. In the next section, we will formulate a model whose underlying assumption is that bonding depends directly on differential motion and the amount of friction at the interface. This model will be used to to study how changes is substrate geometry affect differential motion.

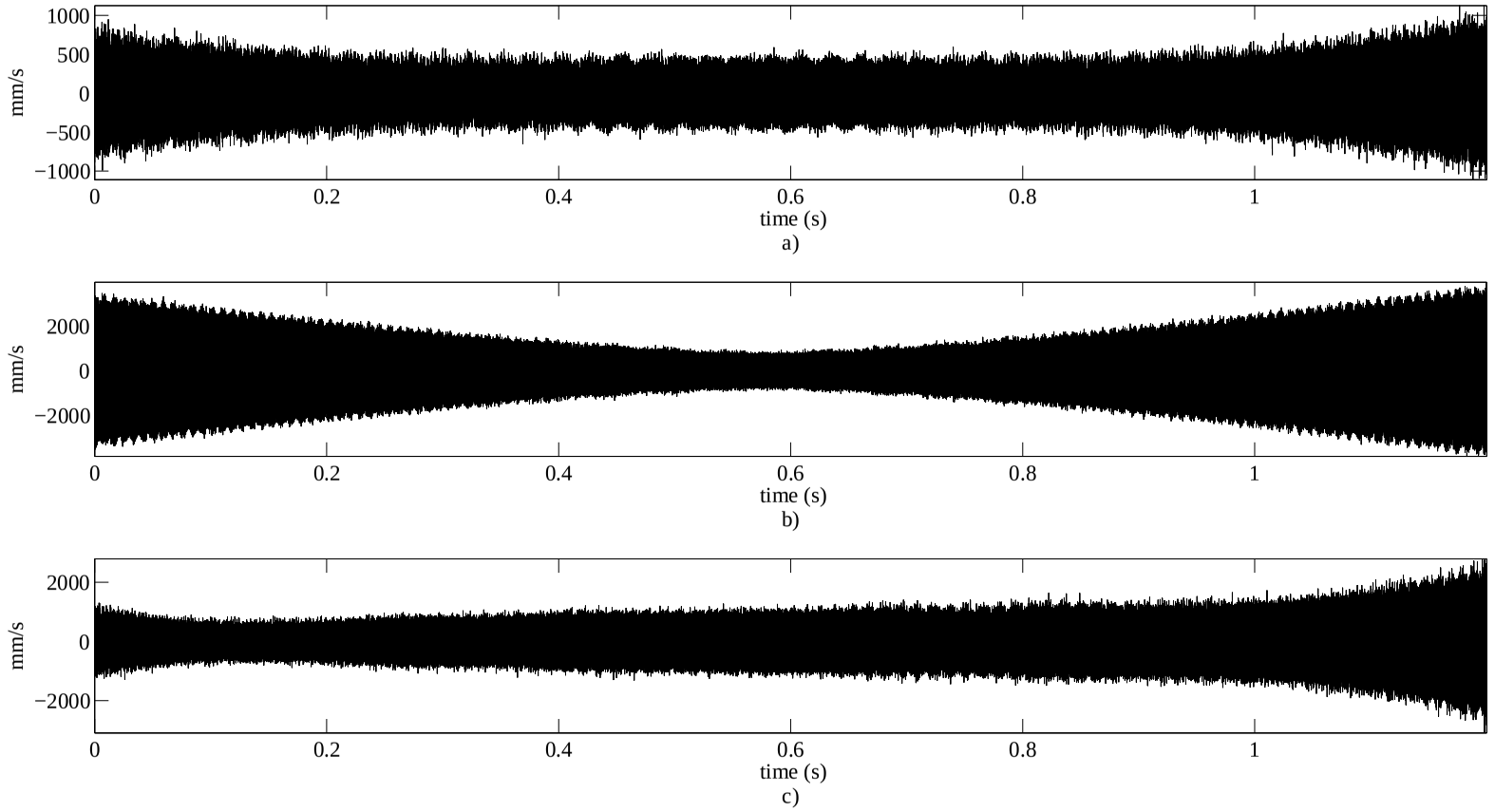

Figure 2.18: Plot of Lateral Velocity Beneath the Contact Patch for specimens with $L = 2.5$ inches, $w = 0.9375$ inches and a) $h = 0.5$ inches, b) $h = 0.9375$ inches, and d) $h = 2.0$ inches

Chapter 3

Lumped-Parameter Model of the UC Process

Previously, we explored the possibility of a resonance excitation of the standard build features of the UC process. In this chapter, we present a phenomological approach to explain how resonance affects the bonding process and explain how both the transverse force and differential motion changes as the height of the build piece increases, i.e., the stiffness decreases. Ultimately, the goal is to determine the necessary feature stiffness for bond formation. The underlying premise of this investigation is that the UC process not only requires differential motion, but a certain minimum level of stress, that causes plastic deformation at the layer feature interface to begin the bonding process [18, 36, 47]. This state of stress is a function of the normal and tangential forces between the bonding layer and build piece. Assuming Coulomb friction describes the interaction between the layers, the tangential force transmitted to the build piece is either the force needed to prevent slipping, the break away force at the transition from stick to slip, or the friction force in slip. The value of the transverse force is a function of the material's coefficient of friction, the normal load, the build piece's mass and stiffness (modulus and geometry). The minimum value of the force of friction must be enough to cause plastic deformation. This paper adopts a nonlinear dynamics approach to explaining this phenomenon. It is based on the reduction

of the build feature to a single-degree-of freedom oscillator. We utilize a stick slip model of Coulomb friction to simulate the interactions between a bonding tape and the build feature.

3.1 Simple Model

Figure 3.1 presents the proposed model. The model focuses solely on the dynamics of the system as the substrate stiffness decreases. Neglected are the effects of heat, and acoustic softening. The model consists of a tape with mass m_t and m_{eff} the modal mass of the feature. A linear spring k_{eff} represents the modal stiffness of the workpiece. We assume no slipping between the sonotrode and bonding tape. Thus the tape's position is enforced as $Y \sin \Omega t$. We also assume that the material behaves linearly. In addition we assume that material losses are negligible and the sonotrode's excitation frequency is constant. The latter assumption is made to simplify the dynamics. In practice, the sontrode's control system adjusts the frequency using a phase lock loop algorithm. The Coulomb friction

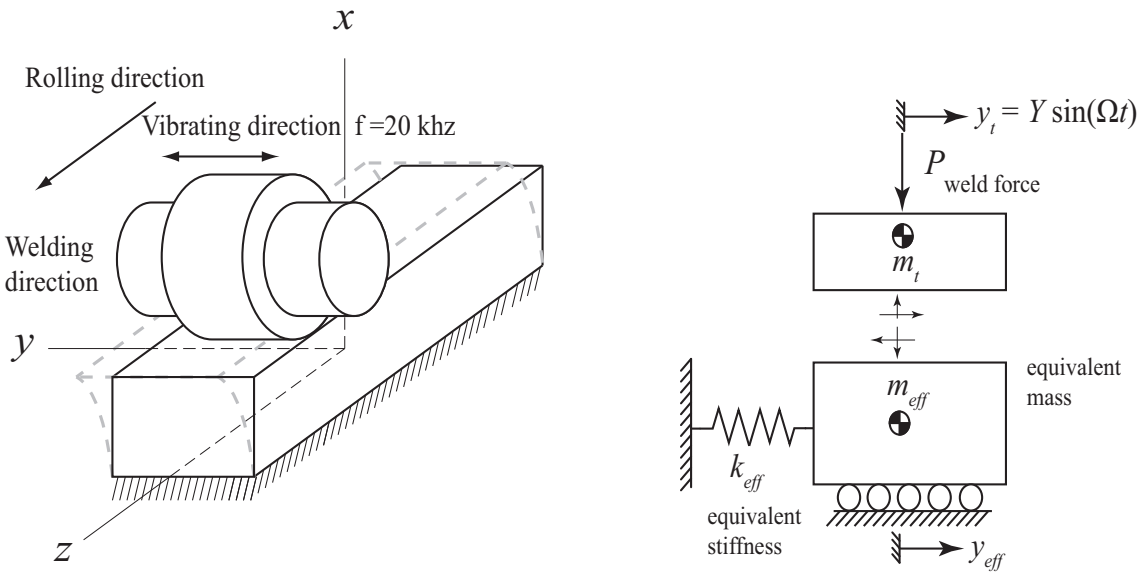

Figure 3.1: Bending Mode of the Build Piece and the Mass-Spring Approximation

based interaction between the layer and the feature is represented using a switch based

model where the resulting equations of motion are in non-dimensional form:

if $|\dot{y}_r| \geq 0$ slip

$$\ddot{\hat{y}}_r = -\frac{\hat{y}_r}{\alpha^2} + \left(1 - \frac{1}{\alpha^2}\right)\sin\tau - \frac{\gamma}{\alpha^2}\beta\text{sign}(\dot{\hat{y}}_r) \tag{3.1}$$

else

if $\left|\frac{\hat{y}_r}{\alpha^2} + \left(\frac{1}{\alpha^2} - 1\right)\sin\tau\right| > \frac{\gamma}{\alpha^2}$ stick-slip transition

$$\ddot{\hat{y}}_r = -\frac{\hat{y}_r}{\alpha^2} + \left(1 - \frac{1}{\alpha^2}\right)\sin\tau - \frac{\gamma}{\alpha^2}\text{sign}\left(\frac{\hat{y}_r}{\alpha^2} + \left(\frac{1}{\alpha^2} - 1\right)\sin\tau\right) \tag{3.2}$$

else $\left|\frac{\hat{y}_r}{\alpha^2} + \left(\frac{1}{\alpha^2} - 1\right)\sin\tau\right| \leq \frac{\gamma}{\alpha^2}$ stick

$$\ddot{\hat{y}}_r = 0 \tag{3.3}$$

end

where

$\omega_e^2 = \frac{k_{eff}}{m_{eff}}$: the first natural frequency of the parallelepiped in bending,

$\alpha = \frac{\Omega}{\omega_{eff}}$: ratio of the forcing frequency to the natural frequency,

$\gamma = \frac{\mu_s P}{k_{eff} Y}$: slip parameter,

$\beta = \frac{\mu_k}{\mu_s}$: ratio of static coefficient to kinetic coefficient of friction ,

$\tau = \Omega t$: non-dimensional time,

$y_r = y_{eff} - y_t$,: relative position between tape and feature,

$\hat{y}_r = \frac{y_r}{Y}$: non-dimensional relative position,

$\frac{d\hat{y}_r}{d\tau} = \dot{\hat{y}}_r$: non-dimensional velocity,

$\frac{d^2\hat{y}_r}{d\tau^2} = \ddot{\hat{y}}_r$: non-dimensional acceleration.

The non-dimensional force of friction takes on the following values:

$$F_{\text{slip}} = -\frac{\gamma}{\alpha^2}\beta \text{sign}(\dot{\hat{y}}_r), \tag{3.4}$$

$$F_{\text{stick slip}} = \frac{\gamma}{\alpha^2}\text{sign}\left(\frac{\hat{y}_r}{\alpha^2} + \left(\frac{1}{\alpha^2} - 1\right)\sin\tau\right), \tag{3.5}$$

$$F_{\text{stick}} = \frac{\hat{y}_r}{\alpha^2} + \left(\frac{1}{\alpha^2} - 1\right)\sin\tau. \tag{3.6}$$

The stick condition

$$\left|\frac{\hat{y}_r}{\alpha^2} + \left(\frac{1}{\alpha^2} - 1\right)\sin\tau\right| \leq \frac{\gamma}{\alpha^2} \tag{3.7}$$

can be used to derive a relationship that separates the regions of stick and stick-slip motion

$$\left|\frac{1-\alpha^2}{\gamma}\right| \leq 1. \tag{3.8}$$

In terms of physical parameters this relationship is

$$\left|\frac{(k_{eff} - m_{eff}\Omega^2)Y}{\mu_s P}\right| \leq 1. \tag{3.9}$$

The inequality indicates that the maximum value of friction force $F_{max} = |k_{eff}Y - m_{eff}Y\Omega^2|$ needed to enforce slip must be less than the limiting value of the friction force, $\mu_s P$. Equation 3.9 indicates the maximum force transmitted to the weld as well as delineates region of stick and stick-slip. In fact, it allows us to study changes in the material's coefficient of friction, the normal load, the build piece's mass and stiffness (modulus and geometry) on the process. Factoring m_{eff} out of Equation 3.9 yields a more attractive form of Equation 3.9 that describes the effect of a resonance excitation to the system is:

$$\left|\frac{m_{eff}(\omega^2 - \Omega^2)Y}{\mu_s P}\right| \leq 1. \tag{3.10}$$

Obviously as ω approaches the driving frequency Ω, the left hand side of 3.1 goes to zero, i.e., the system becomes more compliant and the feature sticks to the tape.

3.1.1 Modeling the Effective Properties of the WorkPiece

The effective stiffness, k_{eff}, and mass, m_{eff}, of the build piece changes with its geometry. Any model of the build piece must accurately predict these changes. We utilize the Rayleigh-Ritz model described in Chapter 2 to determine effective properties of the workpiece.

We reduce the parallelepiped to a single degree of freedom (sdof) oscillator by normalizing each of the mode shape vectors in Eqn. 2.5 to have a norm of 1. The effective masses are calculated as

$$m_{\text{eff},j} = \{\boldsymbol{U}_j\}^T \boldsymbol{M}_{ij} \{\boldsymbol{U}_j\}, \quad i,j = 1,2,3, \tag{3.11}$$

where $\boldsymbol{M}_{ij}$, $\{\boldsymbol{U}_j\}$ are the mass matrix and the mode shape from the Rayleigh-Ritz model. The modal stiffness in each direction is now simply

$$k_{\text{eff},j} = \omega_i^2 m_{\text{eff},j} \quad j = 1,2,3 \tag{3.12}$$

where ω is the natural frequency of the mode that is approximated. In the stick-slip model we use the effective stiffness and mass, $k_{\text{eff},2}$, $m_{\text{eff},2}$, respectively.

3.1.2 Dimensional Studies

In this section, we compare the predictions of our model to published results. However, we begin by examining how differential motion changes with geometry. Figure 3.2 shows the non -dimensional velocity of the lumped parameter model for h/w of 0.5, 0.75, 8, 1, and 2. The lumped parameter model also shows that there is a drop in differential motion near a resonance corresponding to an h/w of 0.8.

The effect of substrate stiffness was explored experimentally by Robinson *et. al.* [18]. The researchers constructed build features at widths of 15/16 in., 1/2 in., 1/4 in., 1/8 in.,, and 1/16 in. at three orientations: longitudinal, lateral, and at an angle of 45 degrees to

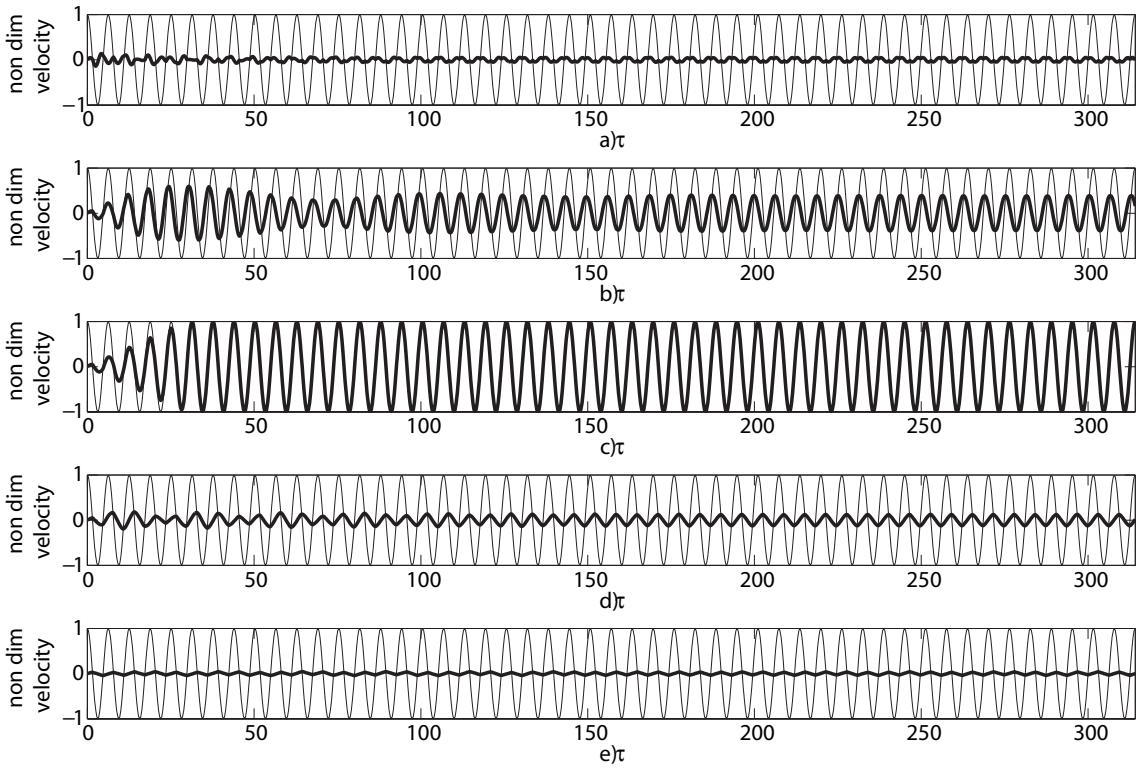

Figure 3.2: Sonotrode, Substrate Non-Dimensional Velocity a) $h/w = 0.5$, b) $h/w = 0.75$, c) $h/w = 0.8$, d) $h/w = 1$, e) $h/w = 2$ for Lumped Parameter Model

the rolling direction of the sonotrode. Widths smaller than the nominal width of the tape 15/16 in. were trimmed to the correct thickness after each machine pass. The researchers found that features of 1/16 in., were able to be built to the higher h/w ratios. Figure 3.3 presents a contour plot $\log|(1-\alpha^2)/\gamma|$ for various heights and depths. Points $\bullet$ indicate experimental values from [18]. The gray region indicates regions of slip and the white region indicates the stick region. The dotted lines indicate geometries of constant h/w. There is clear indication that the geometry affects whether the feature sticks or slips and sticks with respect to the tape. However, all widths of Robinson [18] clearly lie in the stick-slip region. Ideally, some of the data should lie in the stick region. This discrepancy may be due to the model; we have relatively simple assumptions on the effective stiffness, mass and frictional behavior. We also note that as features of the nominal build width pass through the first natural frequency, the feature sticks; again, this is to be expected since the compliance

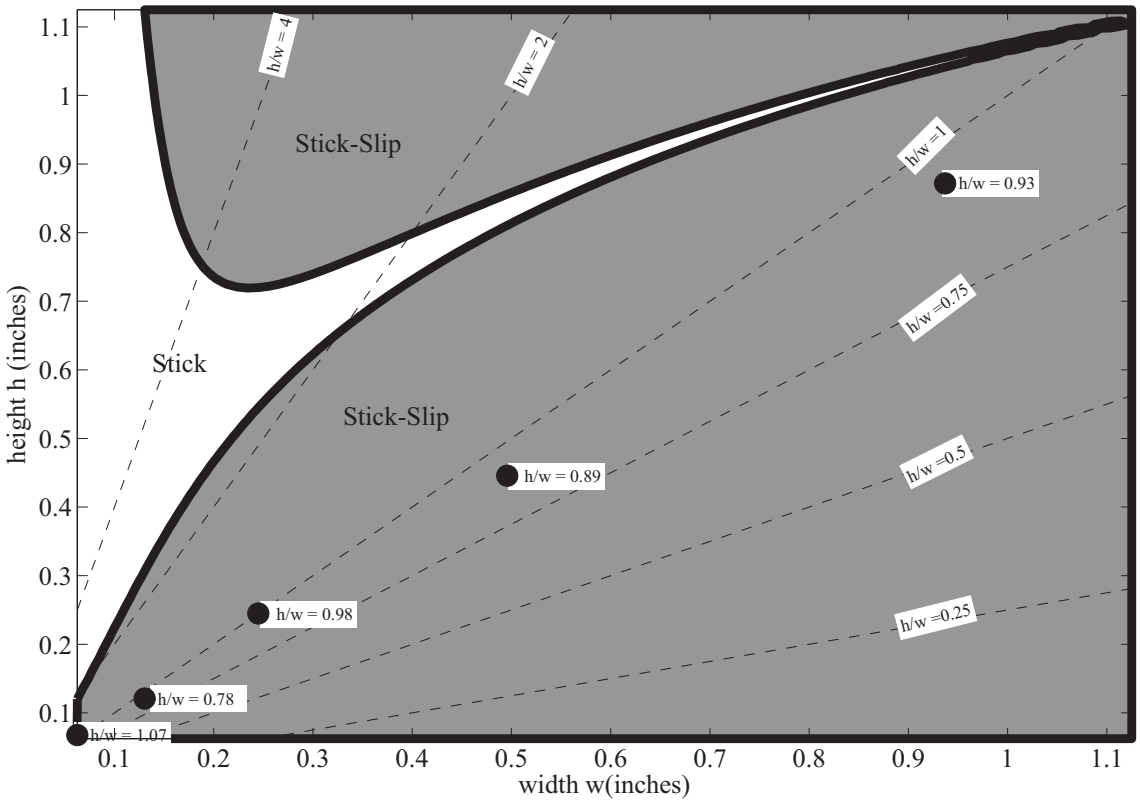

Figure 3.3: Contours of $\log(|(1-\alpha^2)/\gamma|)$ for Aluminum 3003 with $L/d = 10$, $\mu_s = 1.4$, • indicates experimental build heights from [18]

would decrease. This indicates that it may be possible to weld on features that are already past the apparent limit on build height or even to temporarily stiffen the feature at the build height limit and once this limit is passed to continue, the UC process. In features that are relatively thin (build width of approximately 0.2 inches) there is no increase in stiffness as the feature's first natural frequency passes through resonance.

3.2 Effect of Coefficient of Friction

The force transmitted by friction is directly proportional to the coefficient of friction between the foil and the substrate. We hypothesize that the coefficient of friction is dependent upon the surface topography of the tape. The topography changes based on the roughness of the sonotrode due to the damage it does to the bonding tape's surface. Fur-

thermore, as the surface topography changes: due to colliding asperities, removal of oxides, temperature rise at the interface and local metallic contact of asperities may increase the coefficient of friction changing the stick-slip boundary. While the model is limited in that it does not incorporate a time dependent coefficient of friction based on the wear at the bonding interface, we can use it to examine the overall effect of changes in the coefficient of friction by letting μ_s vary from 1/4 to 10 times the nominal value of 0.4. Physically, the coefficient of friction is limited to the product of the shear strength of the material and the real area of contact at the bonding interface. Figure 3.2 illustrates the sensitivity of the coefficient of friction on the stick slip boundary. A large increase in the coefficient of friction increases the stick region. Based on the research by Gao and Doumandis [19] the coefficient of friction for aluminum may change from approximately 0.3 to 0.58 a negligible effect on our stick slip boundary.

3.3 Effect of Loss of Sonotrode Amplitude

The model assumes that the sonotrode amplitude is constant. However, recent research by Solidica, Inc. indicates that amplitude is lost under load. In addition, Huang and Ghaseemieh [38] show amplitude transmitted to the bonding interface is reduced due to deformation in the tape. Figure 3.3 shows the effect of a loss of amplitude on the stick-slip boundary. The amplitude is varied to from 25, 50 to 75 percent of the sonotrodes amplitude of 16 μm. Clearly as the amplitude is decreased the stick slip boundary grows in size.

3.4 Summary

We have explored the possibility of the UC process exciting a resonance in the build feature and the tradeoff between force, stiffness and geometry at the work piece. We modeled the vibrations build feature as stick slip oscillator with effective properties obtained from Rayleigh-Ritz model. The lumped parameter model has several advantages. First, it is a relatively simple conceptual model. Second, it is computationally inexpensive. Both

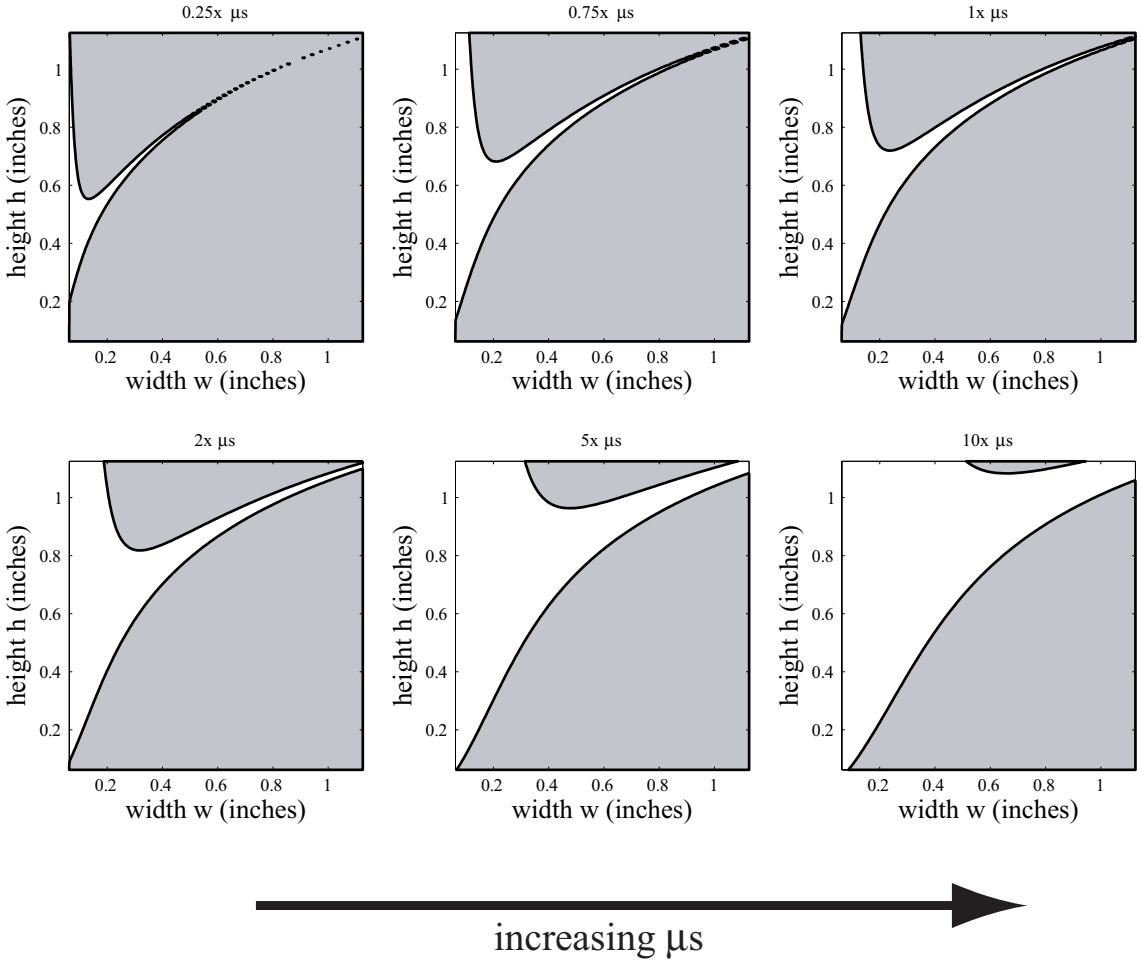

Figure 3.4: Effect of Changing Coefficient of Friction on Stick Slip Behavior

these characteristics make it ideal to study the effect of changes in process parameters. However, this insight comes at the cost of simplifying the forces and stresses at the contact interface. The underlying assumption is that modal effects are the dominant factor in determining when bonding occurs. We constructed this model using the first bending mode of vibration. The rationale for this is that the primary mode has no nodal region and thus will be present regardless of the location of the sonotrode and it is relatively length independent. The main drawback to using this single mode construction is that it neglects the effects of higher modes. However, the same bifurcation diagrams may be produced using high order modes.

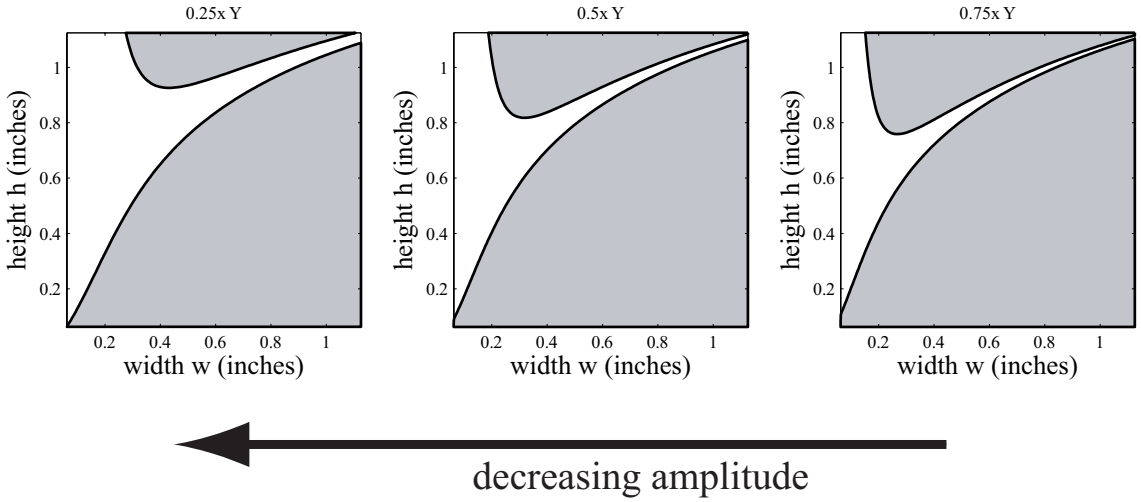

Figure 3.5: Contours of $\log(|(1-\alpha^2)/\gamma|)$ for Aluminum 3003 with $L/w = 10$ with Y Reduced by 25%, 50%, 75%

The model approximates the effect of the compliance increasing as the feature approaches resonance. Comparing the results to experimental observations from Robinson [18] we see some correlation to the friction force, and energy to build height. In the next sections we would explore the limit on h/w experimentally by designing tests that specifically isolate the stiffness feature and force transmitted to the weld. One method of doing this would be to weld over wrought features while varying the normal pressure and amplitude of the sonotrode. Welding over wrought feature would eliminate the effects of previous bonds. Using our model, we expect to see degradation in bonding when welding wrought samples that have natural frequencies close to 20 kHz. This bonding degradation may result in incomplete welds that have low peel strength, or a decrease in linear density of the weld, i.e., ratio of bonded to non bonded areas at the interface. This observation needs to be experimentally validated. Another interesting possibility indicated by our work is that it may be possible to bond features much higher than the current build limit if we start with features of sufficient height that do not lie in the stick region.

Chapter 4

Experimental Procedures

This chapter details a set of tests to examine the differential motion, bonding and process parameters such as changes in the sonotrode' s amplitude during the consolidation process due to changes in the build feature's geometry. The first published research documenting the height to width limit was conducted by Robinson *et al.* [18]. This chapter details a set of experiments that examine bonding both below and above the apparent aspect ratio limit. The model in Chapters 3 indicate that differential motion increases once the build limit is passed for certain widths. Using the assumption that a certain amount of differential motion at the interface is necessary for bonding these models indicate that once apparent aspect ratio limit of h/w of one is passed, bonding can occur. This chapter outlines the procedure for two tests to confirm our predictions these are

Resonance Excitation of Build Feature - to quantify the effect of resonance at various geometries on bonding,

Controlled Geometry Rolling - designed to eliminate the cumulative effective of porosity at the welding interface and to further quantify the effect of resonance at various geometries on bonding,

4.1 General Test Setup

In each test we monitored the vibration of the build feature and the sonotrode during welding, i.e., each test uses the same measuring devices and data acquisition, system. Before we describe the general test setup it is worth noting the challenges in measuring the motion of the sonotorode, foil and build piece. The Formation machince in constructed in a manner that provides limited access to the sonotrode. The metal foil is very thin (150 μm) making direct measurements of its movements extremely difficult. Furthermore, the bonding area is obscured by the sonotrode. Finally, a sonotrode vibrating at a 5-40 μm peak to peak amplitude would experience 8.0×10^3 to 7.9×10^4 g's, effectively out of the measurement range of accelerometers. Therefore, the only measurement options are non contact methods.

Figure 4.1 shows the experimental setup. Specifically, the test equipment consisted of a Polytec OFV 501 fiber interferometer to measure the vibration of the sonotrode, a Polytec OFV 505 vibrometer measures the build feature's velocity below the contact patch with the sonotrode, and a USB 1608 HS high speed analog input module from Measurement Computing to capture data. In addition, to monitoring the velocities of the build piece and sontorode we also record the power in the piezoelectric actuator, and the normal load applied by the sonotrode. The sonotrode excites the system at 20 Khz. Numerically, we predict that the largest frequency component in the signal due to stick-slip phenomena between the sonotrode and build piece is 120 Khz. Using *Shannon's Sampling Theorem* [48] the sampling rate should be at least 2.5 times the largest frequency component in the signal, i.e., 300 kHz. However, twice the largest frequency component or 240 kHz provides the minimum number of points to represent the waveform. We sampled the data at 250 kHz the limit of the USB 1608 HS analog module.

4.2 Material

The UC process can bond a variety of materials. However, in these tests we restrict our attention to Aluminum 3003 H-18; the original material used in the process. Table 4.1

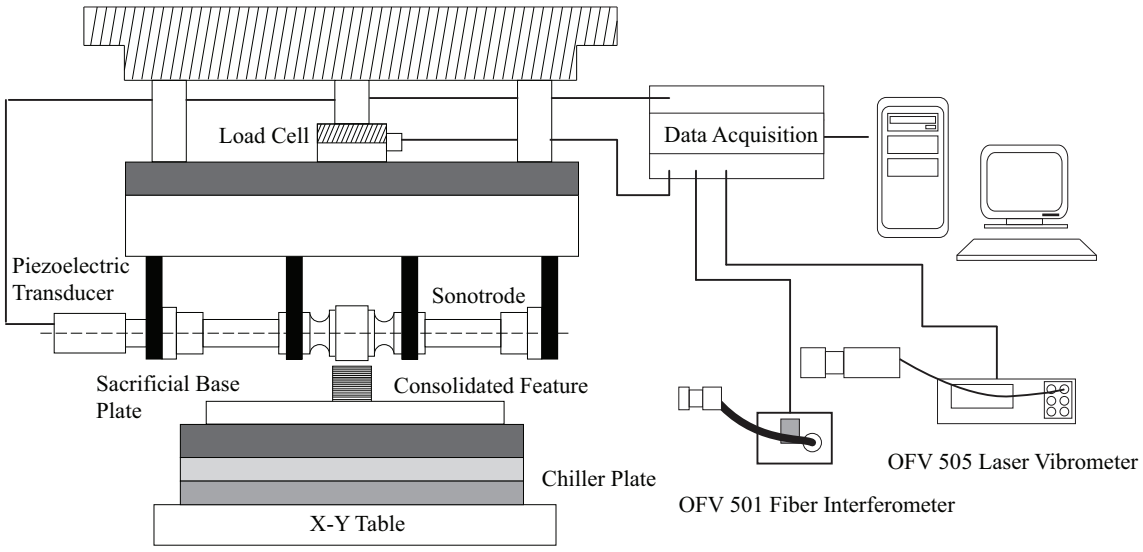

Figure 4.1: Test Setup

provides the chemical composition of the material.

Table 4.1: Chemical Composition of AL 3003-H18 by Percent Weight [49]

Al	Cu	Fe	Mn	Si	Zn
96.7-99.0	0.050-0.200	≤ 0.700	1.00-1.50	≤ 0.600	≤ 0.100

4.3 Resonance Excitation of Build Feature

The SDOF oscillator predicts a substantial loss in differential motion and therefore energy and force transmitted in the interfacial bonding region as the build feature approaches the primary resonance. We hypothesize that this loss of force and energy are the principal reasons for a lack of bonding. The models also predict at the nominal tape width (23.4 mm or 15/16 inches) after the primary resonance has passed, that differential motion increases and bonding can again occur. These predictions are easily testable by constructing test samples with geometries that place the primary resonance below, at and above the frequency of the sonotrode. The actual geometries were chosen using the "Mode" Map in Figure 2.16.

4.3.1 Test Samples

Sixteen, 2.5 inches long specimens were used in this study. We placed eight samples of two different widths and various heights on two base plates. The first base plate contained samples of widths of 15/16 inches (93.75mm) with heights that are 0.5, 0.75, 1, and 2 inches. The second base plate contained samples of widths 0.5 in (12.75 mm) with heights of 0.25, 0.5, 0.879, and 1.7 inches. In order to produce samples at an aspect ratio of h/w greater than one, the specimens are milled from an stack of width 3 inches, height of 2 inches and a length of 10 inches. Figure 4.2 shows the nominal width specimens.

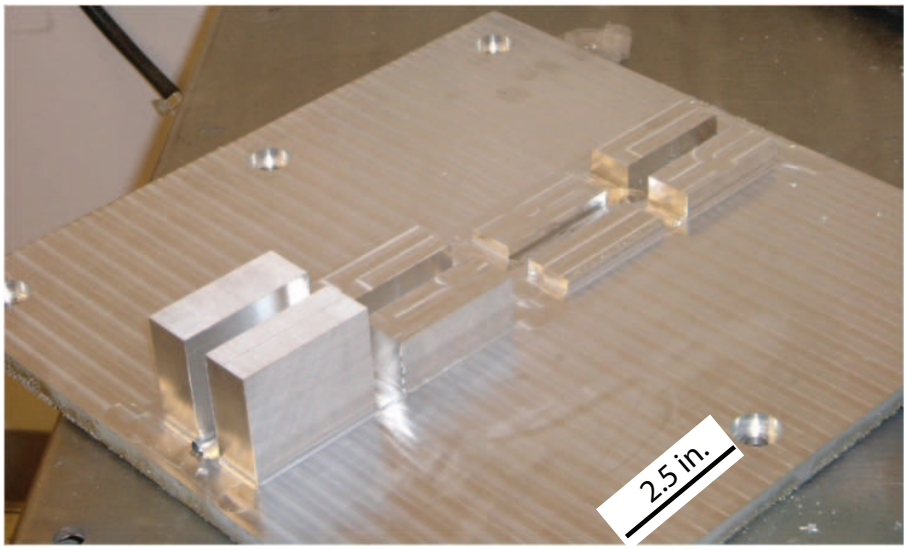

Figure 4.2: Nominal Width Specimen for Resonance Test

4.3.2 Test Parameters

During the test we used the following parameters:

- 1400 N (315 lb) compressive load applied to the tape and build specimen,
- heated base plate that reached a temperature of 150 °C (300 °F) ,
- rolling speed of 42.33 mm/s (100 in./min),

- 25 μm (9.84×10^{-4} in) sonotrode vibratory amplitude.

These parameters were chosen based on guidelines from Solidica, Inc. [50].

4.3.3 Procedure

The specimens were heated for several hours, therefore we assume that the temperature of each reached steady state. During the tests the sonotrode would move downward on the part at the specified normal load at one end of the part. The sonotrode would then begin to vibrate at the specified amplitude and roll for 2.5 inches. We trigger data acquisition when the power of the actuator reached 1 volt out of a ± 10 volt range.

4.4 Controlled Geometry Rolling

This test is a supplement to the resonance tests. Again, due to the difficulty in obtaining wrought Aluminum 3003 H-18 at geometries other than plates and foils; we focus on specimens of width 0.5 inches that are placed in the text fixture. This test was designed to further explore how wrought samples act in bonding when compared to consolidated samples by eliminating the effects of posorosity and damage at the sonotrode interface, that results in voids in the bonding interface.

4.4.1 Manufacturing Specimens

Unfortunately, Aluminum 3003 H18 in geometries other than foils and plates is not readily available. In order to construct specimens of suitable dimensions, we manufactured the samples from the standard Aluminum 3003 H18 base plate used in the UC process. Furthermore, the specimens are machined to the final height when attached to the formation machine. This is done to ensure the sonotrode comes in contact with a surface that is flat with respect to the machine. We manufactured 4 specimens with the with heights of the sample above the test fixture are 0.5, 1, 1.25, and 1.5 inches. The exact dimensions of the specimens are given in Table 4.2 . The tolerance for each specimen was $\pm .0005$ of an inch.

Table 4.2: Dimensions of Test Specimens for Controlled Geometry Rolling

Specimen	Height (in.)	Width (in.)	Length(in.)
1	1.4375	0.5	2.5
2	1.9375	0.5	2.5
3	2.1875	0.5	2.5
4	2.4375	0.5	2.5

4.4.2 Design of Test Fixture

Using samples machined from the base plate proved problematic; they needed to be cantilevered to the Formation Machines bed in a manner that:

1. does not affect the dynamics of the test sample,
2. allows for relative ease of changing specimens,
3. relatively light weight (the fixture needed to be transported to Solidica, Inc. facilities in Ann Arbor, M.I.),
4. attaches easily to the Formation machine.

The most important of these requirements was the first. If the modal characteristics of a specimen were drastically altered, the sample may become too stiff and not accurately represent a cantilevered specimen. Alternatively, if the support itself has a mode of vibration near the excitation frequency, the whole structure may vibrate with the excitation and adversely affect the bonding at the interface. The text fixture was designed heuristically. Ideally, having the specimens wedged between two solid sections of metal that are in turn bolted to bed of the Formation machine would minimize any affect of the support structure. However, this setup is heavy and awkward. Ultimately, we decided on the steel, ribbed structure in Figure 4.3.

As an example of the effect of the fixture on the modal characteristics of a sample, Table 6.4 compares the numerical predictions of a freestanding specimen of dimensions $0.125 \times 0.69 \times 2.5$ inches to a specimen of the same dimensions in the text fixture. There is

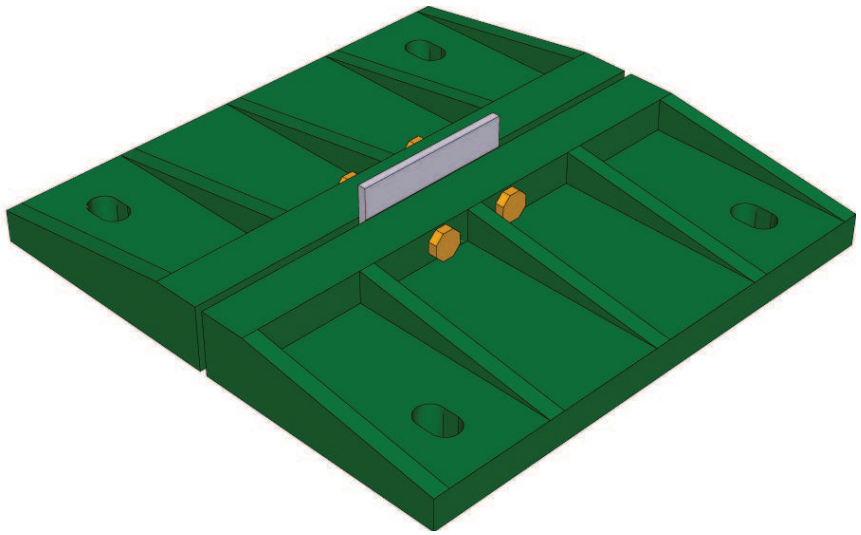

Figure 4.3: CAD Model of Test Fixture Used in Controlled Geometry Rolling

less than a 12% difference in the first four modes in each configuration. The support does not significantly change the modal characteristics of the test coupons until the fifth mode when there is a 45% difference in the natural frequencies. Similar, trends were found for the other geometries used in the test.

Table 4.3: Comparison of Simulated Primary Modes for Wrought Sample Fixtured and Unfixtured for 0.125 in. $\times$ 0.69 in. $\times$ 2.5 in. sample

Mode	Freq. Cantilevered Specimen (kHz)	Freq. Specimen in Text Fixture (kHz)	% Difference
1	16.784	17.372	3.51
2	17.955	18.962	5.61
3	23.419	22.268	0.03
4	33.809	30.448	11.48
5	58.848	31.582	45.99

4.4.3 Test Parameters

We used the same parameters as the resonance test:

- 1400 N (315 lb) compressive load applied to the tape and build specimen,

- heated base plate that reached a temperature of 150 °C (300 °F) ,
- rolling speed of 42.33 mm/s (100 in./min),
- 25 μm (0.000984 in.) sonotrode vibratory amplitude.

4.4.4 Procedure

Similar to the resonance test the sonotrode would move downward on the part at the specified normal load at one end of the part. The sontrode would then begin to vibrate at the specified amplitude and roll for 2.5 inches. We trigger the acquisition when the power suppy to the actuator outputed 1 volt to the data acquisition system out of a ± 10 volt range.

4.5 Summary

These test are designed to provide answers to some of the research question posed in Chapter 1. Specifically, by monitoring the sonotrode's load, amplitude and power we can study how its motion is impacted by changing the build feature's geometry. These tests are also designed to explore the geometries where bonding degradation occurs. Finally, by monitoring both deflection of the feature and the sonotrode it may be possible to ascertain the dynamic conditions when bonding degradation occurs. The results of each test are discussed in the next chapter.

Chapter 5

Experimental Results

The previous chapter outlined the procedure for two test designed to quantify our theory of the role of geometry on Ultrasonic Consolidation and to explore the effect of geometry has on process parameters during the consolidation operation. These tests included:

Resonance Excitation of Build Feature - to quantify the effect of resonance at various geometries on bonding,

Controlled Geometry Rolling - to quantify the effect of resonance at various geometries on bonding.

In this chapter we will discuss the results of each test.

5.1 General Observations from Test Data

As stated previously the tests were designed to examine the change in process parameters during welding. Figure 5.1 shows a sample of the data taken in each test. The first thing to note is the presence of speckle noise in the velocity of the build feature. The noise is caused when the coherent waves of an incident laser beam are dephased during back spatter from a surface that is rough on the scale of the optical wavelength [51]. We use a modified form of the algorithm used by Vass *et al.* [52] to minimize the effect of this speckle

noise without significantly altering the signal. The data presented in the next section will have been filtered unless otherwise noted. Unless noted the algorithm will be applied to the data presented in the following sections with exception of the data used in the Fourier transforms. Secondly, the measured quantities such as power, build feature velocity, sonotrode velocity, and load vary along the length of the build feature.

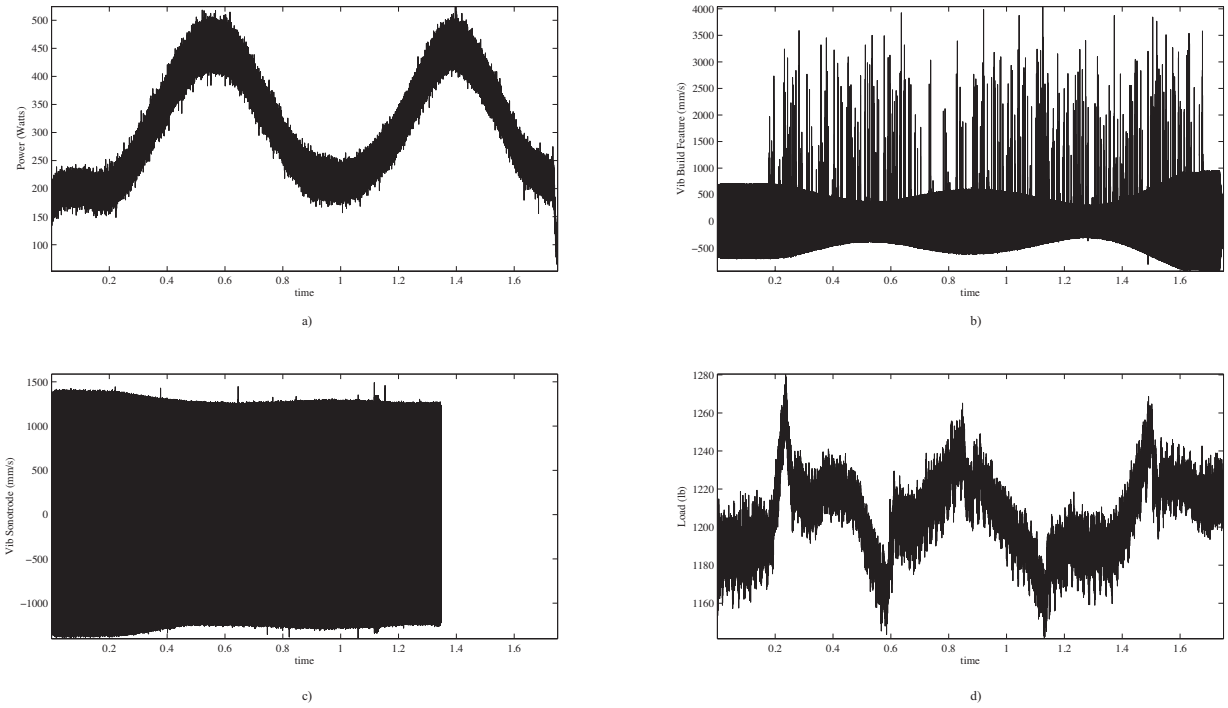

Figure 5.1: Sample of typical measurement a) Power, b) Substrate Velocity, c) Sonotrode Velocity, d) Load

5.2 Resonance Excitation of Build Feature

The phenomena exhibited during the resonance tests have been unreported in the published literature. The limits on the build height for the nominal width (0.975 inch) and half width (0.5 inch) specimen are given in Tables 5.1, and 5.5, respectively. Depending on the geometries the failures range from fatigue in the bonding layers, to overloading the

power supply of the ultrasonic welding assembly.

5.2.1 Nominal Width Specimens of Aluminum 3003 H-18

For the nominal width specimen with an initial height of 0.5 inches bonding failure was due to a detachment of the first layer after a number of layers were built, Figure 5.2. This is most likely due to fatigue failure of the initially bonded layer, supporting the contention that an excitation near one of the natural frequencies of the feature causes failure. An excitation near a resonant frequency would drastically increase the amount of strain energy in the vibrating specimen making the specimen more susceptible to fatigue failure. Welding over the nominal width specimen that has an initial height of 0.9375 inches causes the power supply of the transducer sonotrode assembly to overload. We repeated the operation four times with the same result. Note the specimens were built so that their first bending frequency is close to the operating frequency of the sonotrode. Personal communication with Branson, Inc, the makers of the power supply indicates that this power supply failure is very probably due to the sonotrode trying to couple to a frequency just outside the power supply's range or by a mode in the build feature interacting with the sonotrode in a manner that alter its operation. The phase lock loop control algorithm can adjust the frequency of excitation only within a narrow band ($\pm$ 500 Hz). A resonant frequency of the build piece just outside this band would cause the sonotrode to couple to the build piece and vibrate at the piece's resonant frequency; approximately 21 kHz if the sample was wrought. The power supply overloads when trying to adjust the frequency of the voltage that excites the piezoelectric actuator to lie in the the operating bounds. The same behavior was observed for specimens of an initial height of 0.75 inches of sonotrode. However, the predicted first natural frequency of the specimens was much higher, i.e., 24 kHz. Interestingly as predicted, for the nominal width case, the specimen of initial height of 2.00 inches allowed the welding of 55 layers without failure, Figure 5.3.

We arbitrarily chose to take data at the 1st, 2nd, 15th, 27th, 35th, and 55th welds when possible. The limit of 55 layers war arbitrarily set as indication of successful bonding

Table 5.1: Resonance Test Failure for Specimens of Width 0.975 inches

Height(inches)	Layer at Failure	Method of Failure	Total Build Height
0.5000	41	Detachment of 1st layer	0.7460
0.7500	19	Welder Fault	0.8430
0.9375	–	Welder Fault	0.9375
2.0000	55(No Failure)	–	2.3300

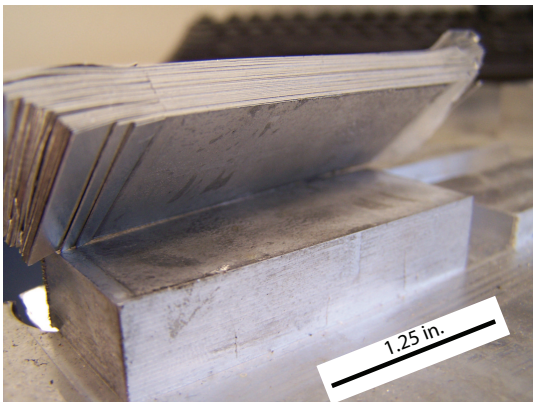

Figure 5.2: Failure of Specimen with width 0.9375 inches and initial height of 0.25 Inches

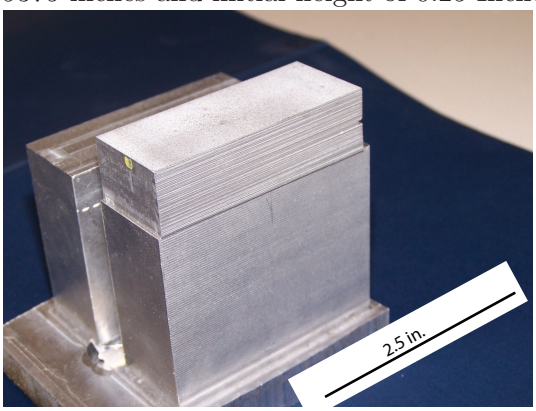

Figure 5.3: Bonding of Specimen with width 0.9375 inches and initial height of 2.00 Inches

taking into consideration the time and materials used on the specimens. Figure 5.4 plots the first weld for the 0.9375 inch specimens at heights of 0.50, 0.75, 0.94, and 2.00 inches over the whole weld interval and for a zoomed window at the initial sonotrode dwell time. Several points are worth noting about Figure 5.4. First, it is similar to the deformation predicted by the moving load model in Figure, 2.18. Obviously, the deformation is dependent on the sonotrode's location on the specimen. Second, the most compliant portion of each specimen changes with height. If we crudely estimate the minimal stiffness of the feature by the minimum of the motion envelope in each feature we note that the specimen with height of 0.5 inches is stiffer near the middle while the height of 2.00 inch specimen is stiffer nearer to the ends. Finally, examining the magnitude of motion we see slight increase in velocity of the feature as the height increases from 0.5 to 1 inches and a decrease when the height reaches 2.00 inches. In fact, the RMS values in the zoomed window are presented in Table 5.2

Table 5.2: RMS Values for Substrate Velocity of Windowed Sample

Height(inches)	RMS (mm/s)
0.25	624.27
0.75	735.07
0.94	699.83
2.00	407.47

This behavior is unexpected if you considered the build feature as a simple beam that deforms statically. However, it is entirely consistent with the lumped parameter model presented in Chapter 3. Also note that in Figure 5.4 e) and f) the welder faulted.

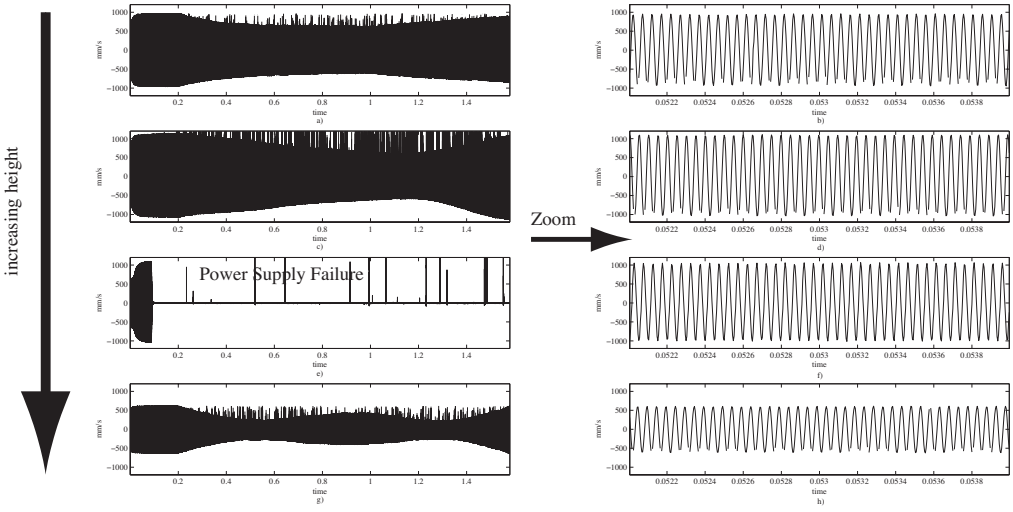

Figure 5.4: Overall and Zoom Time Response of First Weld for 0.9375 inch Width Specimens a) and b) h= 0.5 inches, c) and d) h=0.75 inches, e) and f) h=1.0 inches, g) and h) h=2.0 inches

5.2.1.1 Prescence of Higher Order Harmonics

One of the initial research questions, *could we experimentally detect a change in the dynamic response of the build piece and or sonotrode from optimal build geometries to those at or near bonding degradation*, may be answered by quantifying stick-slip motion from the respective time signals of the the substrate and sonotrode. Rozenburg [6] notes that there is no practical way to observe stick slip behavior during the ultrasonic welding process. He, however, postulates that the vibration of the build feature would be not be purely sinusoidal. The vibration of the build feature would contain other harmonic components due to stick-slip behavior. Similarly, Ditri and Eder [53] theorize that at stick, the deformation would be composed of only one frequency and higher harmonics in the vibration of the build piece are due to stick slip motion. They conducted several experiments that showed the feature vibrated not only at the dominant frequency of the ultrasonic welder but also at several overtones. Ditri and Eder [53] explain the presence of these harmonics in terms of ultrasonic capillary bonding. In fact they note the peaks of the velocity signal are "cut" due to slip. In addition, they found that a Fast Fourier transform (FFT) of the time response of the substrate indicated the presence of higher order harmonics.

However, before making a direct assertion of the presence of stick slip motion we examine the velocity signal of the sonotrode under no load, Figure 5.5. We expect to see that an Fourier transform of the time signal would indicate a single peak at the operating frequency of 20 kHz. In fact, if we look at a magnitude plot of the Fourier transform in Figure 5.5 c), we see only one frequency at 20.15 kHz. However, plotting the Fast Fourier transform on log scale, Figure 5.5 d), we see the dominant frequency at approximately 20.15 kHz. The plot also shows higher order harmonics at multiples of 2, 3, 4, 5, and 6, i.e., at 40.3, 60.45, 80.6, 100.75, 120.9 kHz, respectively. The higher order harmonics are several orders of magnitude smaller that the operating frequency. Furthermore, the cause of these higher order harmonics is not known. We believe that it may due to material nonlinearities in the piezoelectric actuator [54].

Figure 5.6 shows their presence during the consolidation process. However, their

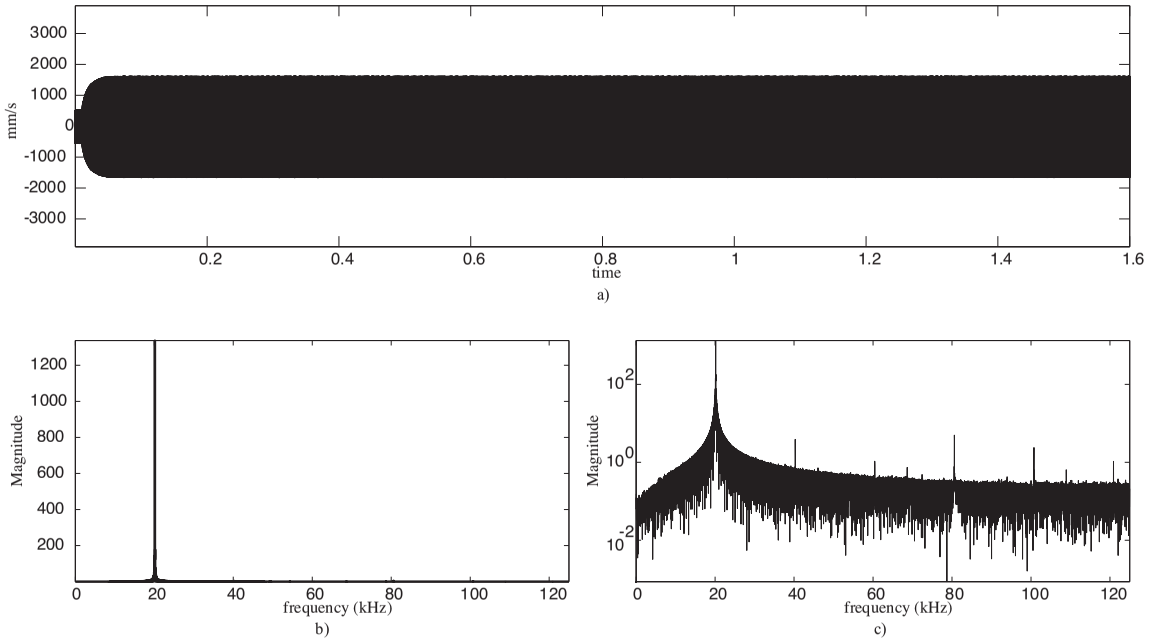

Figure 5.5: Time and FFT of Free Air Response of Sonotrode, a) Sonotrode Full Time Response, b) Sonotrode Zoomed Response, c) Magnitude Plot of FT, and d) Log Plot of Ft

effect is increased on the sonotrode. Without further analysis of the transducer-horn assembly it is impossible to conclusively use a FFT of the time response to quantity stick slip. Indeed, it appears that the features only vibrates at the operating frequencies of the sonotrode.

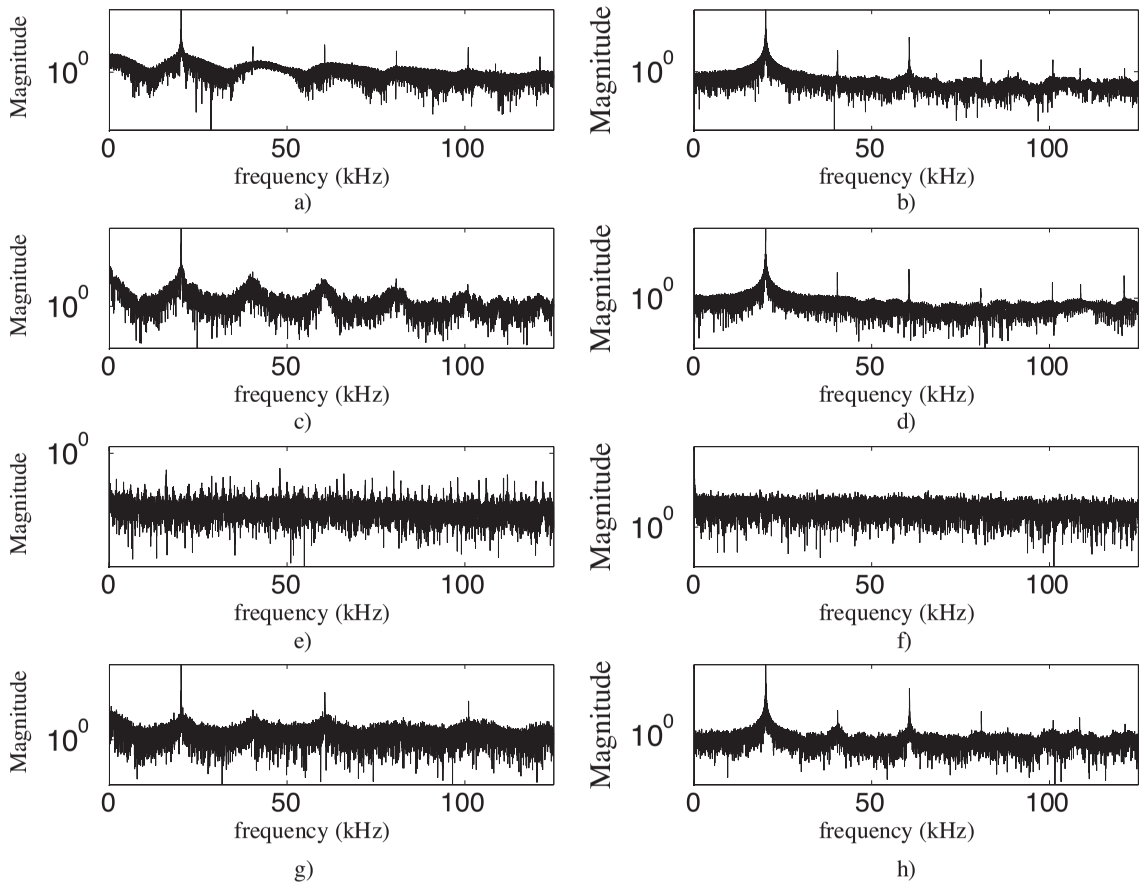

Figure 5.6: Feature and Sonotrode FFT of Time Response of First Weld of 0.9375 Inch Width a) $h = 0.25$ inches Feature Response, b) $h = 0.25$ inches Sonotrode Response, c) $h = 0.50$ inches Feature Response, d) $h = 0.50$ inches Sonotrode Response, e)$h = 0.75$ inches Feature Response, f) $h = 0.75$ inches Sonotrode Response , g) $h = 1.0$ inches Feature Response, and h) $h = 1.0$ inches Sonotrode Response

5.2.1.2 Load and Power

Figure 5.7 shows plots of load and power of the welder when consolidating the 0.9375 inch test specimens. Note that in each plot the load varies slightly from the nominal load and that the variation depends upon the location of the welder along the specimen. Tables 5.3 presents the maximum, minimum, and average values of load during the entire welding interval. However, the minimum and average load calculation are meaningless when the

Table 5.3: Maximum, Minimum and Average Load during the Welding of 0.9375 inch Specimens

Height (inches)	Max. (N)	Min. (N)	Avg. (N)
0.50	1281.5	1140.0	1199.1
0.75	1262.3	1153.3	1202.6
0.94	1373.6	–	–
2.00	1262.1	1162.5	1205.5

welder faulted on the specimen. Clearly, the maximum load spikes when the welder faulted.

Like the load ,the power also varies during the ultrasonic consolidation process. Note that for $h = w = 0.93675$ inches, Figure 5.7 f), the power spikes above the values seen during the other tests. Table 5.4 shows the maximum, minimum and RMS power consumed during the welding cycle. Interestingly, as the height of the specimen increases, both the

Table 5.4: Maximum, Minimum and RMS Powesduring the Welding of 0.9375 inch Specimens

Height (inches)	Max. (Watts)	RMS. (Watts)
0.50	582.3	450.4
0.75	829.7	574.6
0.94	1225.45	–
2.00	653.36	457.768

maximum amount of instantaneous power supplied to the welder and the RMS value of the power consumed over the weld cycle increased. Similarly, to the load, the maximum power

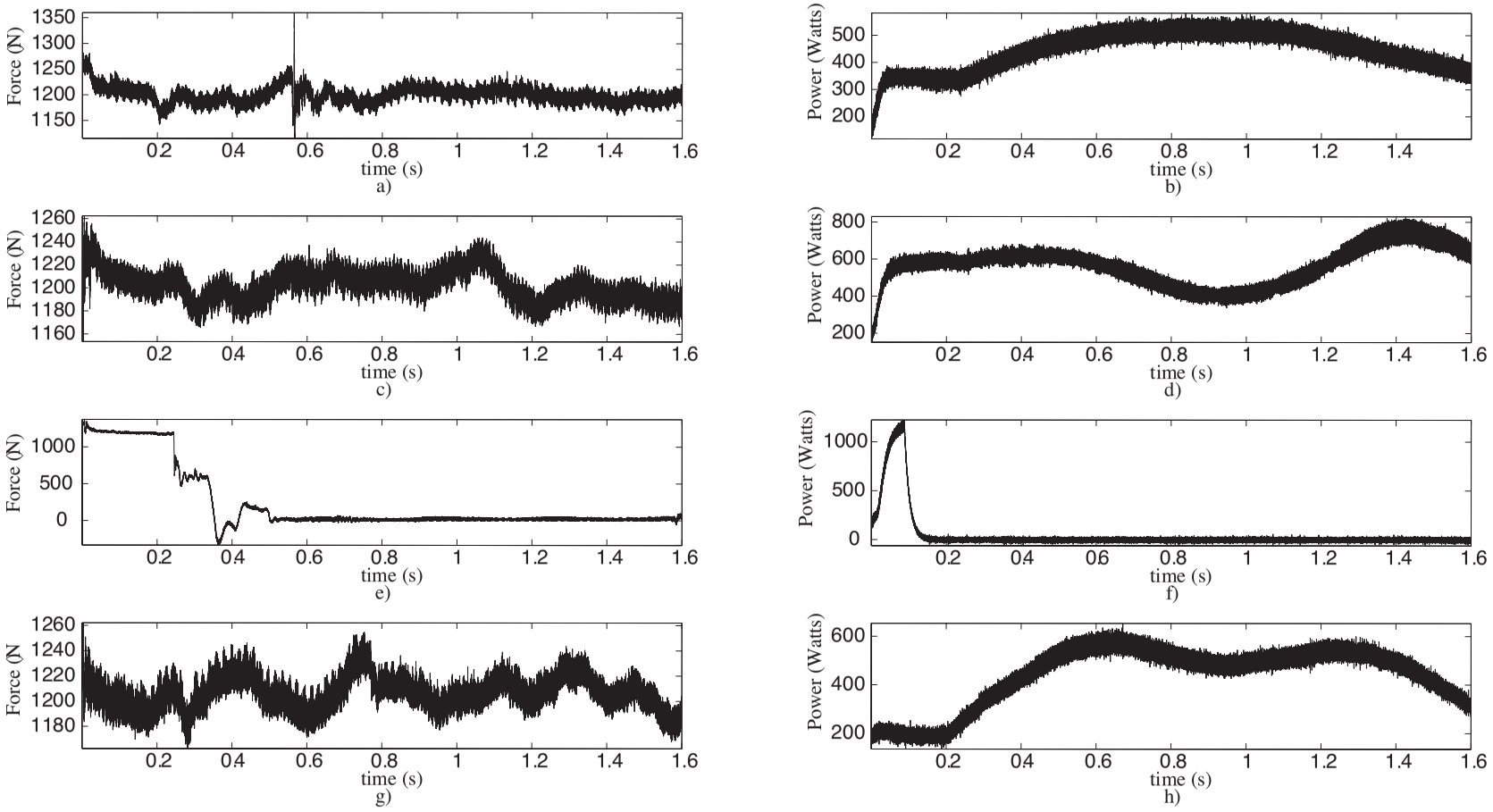

Figure 5.7: Load and Power of Nominal Width Specimens a) Load for $h = 0.50$ inches, b) Power for $h = 0.50$ inches, c) Load for $h = 0.75$ inches, d) Power for $h = 0.75$ inches, e) Load for $h = 1.00$ inches, f) Power for $h = 1.00$ inches, g) Load for $h = 2.00$ inches, and h) Power for $h = 2.00$ inches

draw occurred when the welder faulted.

5.2.2 Half Inch Width Specimens of Aluminum 3003 H-18

While the 0.9375 inch width specimens showed that for a given width if one starts past the apparent build height limit, bonding could again occur, the same was not true for the 0.5 inch width specimens, see Table 5.5. Welding over the specimen with an initial height from 0.25 inches we were able to add 48 layers before the failure to bond occurred. While the specimens of width 0.750 and 0.879 inches, the first layer would not bond. Finally, in the specimen of height 1.700 inches the first layer bonded in the middle and not on the edges, Figure 5.8. More tests are needed to determine the exact cause of failure.

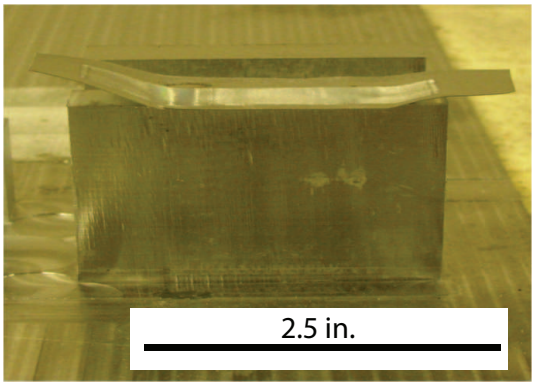

Figure 5.8: Failure of Specimen with width 0.5 inches and initial height of 1.7 Inches

Table 5.5: Resonance Test Failure for Specimens of Width 0.50 inches

Height(inches)	Layer at Failure	Method of Failure	Total Build Height
0.25	48	Debonding of 38th layer	0.530
0.75	1	Failure of of 1^{st} layer to bond	0.750
0.88	1	Failure of of 1^{st} layer to bond	0.879
1.70	1	Partial bonding of 1^{st} layer	1.700

5.3 Controlled Geometry Rolling

The controlled geometry test were designed to identify the ideal stiffness needed for optimal bonding at various heights by eliminating the cumulative effective of porosity at the welding interface. Four specimens were used in this test each was 0.50 inches in width and 2.50 inches long. The specimens had heights of 0.25, 0.50, 0.75, 1.00 inches. We were able to deposit at least three layers with no apparent evidence of bonding degration on all the specimens with the exception of the specimen of height 0.50 inches, in this specimen the first layer would not adhere to the substrate.

Figure 5.9 plots the time response of the build feature and the sonotrode during the consolidation process. Again,we see the trend that the amplitude increases as the height approaches the width and decrease as the height further increases. The second notable observation is that the sonotrode's velocity is constant for welding over all specimens with the exception of welding over the specimen of height of 1.00 inches. Examining the power consumption Table 5.6 trend is similar to the resonance test. The power consumption reaches a maximum when the height of the specimen is 0.75 inches and then decrease. Since the specimens are wrought these test seems to indicate that cumulative effects of

Table 5.6: Maximum and RMS Power during the Welding for Clamped Specimens

Height (inches)	Max. (Watts)	RMS. (Watts)
0.25	209.02	141.2
0.50	338.60	214.21
0.75	11935.00	887.13
1.00	10376.00	557.67

porosity due to bonding defects are not the cause of bonding degradation.

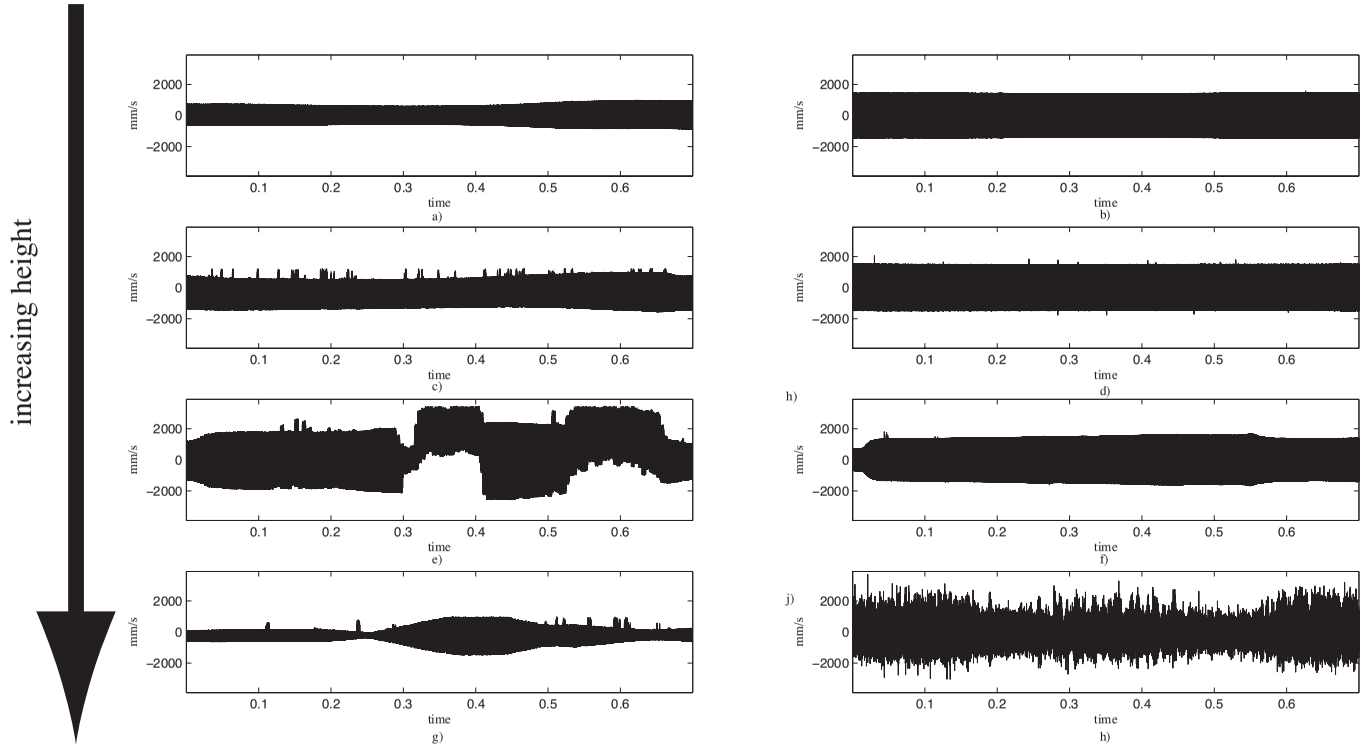

Figure 5.9: Feature and Sonotrode Time Response of First Weld of Clamped Specimens of 0.50 inch Width a) $h = 0.25$ inches Feature Response, b) $h = 0.25$ inches Sonotrode Response, c) $h = 0.50$ inches Feature Response, d) $h = 0.50$ inches Sonotrode Response, e)$h = 0.75$ inches Feature Response, f) $h = 0.75$ inches Sonotrode Response , g) $h = 1.0$ inches Feature Response, and h) $h = 1.0$ inches Sonotrode Response

5.4 Summary

The Rayleigh-Ritz Model, finite element model, and lumped parameter model all predict a decrease in compliance as the h/w approaches unity for the nominal width specimen. Furthermore,the h/w ratio obscures the true reason that bonding degradation occurs. Examining the limits on build height and the RMS vibration of the build feature, supports the contention that the feature becomes more compliant as it nears a build feature's natural frequency and moves away from the problematic region to allow bonding once this limit is passed. We see the same behavior occurring for half width specimens. However, the models do not predict any modal interactions unless the modulus of the material is drastically lowered. The cumulative effects of subsequent bonding seems to play no role in the limit on build height since wrought specimens exhibited the same behavior as consolidated specimens.

In trying to use the process parameters to quantify bonding failure we see both a spike in the substrate's motion and the power draw by the piezoelectric actuator. However, further tests are needed to quantify the exact troubled regions of deflection and power draw. The results show that for nominal widths that, the h/w limit is not an absolute limit on the UC process. If the structure is constrained or altered as to temporarily change its modal characteristics, it may be possible to build higher. In the next chapter, we test this hypothesis by examining the use of support materials in extending build height.

Chapter 6

Extending Build Height through the Use of Support Materials

Anecdotal evidence by Solidica, Inc. shows that the addition of support materials can increase the build height of freestanding features. In simple mechanical terms, the stiffness of the build piece can be represented by springs through which forces are transmitted in the normal and transverse directions to the ground, i.e., to the Formation machine. The transverse force depends on how the build piece resists the sonotrodes attempt to oscillate by a prescribed amplitude (X_s) at 20 kHz. This enforced motion in the transverse direction is fundamentally different from the applied force in the normal direction. The lateral force only has to be large enough to displace the build piece by X_s, and the transverse stiffness of the build piece decreases rapidly as the height increases through layering. Lower lateral force means lower surface shear tractions and lower Von Mises stresses at the bonding interface. This chapter begins by hypothesizing the effect of support materials on the build height. It then progresses to a material characterization of the two candidate support materials, a sugar glucose mixture and tin bismuth. Finally, each support material is evaluated for its effectiveness in extending the build height of nominal width build features.

The addition of support materials has three possible effects on a freestanding build feature: 1) increases the lateral stiffness of build pieces, 2) if the support material adheres to

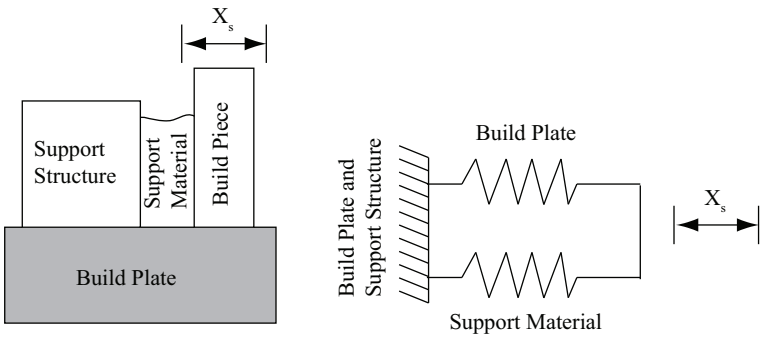

Figure 6.1: Conceptual Model of Support Material

the sides of the feature, it changes the fundamental frequencies of the build feature, 3) adds dampening to structure. However, using our previous analysis of the modal characteristics as a guideline, it is reasonable to conclude that the second effect is dominant in influencing build height of the nominal width specimens. At other widths, the other two effects may be dominant in influencing the build height. The left side of Figure 6.1 shows the gap between a build piece and a support structure filled by a support material, and the right side of the figure shows how the support material acts in parallel with the build piece to provide additional transverse stiffness. Unpublished observations by Solidica, Inc. indicates tin bismuth (SnBi) is an effective support material. However, removing SnBi from the build piece is cumbersome and inconvenient. The ideal support material would both provide sufficient stiffness and be convenient to remove. At the other extreme, a soft polymer might be easy to melt away, but it would probably not supply enough stiffness to enable the bonding process. The tradeoff between stiffness and convenience of removal is shown schematically in Figure 6.2. It is with these goals in mind that we know try to directly quanitify the effect of two candidate support materials; SnBi and "candy". The candy is a mixture of sugar, glucose, and water. These materials can be seen as extreme points on the stiffness versus convenience curve.

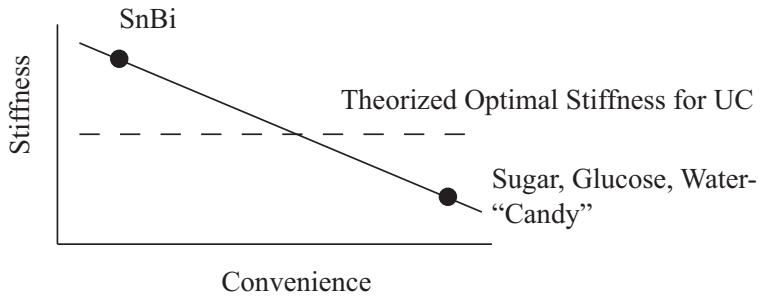

Figure 6.2: Tradeoff between Stiffness of Support Material and Convenience of Removal

6.1 Hypothesized Effect of SnB Support

The exact effect of SnBi has not been quantified, however, we have formed a hypothesis bases on experimental observations: Tin Bismuth provides an increase in stiffness that causes it to effectively act as a boundary condition shortening and reducing the effective height of the specimen. This hypothesis is based on the aforementioned observations by Solidica, Inc. and experiments to characterize the stiffness of several high aspect ratio test features through modal testing. The tests samples were machined from a slab of 50mm thick wrought Al 6061. The rectangular test features machined from the slabs were 63.5 mm (2.5 inch) long by 25.4 mm (1 inch) high. Three samples of each of the following thicknesses: 3.175 mm (1/8 inch), 6.35 mm (1/4 inch), 12.7 mm (1/2 inch), and 25.4 mm (1inch). Slots were placed behind the feature for tests with support materials. In order to quantify the effect of Tin Bismuth (SnBi) we filled the gap behind the three 3.175-mm-thick wrought specimens to depths of 3.175, 6.35, and 9.525 mm, effectively decreasing the height of the specimens to 22.225, 19.050, and 15.875 mm, respectively. We modeled the test feature as a rectangular parallelepiped with the effective heights mentioned previously. The test setup was the exact same procedure and setup shown in Figure 2.8. The results in Table 6.1 confirms this theory by showing that the support material affects the feature by making it vibrate in the same manner as a feature of a lower aspect ratio.

Table 6.1: Comparison of Natural Frequencies of Sn Bi height with Reduced Stack Height

Sn Bi fill Height	Mode	Experimental (kHz)	Model Height	Analytical (kHz)
1/8”	1	5.45	7/8”	5.56
	2	6.68		6.91
	3	10.65		10.65
	4	17.15		17.43
1/4”	1	7.45	3/4”	6.32
	2	8.86		7.55
	3	12.65		11.59
	4	19.42		18.16

6.1.1 Indirect Material Characterization of SnBi

We characterize the Youngs Modulus of SnBi by modifying the ASTM Standard 1876 E [55]. The specimens dimensions were nominally 7/16 × 7/16 × 10 inches. The test uses the first natural frequency in bending or torsion frequencies to estimate the Youngs Modulus. Figure 6.3 shows the experimental setup for the tests: a data acquisition system, signal conditioner, impact hammer and accelerometer.

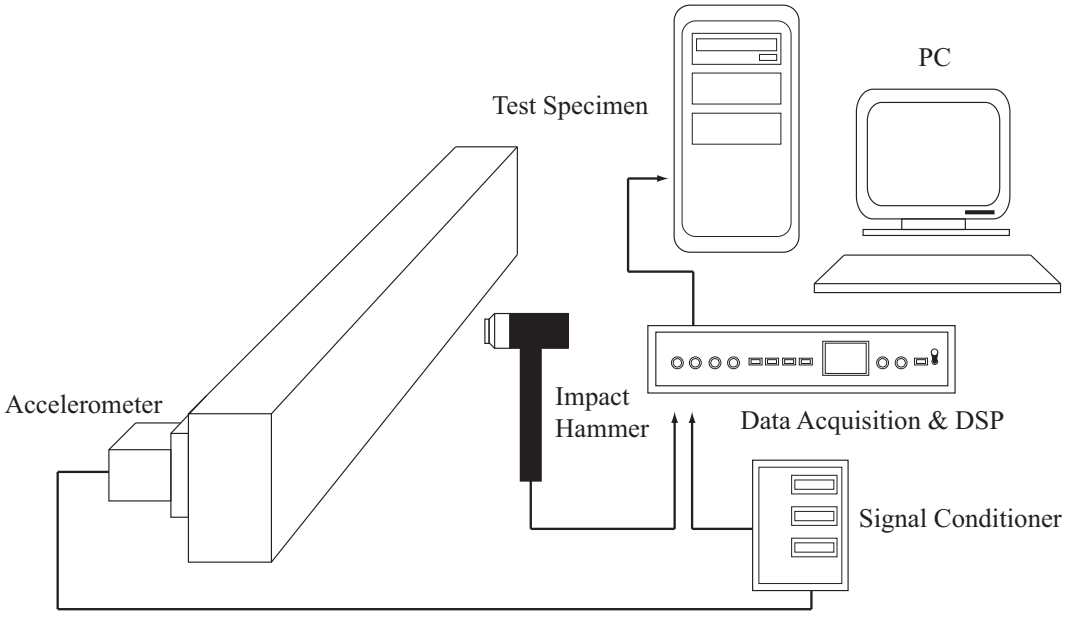

Figure 6.3: Test Setup for Support Material Characterization

The specimens were suspended in air with fishing line attached approximately at the nodal lines for the first flexural bending mode. An impact hammer was used to excite the structure and the natural frequencies were noted. Each estimate of the natural frequency is the average of seven tests to ensure consistency. Once the primary flexural mode is identified the Youngs Modulus can be determined from

$$E = 0.9465 \left(\frac{m f_f}{b} \right) \left(\frac{L^3}{t^3} \right) T_1 \tag{6.1}$$

where E is Youngs Modulus (Pa), m is the mass of the bar (g),L is the length of the bar (mm),b is the width of the bar (mm), t is thickness of the bar (mm), f_f fundamental resonant frequency of the bar in flexure (Hz) and T_1 [55] is a correction factor. The correction factor is defined as

$$T_1 = 1.00 + 6.585 \left(\frac{t}{L} \right)^2 \tag{6.2}$$

The results are given in Table 6.2 .

Table 6.2: Measured Frequencies and Computed Young's Modulus of SnBi Test Specimens

Specimen	Mass(g)	Measured Frequency (Hz)	Computed Young's Modulus
1	358	425.00	60.83
2	346	430.00	60.18
3	351	431.25	61.41

The first thing to note is that the mass of the specimens vary from 346 to 358 g causing the natural frequency to vary from 425 to 431.25 Hz. However, the effect on the modulus in minimal with the mean calculated modulus being 60.8084 GPA with a standard deviation of $\pm$ 0.6129 GPa. This is roughly 87 percent of the modulus of Aluminum 3003 H-18 (69 GPa).

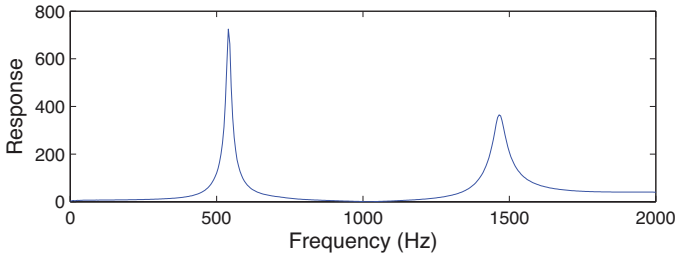

Figure 6.4: Sample Frequency Response Plot used for ASTM Standard 1876 E for Sugar Glucose Water Specimen

6.1.2 Candy-Combination of Sugar, Glucose and H20

The dimension of each specimen was roughly 7/16 × 7/16 × 10 inches. Figure 6.4 shows a sample Frequency Response plot obtained from the specimens. The tests were conducted in the same manner as the SnBi tests. Note that the two bending frequencies are near 500 Hz and 1500 Hz. In this test we have tried to minimize their affect by using accelerometers; they have a mass roughly 2% of the mass of the sample. Table 6.3 summarizes our results for each specimen.

Table 6.3: Measured Frequencies and Computed Young's Modulus of Candy Test Specimens

Specimen	Mass(g)	Measured Frequency (Hz)	Computed Young's Modulus
1	59	495	14.3425
2	60	530	16.7212
3	60	540	17.3581
4	58	510	14.9669
5	59	525	16.1337
6	61	535	17.3221

Table 6.3 inidicates that the bending frequencies differ somewhat from specimen to specimen; they range from 495 to 540 Hz. This could be due to variations in the manufacturing process or in the geometry of each specimen. The deviation in bending frequency causes the calculated Youngs Modulus to vary for 14.34 to 17.35 GPa. The mean Modulus is 16.14 GPa with a standard deviation of ± 1.25 GPa.

6.2 *In-Situ* Support Material Characterization

While the results of the material characterization indicate that SnBi is much stiffer than the candy, this does not indicate how each material will perform under actual UC process conditions. It should also be noted that the stiffness characterizations were at room temperature. During the actual welding operation, the support material will be heated externally. The temperature of the base plate is lowered so that both materials will not be heated near their melting points and should remain solid. In designing the next series of tests to quantify the effect of support material on the build height limit we assume that any difference in modulus at room temperature is proportional to the temperature difference during bonding. Furthermore, we chose to examine several extreme cases of geometry due to time constraints.

6.2.1 Test Specimens

Finite element simulations performed by McCullough [56] indicate that the height was the most dominant factor affecting the deflection of height was the dominant factor in affecting the deflection of the feature, the second dominant factor is modulus. McCullough [56]. The build features had a height, width and length of 0.9375 inches, 0.9375 inches and 2.5 inches, respectively. Figure shows the trough arrangement of the support material and Figures 6.5 shows the actual specimens, Figures 6.6 and 6.7 show the support test materials filled.

6.2.2 Test Parameters

We initially decided to use the following parameters:

- 1400 N (315 lb) compressive load applied to the tape and build specimen,
- heated base plate that reached a temperature of 120 °F (50°C) for the sugar glucose and 200 °F (93 °C) for SnBi,
- rolling speed of 42.33 mm/s (100 in/min),

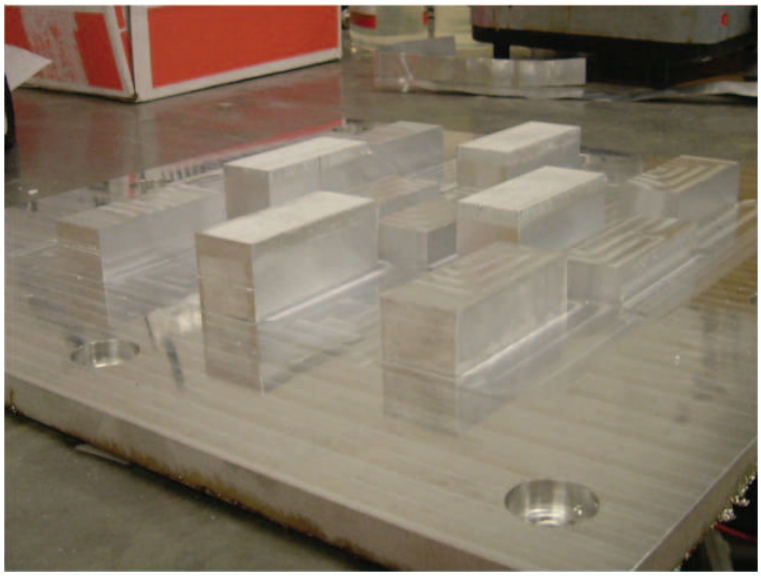

Figure 6.5: Specimens before filling used in the *In-Situ* Support Material Characterization

- 25 μm (9.84×10^{-4} in) sonotrode vibratory amplitude.

The load of 1400 N had to be reduced; welding at this load shorted out the power supply with no layer be able to adhere to the top surface. This result was the exact same phenomenon that we encountered during the resonance test. After consultation with Solidica, Inc. the normal load and amplitude were reduced until bonding occurred at a load of 179.8 lbs (800 N) for the combination of sugar and glucose, and 269.8 lbs (1200 N) for SnBi. The amplitude also had to be reduced to 18 μm for both sets of specimens. We also note that while welding aluminum the Formation machine heats the base plate to 300 °F (150°C). This temperature exceeded the melting temperature of both support materialsand had to be reduced accordingly. Before testing both tin bismuth and "candy" were poured into the "troughs" in their liquid state and allowed to cool. After each material solidified they were then reheated to the temperatures list above during the bonding operation.

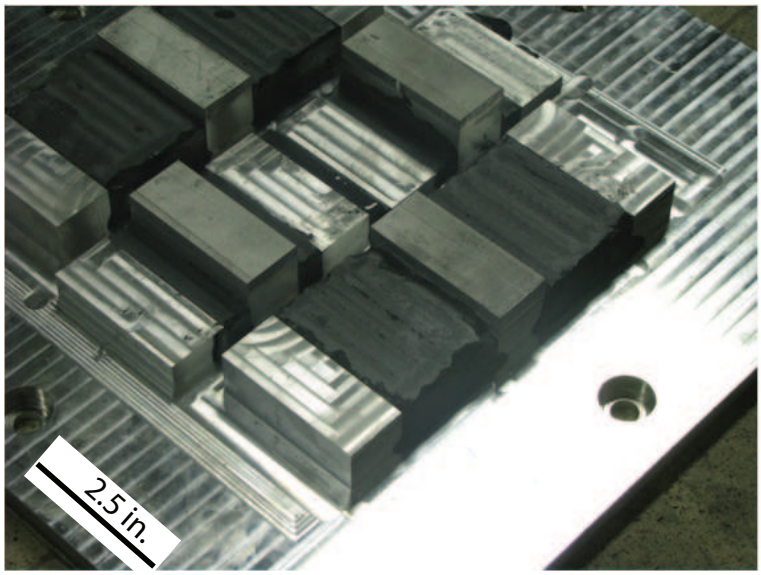

Figure 6.6: SnBi Support used in the *In-Situ* Support Material Characterization

Table 6.4: Test Specimens and Process Parameters used in Support Material Test

Test No.	h_s	w_s	Support Material	Baseplate Temp.	Normal Load
1	0.25	0.5	Sugar Glucose	120°F	179.8 lbs (800 N)
2	0.50	0.5		(50°C)	
3	0.75	2.0			
4	0.25	0.5	SnBi	200°F	269.8 lbs (1200 N)
5	0.50	0.5		(93°C)	
6	0.75	2.0			

6.3 Results

Each specimen was welded to failure or 55 layers; whichever occurred first. The results of the tests are in Tables 6.5 and 6.6. Overall the candy out performed the SnBi. Only one support configuration for the candy failed, conversely for two configurations the SnBi failed. Candys superior performance does not appear to be related to stiffness but is due to its adherence to the build feature and back wall of the trough. Despite cracking the candy specimens remained attached to the build feature for the duration of the welding process, Figure 6.8. In contrast the SnBi specimens detached from the build features and

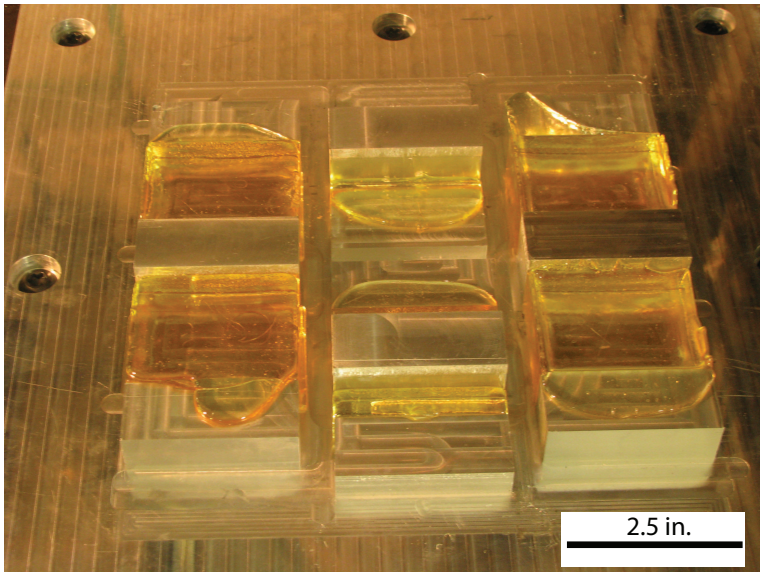

Figure 6.7: Candy Support used in the *In-Situ* Support Material Characterization

back walls, Figure 6.9. No crack or stress related defect was observed in the SnBi during the bonding process. The detachment was most likely due to the support vibrating and shifting loose during the welding process. We hypothesis that candy outperformed the SnBi based

Table 6.5: Failure for Sugar, Glucose, H20 Support Material

Support Height (inches)	Support Width (inches)	Method of Failure	Layer at Failure
0.25	0.50	No Failure	55
0.50	0.50	Crack Formed	48
0.75	2.00	No Failure	55

on two factors: 1) superior surface adhesion 2) and mismatch in the thermal expansion between SnBi and aluminum that left a gap after initial cooling and reheating. Adhesion depends on the relative surface energies of the liquid and the solid. When the surface energy of the liquid is greater than solid, that of the liquid will have a large contact angle and appear as bead on the solid. Conversely, if the surface energy of the liquid is less than the solid's the liquid will have small contact angle and appear spread out over the solid. Lee [57] shows that the surface energy of molten SnBi is approximately 340 dynes/cm, much

larger than the surface energy of the solid aluminum which is 35-45 dynes/cm depending on the alloy. The larger value of molten SnBi indicates a large contact angle and pour sticking to aluminum. Finally the brittleness and cracking of the candy suggested it was reheated

Table 6.6: Failure for SnBi Support Material

Support Height (inches)	Support Width (inches)	Method of Failure	Layer at Failure
0.25	0.50	Crack formed	28
0.50	0.50	No Failure	55
0.75	2.00	Detachment of 1st layer	24

to below its glass transition temperature. While we cannot find data on the glass transition of the candy used in this study. Upon examining the literature we find that glass transition temperatures of similar substances ranging from 140 °F (60 °C) to 163 °F (73 °C) which is above the reheating temperature of 120 °F (50°C) [58].

A finite element analysis of the initial cooling and reheating of the SnBi support structure and aluminum build feature can be found in McCullough [56]. The researcher applied an initial temperature of 450 °F to SnBi before allowing it to cool to an ambient temperature of 68 °F. He then applied a 200 °F temperature constraint on the bottom surface of the test fixture simulating the reheating caused by the Formation Machine. While the model is rudimentary in that it does not account for the phase changes in SnBi as it solidified or include any type of surface interactions between the tin bismuth and the aluminum, the work does point to 34 μm difference between the width of the trough and the width of the support material. The researcher notes that the model is an initial investigation but the mismatch in thermal expansion warrants further consideration. He did not analyze candy due to a lack of thermal properties. Arguably, one may point out that candy performed better due to the tin bismuth being improperly constrained, i.e., two faces of the support material were exposed and allowed to deform freely and escape. In order, for UC to mature as robust manufacturing technology the support materials performance should not be limited by its attachment to the build feature.

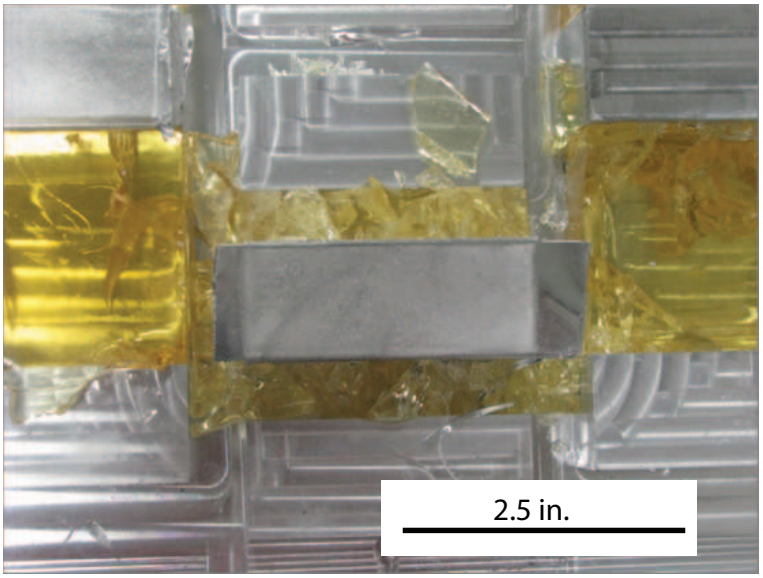

Figure 6.8: Cracking of Sugar Glucose Support Material during *In-Situ* Support Material Characterization

6.4 Summary

The chapter begins by examining the ideal characteristics of a candidate support material and proposing the effect of support materials on the build height. It then proceeds to a material characterization of the two candidate support materials, a sugar glucose mixture and tin bismuth. Finally, each support material is evaluated for its effectiveness in extending the build height of nominal width build features through a series of tests. The test show that the sugar glucose mixture outperforms the tin bismuth. These results point out that support material properties such as height, width and stiffness are not the only factors determining the effectiveness of a support material. Factors such as surface adhesion and thermal expansion may also play an important role in their performance.

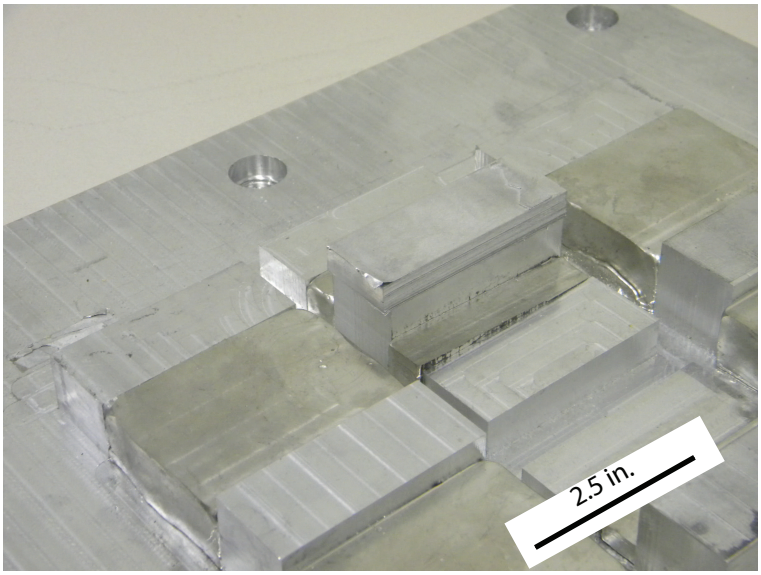

Figure 6.9: Detachment of SnBi Support Material during *In-Situ* Support Material Characterization

Chapter 7

Concluding Remarks

We put forth several research questions at the beginning of this dissertation.

1. Are parasitic vibrations caused by a change in geometry of the workpiece responsible for bonding degradation?

2. Under what exact geometries does bonding degradation occur?

   - Degradation for all heights and widths that have ratios of h/w ranging from 0.8 to 1.2?
   - Are there quantifiable differences between a wrought build feature and consolidated feature?

3. Can we experimentally detect a change in the dynamic response of the build piece and or sonotrode from optimal build geometries to those at or near bonding degradation? Perhaps by considering changes in amplitude or the frequencies present in the time response.

4. How does friction act at both tape interfaces, i.e., between the tape and the sonotrode and between the tape and build feature? Is it gross sliding versus micro slip? Can we determine how friction acts based on experimental evidence or thru analytical methods such as Finite Element modeling?

5. How do we determine a reasonable estimate of the effective stiffness and mass of the feature and / or sonotrode?

6. What is a suitable model of the sonotrode? Under what process conditions, if any, can we assume the sonotrode displacement, velocity and acceleration to be enforced?

Each of these items have been addressed below.

Item 1

At nominal tape widths, both analytical and experimental evidence clearly indicate that parasitic vibrations are responsible for failure in the build piece. However, the experiments indicate three types of failure:

- A weakening of the previously bonding region until they shear off from the feature. We attribute this failure to an increase in strain energy and fatigue loading as the system absorbs more energy due to its approaching a resonance excitation.

- A complete lack of welding of a layer. We theorize that under these conditions no differential motion exist between the build feature and tape or the tape is not pressed down adequately upon the feature. This drastically reduces the force of friction and consequently the pressure at the flaying interface is insufficient to cause the plastic state.

- The last bonded layers are sufficiently weak so that subsequent machining operations remove them form the substrate.

Item 2

The experiments presented in this dissertation do not contradict the observation that the h/w holds for all widths. Instead the models and experiments help clarify why this behavior occurs for the bonding of types at the nominal widths. Both numerical simulations and experimental evidence indicate that bonding degradation at this width is due to the proximity of the excitation to the natural frequency. As one or more frequencies converge by increasing the build height, the feature vibrates in phase with the sonotrode. We postulate that

this causes a decrease in the stress state at the interface that results in flaying interface not reaching plasticity and therefore not bonding. In addition welding of 0.5 width specimens in the vibrating fixture exhibited some of the same behavior as the consolidated features. If we also consider that we could weld over previous welded specimens once they were past the aspect ratio limit for nominal width specimens the chances of accumulated porosity or some other aspect of the consolidated feature such as work hardening determining the limit on build height seems remotes.

Item 3

Experimentally, we observe both a spike in the substrate's motion and the power draw by the piezoelectric actuator regardless of the feature's width. However, further tests are needed to quantify the exact troubled regions of deflection and power draw.

Item 4

Experimentally, it is difficult to verify how friction acts on the surface. Using the substrate and sonotrode deformation to deduce where slip occurrs based on the presence of higher order harmonics in the signal proved problematic. Higher order harmonics existed in the sonotrode deformation under no load in free air. While their effect was great amplified during the consolidation process there is not a way to point to individual frequency components and show that they indicate slip.

Item 5

The correlation between the lumped parameter model and experimental evidence indicates that reducing the parallelepiped to a single degree of freedom oscillator works well in determining its effective properties for lumped parameter models. While not addressed in this work, recent research by the Edison Welding Institute [59] indicates that the sonotrode acts like a three degree of freedom oscillator operating in its third mode. It may be possible to extend the lumped parameter models presented in this work to accurately capture the sonotrode's dynamics and to model fluctuations in power flow. The fluctuations in power may ultimately correlate to the strength of the bond since at failure the sonotrode's power draw increased.

Item 6

Clearly, by examining the fluctuations in load and power our model of the sonotrode is an idealization. However, these fluctuations seem to have a minimal effect on the sonotrode amplitude in our tests and thus we are justified in assuming the amplitude and frequency are prescribed. However, when predicting under what conditions a welder fault will occur it would be beneficial to model the sonotrode as an ultrasonic resonator.

7.1 Contributions

This work presents several advances in understanding the mechanics of the Ultrasonic Consolidation Process. These include

- The first real time recorded measurements of both sonotrode and substrate deformations during the UC process.
- The research presented in this work is formal theory that modal interactions are responsible for bonding degradations.
- The work experimentally proved that the h/w build limit of the build piece is one sided build limit. for nominal width specimens
- The models generated in this work the first stage in developing a predictive capability in addressing build height limits in the UC process. The work to date has explored process limits only through experimental studies.
- Extended the current body of finite element models of the UC process to explicitly include the effect of surface topography on the bonding process.

7.2 Discussion

The models and theories in this dissertation, generally predict the observed behavior of bonding failure for nominal width specimens. Using a combination of the "Mode" Map,

Figure 2.17 , the lumped parameter model, and the finite element model we can draw a clear picture of how the modal interaction of the first mode and second modes of vibration cause fatigue, and loss of differential motion leading to the various bonding failures experienced by the nominal width test specimens

However, for specimens of width 0.5 inches the picture is not clear. The results are even more ambiguous when considering why failure occurs when the height approaches 0.5 inches. The first natural frequencies of the specimens are in the neighborhood of 40 kHz. One possible explanation is the material characterization. Clearly, the modulus is lowered due to temperature and the application of ultrasonic energy. However, few published results address this change in modulus. The only alternative is to adjust the modulus to fit our accepted theory. However, the nature of the failure of these specimens is different than the failure of the other specimens. In the nominal width specimens failed due to fracture in the layers. This can easily be attributed to increase in fatigue due to an increase in compliance that would occur as the feature is excited at one of its natural frequencies. In the clamped wrought samples as the h/w approached unity for the 0.5 width specimens there was a complete lack of bonding. It would almost seem as if the tape was not pressed down on by the sonotrode. Again, this behavior could be explained if the sonotrode excited one of the normal modes during the welding operation

7.3 Future Work

Ultrasonic consolidation is a burgeoning new manufacturing process. However, before it can become a robust technology many issues need to be addressed. Specifically, in regards to building high aspect ratio features we outline several issues that should immediately be addressed.

7.3.1 Material Characterization

Ultrasonic consolidation differs from traditional ultrasonic joining processes in that the geometry of the bonding substrate constantly changes during the welding process. Understanding the material properties in conventional ultrasonic proccess is important. It becomes paramount when extending the technology to produce finished product or parts through a series of welding operations. The research in this dissertation shows that at the nominal tape width, that modal properties, specifically the proximity to a natural frequency of the build feature clearly influences the ability to bond to the substrate. The findings also suggest that modal effects are to blame for the bonding degradation at other widths. However, natural frequencies are influenced by both modulus and geometry. Furthermore, heat and the very presence of ultrasonic irradiation drastically change the modulus of the material. In order to develop a predictive model of geometries that may be problematic the changes in modulus due to heat and ultrasonic irradiation must be known for any candidate material used in the process. In fact other, materials may not exhibit the same limit on build geometry.

7.3.2 Sonotrode Characterization and Design

Researchers have made several assumptions about the Ultrasonic horn in the UC process: 1) the horns amplitude is constant under load , 2) it operates at only one frequency. Research by Sheridan [59] and presented in this dissertation show that both of these assumptions are false. The sonotrode's load varies slightly during the UC process, and while the signal is composed of mainly the nominal 20 Khz component, other higher order harmonics are excited and become more pronounced under load. Finally, and perhaps most problematic, is the finding that due to the phase lock loop algorithm, the welder will shut off if the sonotrode couples to the build piece and the coupled assembly vibrates at a natural frequency outside of its operating range. Clearly, in exploring process limits, a better model of the sonotrode is needed. Furthermore, it may be beneficial to use an alternate sonotrode design that operates at two frequencies that may be shifted during the

consolidation process as needed.

7.3.3 Bond Quality versus Geometry

In this study we only considered failure through the detachment of layers and did not examine how the bonding of each layer changed as a function of build height. As we we approach the problematic geometries we do not know if the bonding becomes progressively worse. Examining the linear weld density of the specimens as the height increases and measuring the bond strength through pull test will provide some answers to the question.

7.3.4 Modeling

The models in this work are limited in that they neglect any effect of temperature and the absorption of ultrasonic energy on the modulus, and yield strength of the material [18]. However, they provide upper bounds on the material parameters effect on the process and thus are a first step in predicting when bonding degradation will occur. An immediate extension of this work is to formulate a finite element model to explore the effect of surface topography on the UC process. The model may used to explain the nature of the motion at bonding interface, i.e., gross sliding versus partial slip and to quantify the effect of differing sonotrode surface textures on the stress at the interface. An immediate extension to this model is to add a thermal analysis, including temperature varying material properties, and due to the high strain rates that may present during the UC process a viscoplastic model of plasticity at the interface. In addition, new phenemological models have been developed that may be included to account for the observed phenomena of acoustic softening [60]. Adding these components, it may be possible to provide a detailed picture of the stress state at the interface and to examine how a resonance excitation alters the interfacial stress state.

7.3.5 Support Materials

In choosing an optimal support material much work remains to be done. The results in this work and research by McCullough [56] indicate that stiffness and geometry, and convenience of removal are not the only criteria necessary for an optimal support material. Factors such as surface adhesion and thermal expansion may also play an important role in their performance. In addition, this work focused on the using the support materials to stiffen the build feature it behaved as if its height was reduced and did not consider the effect of support materials that may also add dampening to the structure such as a viscoelastic damping material. Finally, we only examined two candidate support materials in this work, SnBi and a combination of sugar, glucose, and water or "candy". They were chosen since they were extremes on the stiffness convenience curve. We can easily examine intermediate values of this design space by using water soluble polymers or filling the candy with a filler material such as aluminum fillings.

Bibliography

[1] C. Zhang and Li. L. A friction-based finite element analysis of ultrasonic consolidation. *Welding Journal Supplement*, 87(3):187–194, 2008.

[2] C. K. Chua, K. F. Leong, and C. S. Lim. *Rapid Prototyping: Principles and Application*. World Scientific Publishin Co. Pte. Ltd., Hackensack, N. J., 2nd edition, 2006.

[3] H. Hopinson, R. J. M. Hague, and P.M. Dickens, editors. *Rapid Manufacturing: An Industrial Revolution for the Digital Age*. Joh Wiley & Sons, Ltd., Loughborough Univeristy, UK, 2006.

[4] D. R. White. Ultrasonic consolidation of aluminum tooling. *Advanced Materials and Processes*, 64(2):2, 2003.

[5] C.Y. Kong, R.C. Soar, and P.M. Dickens. A model for weld strength inultrasonically consolidated components. *Proceedings of the Institution of Mechanical Engineers, Part C: Journal of Mechanical Engineering Science*, 219(1):83–91, 2004.

[6] L.D. Rozenberg, editor. *Physical Prinicples of Ultrasonic Technology*, volume 1. Plenum Press, 1971.

[7] R.L. O'Brien, editor. *Welding Handbook*, volume 2 of *Welding Processesa*. American Welding Society, eighth edition, 1991.

[8] C.Y. Kong, R.C. Soar, and P.M. Dickens. Characterisation of aluminum alloy 6061 for the ultrasonic consolidation process. *Materials Science and Engineering*, 363(1-2):99–106, 2003.

[9] T. Tsujino, T. Ueoka, T. Kashino, and F. Sugahara. Transverse and torsional complex vibration systems for ultrasonic. *Ultrasonics*, 38:67–71, 2000.

[10] *The Science and Engineering of materials.* PWS Publishing Company, 3rd edition, 1994.

[11] M. J. Fletcher. *Friction Welding.* Mills and Boons, 1972.

[12] B. Langenecker. Effect of ultrasound on deformation characteristics of metals. *IEEE Transaction on Sonics and Ultrasonics*, 13(1):1–8, 1966.

[13] D. R. Culp and H. T. Gencsoy. Metal deformation with ultrasound. *1973 Ultrasonics Symposium*, pages 195–198, 1973.

[14] Reoprt niti. Technical report, 1964.

[15] N.F. Kozakov. Diffusion welding technique with the aplication of ultrasound, March 1961.

[16] S. Yadev and C. Doumandis. Ultrasonic rapid manfuacturing: Implementation and thermo-mechanical analysis. In *American Society of Mechanical Engineers, EEP*, volume 2, pages 515–521, New Orleans, United States, 2002. American Society of Mechanical Engineers.

[17] J. George and B Stucker. Fabrication of lightwieght structural panels through ultrasonic consolidation. *Virtual and Physical Protoyping*, 1(4):227–241, 2006.

[18] C. J. Robinson, Zhang C., G.D. Janaki Ram, E. J. Siggard, B. Stucker, and Li. L. Maximum height to width ratio of freestanding structures built using ultrasonic consolidation. In *2006 Solid Feeform Fabrication Proceedings*, Austin, TX, 2006.

[19] Y. Gao and Doumanids C. Mechanical analysis of ultrasonic bonding for rapid prototyping. *Transactions of the ASME: Journal of Manufacturing Science and Engineering*, 124:426–434, 2002.

[20] C. Doumandis and Y. Gao. Mechanical modeling of ultrasonic welding. *Welding Journal*, 83(4):140S –146S, 2004.

[21] C.Y. Kong, R.C. Soar, and P.M. Dickens. Optimum process parameters for ultrasonic consoildation of 3003 aluminum. *Journal of Materials Processing Technology*, 146:181–187, 2004.

[22] D. J. Inman. *Engineerig Vibration*. Prentice Hall, London, 2nd edition, 2001.

[23] B. Langenecker. *Plastizitasuntersuchungen an Metallkristallen im Ultrashallfeld*. PhD thesis, University of Wien Austria, 1957.

[24] T. Tsujion and T. Ueoka. Studies on ultrasonic butt welding. *IEEE 1984 Ultrasonics Symposium*, pages 493–496, 184.

[25] Jack Blitz. *Fundamentals of Ultrasonics*. Plenum Press, New York, second edition, 1967.

[26] Kuttruff. *Ultrasonics: Fundamentals and Applications*. Elsevier Applied Science, London and New York, 1991.

[27] B. Fu. *Piezoelectric Actuator Design via Multiobjective Optization Methods*. PhD thesis, HNI-Verlagschriftenreihe, Paderborn, 2005.

[28] R. Opie and A. Gupta. Question and monitoring. Email.

[29] N. Bilgutay, Li X., and McBrearty M. Development of non-destructive bond monitoring techniques for ultrasonic bondeers. *Ultrasonics*, 24(6):307–317, 1986.

[30] F. Blaha and B. Langnecker. Dehun von zink-kristallen unterr ultraschalleinwirkung. *Z. Naturwiss*, 20(556), 1955.

[31] K. C. M. Joshi. The formation of ultrasonic bond between metals. *The Welding Journal*, 16:840–848, 1971.

[32] I. Lum, Mayer M., and Zhou Y. Footprint study of ultrasonic wedge bonding aluminum. *Journal of Elctronic Materials*, 35(3), 2006.

[33] R. D. Mindlin. Compliance of elastic bodies in contact. *Journal of Applied Mechanics*, 15(259), 1949.

[34] U. I. Chang and J. Frish. On optimization of some parameters in ultrasonic metal welding. *The Welding Journal*, 53(1):24–35, 1974.

[35] E. Neppiras. Ultrasonic welding of metals. *Ultrasonics*, 3:128–135, 1965.

[36] J. Harthoorn. Joint formation in ultrasonic welding compared with fretting phenomena for aluminum. *In Ultrasonics International 1973*, pages 43–51, 1973.

[37] C. Zhang, Xu Zhu, and Li L. A 3-d coupled-field dynamic mdel for ultrasonic consolidation. In *In Materials Science and Technology*, 2006.

[38] C. J. Huang and Ghaseemieh E. 3d coupled thermomechanical finite element analysis of ultrasonic consolidation. *Materials Science Forum*, 539-43(3), 2007.

[39] C. Zhang and Li L. A study of dynamic mechanical behavior of substrate in ultrasonic welding. The Seventeeth Solid Freeform Fabrication Symposium.

[40] Ram Janaki G.D., Yang Y., George J., and C. J. Robinson. Improved linear weld density in ultrasonicall consolidated parts. Austin, TX, 2006.

[41] M. Kulakov and H. Rack. Control of 3003 h-18 aluminum ultrasonic consolidation. *Journal of Engineering Materials and Technology*, 131, 2009.

[42] J. Wodara. Relation between component geometry and the quality of ultrasonically welded metallic joints. *Wissenschaftliche Zeitschrift der Technischen Universitaet Ott von Guerick Madgeburg*, 33(8):64–68, August 1989.

[43] Eric v. K. Hill and M. Egle Davis. Response of a rectangular parallelepiped to a simulated acousti emission burst. *The Journal of the Acoustical Society of America*, 71(4):891–901, 1982.

[44] Arthur Leissa and Zhang Zhing-ding. On the three-dimensional vibrations of the cantileerd rectangulra parallelepiped. *Journal of the Acoustial Society of America*, 73(6):2013–2021, 1983.

[45] K. L. Johnson. *Contact Mechanics*. Cambridge University Press, 1985.

[46] R.S. Stepleman et al., editor. *ODEPACK, a systematized collection of ODE solvers*, North-Holland, 1983.

[47] E. Vries. *Mechanics and Mechanisms of Ultrasonic Metal Welding*. PhD thesis, The Ohio State University, 2004.

[48] R. S. Fligliola and D. E. Beasley. *Theory and Design for Mechanical Measurements*. John Wiley & Sons, 4th edition, 2005.

[49] *Metals Handbook*. ASM International, 10th edition, October 1990.

[50] G. K. M. Martin. Al, ti and cu parameters. Presentation, September 2008.

[51] S. J. Rothberg, J.R. Baker, and N.A. Halliwell. Laser vibrometry: Psuedo vibrations. *Journal of Sound and Vibration*, 135(3):516–522, 1989.

[52] J. Vass, R. Smid, R.B. Randall, P. Sovka, C. Cristalli, and B. Torcianti. Avoidance of speckle noise in laser vibromtry by the use of kurtosis ratio: Application to mechanical fault diagnostics. *Mechanical Systems and Signal Processing*, 22:647–671, 2008.

[53] SEMICON. *Real Time Ultrasonic Bond Quality Monitoring*, Singapore, 2002.

[54] S.N. Mahmoodi, M. F. Daqaq, and Jalili N. On the nonlinear-flexural response of piezoelectrically driven microcantilever sensors. *Sensors and Actuators A: Physical*, 153:171–179, 2009.

[55] *Standard test Method for Dynamic Young's Modulus, Shear Modulus, and Poisson's Ratio by Impulse Excitation of Vibration.* ASTM International.

[56] D. McCullough. Dynamic finite element simulation of ultrasonic consolidation. Master's thesis, Clemson Univeristy, August 2009.

[57] J. Lee, H. Chen, H. Chang, and C. Chen. Reactive wetting between molten sn-bi and ni substrate ni substrate. *Journal of Electronic Materials*, 32(3):117–122, 2003.

[58] M. Okuno, S. Kishihara, M. Otsuka, and K. Kawasaki. Glass transition temperature of amorphous solid formed from sucrose crystal with different melting point. *Proceedings of the Research Society of Japan Sugar Refineries' Technologists*, 51:7–12, 2003.

[59] K. Graff, editor. *Ultrasonic Consolidation Symposium.* Edison Welding Institute, 2008.

[60] A. Siddiq and E. Ghassemieh. Thermomechanical analyses of ultrasonic welding process using thermal and acoustic softening effects. *Mechanics of Materials*, 40:982–1000, 2008.